WL-TR-93-2076

(2)

AN INVESTIGATION OF THE SURGE BEHAVIOR OF A HIGH-SPEED TEN-STAGE AXIAL FLOW COMPRESSOR

PATRICK RUSSLER

AERO PROPULSION AND POWER DIRECTORATE
WRIGHT LABORATORY
AIR FORCE MATERIEL COMMAND
WRIGHT PATTERSON AFB OH 45433-7650

MAY 1993

FINAL REPORT FOR 08/01/90-08/01/92

AERO PROPULSION AND POWER DIRECTORATE
WRIGHT LABORATORY
AIR FORCE MATERIEL COMMAND
WRIGHT PATTERSON AFB 0H 45433-7650

NOTICE

When Government drawings, specifications, or other data are used for any purpose other than in connection with a definitely Government-related procurement, the United States Government incurs no responsibility or any obligation whatsoever. The fact that the government may have formulated or in any way supplied the said drawings, specifications, or other data, is not to be regarded by implication, or otherwise in any manner construed, as licensing the holder, or any other person or corporation; or as conveying any rights or permission to manufacture, use, or sell any patented invention that may in any way be related thereto.

This report is releasable to the National Technical Information Service (NTIS). At NTIS, it will be available to the general public, including foreign nations.

This technical report has been reviewed and is approved for publication.

PATRICK M. RUSSLER
AEROSPACE ENGINEER
TEST & EVALUATION SECTION
TECHNOLOGY BRANCH
TURBINE ENGINE DIVISION
AERO PROPULSION & POWER DIRECTORATE

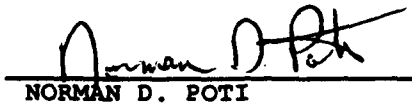

NORMAN D. POTI
CHIEF, TEST & EVALUATION SECTION
TECHNOLOGY BRANCH
TURBINE ENGINE DIVISION
AERO PROPULSION & POWER DIRECTORATE

If your address has changed, if you wish to be removed from our mailing list, or if the addressee is no longer employed by your organization please notify WL/POTX, WPAFB, OH 45433-7650 to help us maintain a current mailing list.

Copies of this report should not be returned unless return is required by security considerations, contractual obligations, or notice on a specific document.

REPORT DOCUMENTATION PAGE

Form Approved
OMB No. 0704-0188

1. AGENCY USE ONLY (Leave blank)	2. REPORT DATE	3. REPORT TYPE AND DATES COVERED
	1993 May	FINAL AUGUST 1990 to AUGUST 1992

4. TITLE AND SUBTITLE
An Investigation of the Surge Behavior of a High-Speed Ten-Stage Axial Flow Compressor

5. FUNDING NUMBERS
PE: 62203F
PR: 3066
TA: 17
WU: 40

6. AUTHOR(S)
Patrick Russler (513) 255-6802

7. PERFORMING ORGANIZATION NAME(S) AND ADDRESS(ES)
Aero Propulsion & Power Directorate
Wright Laboratory
Air Force Materiel Command
Wright-Patterson AFB OH 45433-7650

8. PERFORMING ORGANIZATION REPORT NUMBER
WL-TR-93-2076

9. SPONSORING/MONITORING AGENCY NAME(S) AND ADDRESS(ES)
Aero Propulsion & Power Directorate
Wright Laboratory
Air Force Materiel Command
Wright-Patterson AFB OH 45433-7650

10. SPONSORING/MONITORING AGENCY REPORT NUMBER
WL-TR-93-2076

11. SUPPLEMENTARY NOTES

12a. DISTRIBUTION/AVAILABILITY STATEMENT
Approved for public release; distribution is unlimited

12b. DISTRIBUTION CODE

13. ABSTRACT *(Maximum 200 words)*

During a ten-stage compressor rig test conducted at Wright-Patterson AFB, several instances of compressor surge were observed. While surge is known to occur in high-speed multi-stage compressors, very little transient data pertaining to such events exists in the open literature, exclusive of engine data. In an attempt to make more data of this type available to researchers, surge data from this test are presented in this report. The predictions of a computer-based transient compressor model are compared to the data for study. Furthermore, an unexplained instability phenomenon is investigated: a constant surge/rotating stall boundary.

During the test, it was found that the speed boundary between surge and rotating stall occurred between 80% and 81% rotor speed. This boundary did not change when the compressor discharge volume was changed. This seemed to contradict accepted theory, which predicts a shift in the surge/rotating stall boundary. An investigation into the possible causes of this phenomenon is conducted as part of this report. Several theories are explored, including the possibility of excess volume communicating with the compressor during instability. Although the excess volume theory is not proven, it remains the most likely cause of the unusual surge/rotating stall boundary behavior.

14. SUBJECT TERMS			15. NUMBER OF PAGES
Axial Compressor	Compressor Surge	Surge Performance	161
Aircraft Turbine Engine		Discharge Volume Effects	16. PRICE CODE

17. SECURITY CLASSIFICATION OF REPORT	18. SECURITY CLASSIFICATION OF THIS PAGE	19. SECURITY CLASSIFICATION OF ABSTRACT	20. LIMITATION OF ABSTRACT
Unclassified	Unclassified	Unclassified	Unlimited

TABLE OF CONTENTS

TABLE OF CONTENTS (continued)

LIST OF FIGURES

LIST OF FIGURES (continued)

LIST OF FIGURES (continued)

LIST OF TABLES

SYMBOLS AND NOTATION

a = speed of sound

A = through-flow area

B = dimensionless parameter

FX = compressor forces acting on the fluid

H = total enthalpy

L = effective length of equivalent duct

m = mass flow rate

NBM = dimensionless parameter

P = static pressure

PR = pressure ratio (P_{t2} / P_{t1})

Q = rate of heat addition

t = time

T = static temperature

TR = temperature ratio (T_{t2} / T_{t1})

U = mean rotor velocity

u = through-flow velocity

V = volume

W_{sh} = rate of shaft work

SYMBOLS AND NOTATION (continued)

Greek Symbols

ρ = density

τ_D = compressor time constant; lag

ϕ = flow coefficient

$$= \frac{\frac{W\sqrt{T_t}}{P_t A}\left[\frac{\textit{Design Corrected Speed}}{\textit{Actual Corrected Speed}}\right]}{0.5318}$$

ψ^P = pressure coefficient

$$= [PR^{\frac{\gamma-1}{\gamma}} - 1]\left[\frac{\textit{Design Corrected Speed}}{\textit{Actual Corrected Speed}}\right]^2$$

ψ^T = temperature coefficient

$$= [TR - 1]\left[\frac{\textit{Design Corrected Speed}}{\textit{Actual Corrected Speed}}\right]^2$$

Subscripts

b = stage bleed

c = compressor

d = discharge duct

i = combustor filler volume

p = plenum

ss = steady-state

t = total or stagnation

1.0 INTRODUCTION

Paramount to the previous and continuing development of the aircraft gas turbine engine is an understanding of compressor instability. Compressor instabilities, as evidenced in the axial flow compressors used in modern jet engines, have a detrimental effect upon the operating behavior of such engines. Reduced performance and engine life are only two detriments of compressor instability, but are considered among the most important ones to aircraft engine designers. The lack of understanding and predictability of unstable compressor behavior in the compression systems of jet engines has led to inconvenience and even disaster. As a result, research continues in an effort to better understand the instability behavior of high-speed axial-flow compressors.

This report was written with two separate goals in mind. The first of these was to present some of the surge data obtained from a high-speed 10-stage axial flow compressor. By using some fundamental data analysis techniques as well as computer based flow modeling, the basic surge behavior of this compressor was documented. The second and more challenging goal of this research was to discover the reason for the strange nature of the surge/rotating stall boundary in this compressor. Changes in the discharge plenum volume seem to have had no effect on this boundary, an observation which runs contrary to accepted theory. This report attempts to resolve this apparent contradiction by showing that certain unexpected flow conditions existed during surge which may have affected the surge/rotating stall boundary behavior of this compressor.

1.1 Compressor Behavior and Instability

The purpose of the compressor in a modern jet engine is to increase the total pressure entering the combustion chamber so that the working fluid (air) can be more readily and efficiently heated. Two principal types of compression systems are typically used to perform this task. Centrifugal compressors, which utilize centrifugal force to help compress the working fluid, are usually characterized by a relatively high pressure rise per individual stage. Axial compressors, which rely on the pressure rise produced across rotating airfoils to compress the working fluid, are usually characterized by high mass flow rates. Generally, centrifugal compressors produce higher pressure ratios per stage than do axial compressors, but at the cost of added weight and increased total pressure loss due to flow turning between individual stages. Due to the weight limitations and high mass flow requirements imposed upon present day engines, axial compressors have become the predominant type of compression system employed in modern jet engines. Thus, from a aircraft propulsion stand-point, the stability behavior of axial flow compressors is of great interest.

The performance of all compressors, including the axial type, is often described by what are called a performance characteristics. Performance characteristics relate compressor operating variables such as efficiency, pressure, temperature, mass flow, etc, to one another. As an example, consider the "typical" compressor performance characteristic for stalled and unstalled operation shown in Figure 1.1. This performance characteristic relates the total pressure ratio produced across the compressor to the mass flow through the compressor. The resulting curves define the stable operating points for

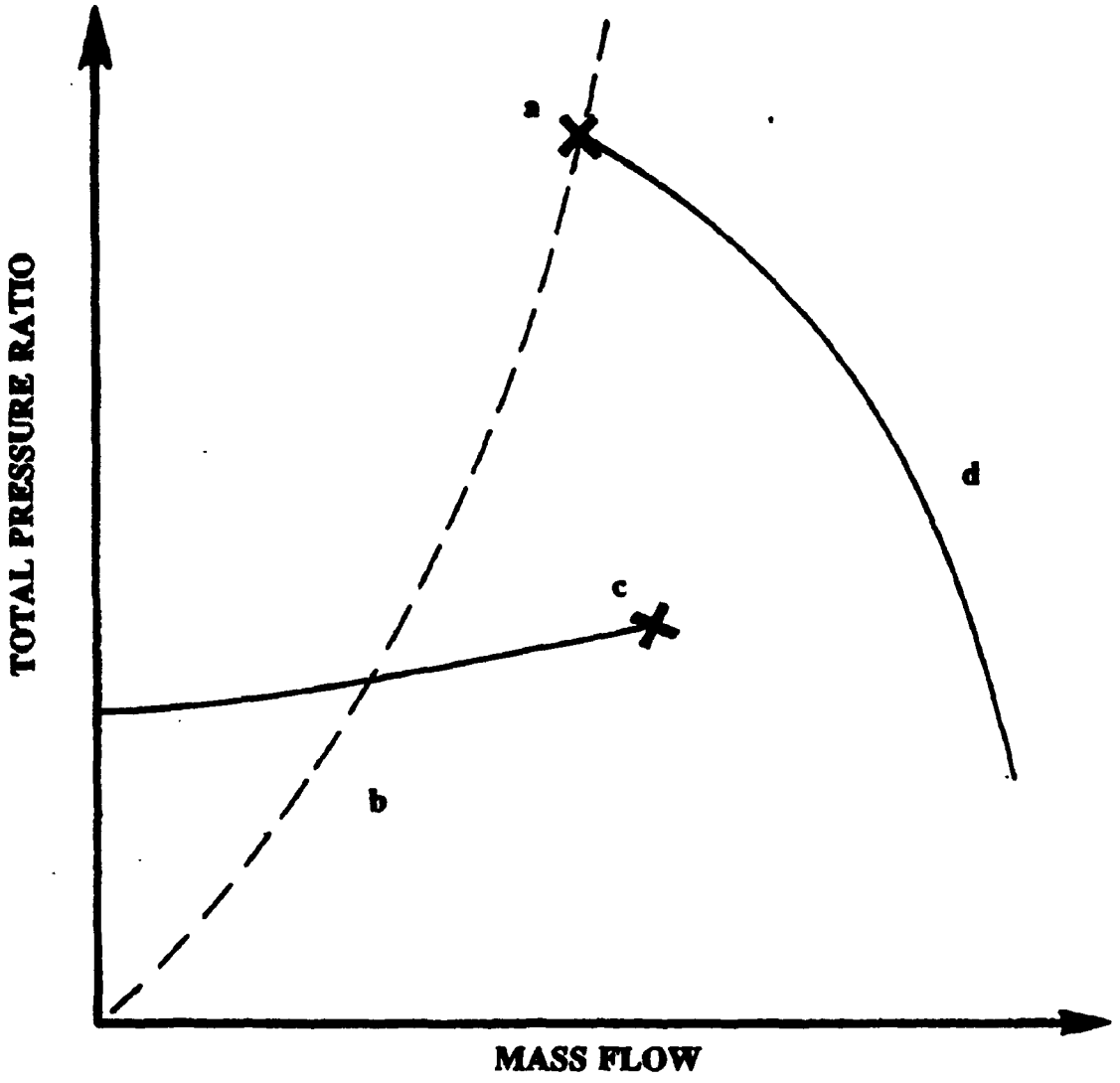

Figure 1.1 "Typical" compressor characteristic

a given compressor at one particular compressor rotor speed. There are an infinite number of curves for an infinite number of compressor speeds, so any given compressor will have a set of compressor characteristics that vary with compressor speed.

Generally, there are two operating regimes for a given compressor. In Figure 1.1, the curve that includes points **d** and **a** is called the unstalled portion of the compressor characteristic. The design point for this specific compressor (if it is to operate at this compressor speed) exists somewhere on this curve. The other part of the characteristic is typically called the stalled portion of the compressor characteristic. When the compressor operates at some point on this curve the compressor blades are stalled, causing an overall reduction in compressor performance.

As suggested above, it is desirable for the compressor to operate on the unstalled portion of the compressor characteristic. However, under certain conditions, the compressor may be forced to operate on the stalled portion. Consider again the compressor pressure characteristic in Figure 1.1. Let us suppose that the compressor is currently operating on the unstalled portion of the characteristic at an operating point somewhere near **d**. Then, holding the speed constant, let's further suppose that the mass flow is reduced. In a compressor test situation where the compressor is not part of an engine, this is usually accomplished with a valve or throttle downstream of the compressor exit. In this case the throttle is slowly closed.

As the throttle is closed, the compressor operating point begins to move up the unstalled portion of the compressor characteristic towards **a**. Let us suppose throttle closure is stopped once the compressor operating point reaches point **a**. The

compressor will continue to operate steadily at this point. Notice the dashed line shown on the "typical" compressor characteristic. This line is called a throttle line, and like the compressor characteristic, it defines all the stable operating points for the throttle, but for a given throttle flow area rather than for a given compressor speed. As is the case for compressor pressure characteristics, there are an infinite number of throttle lines defined by an infinite number of throttle areas, but let us concern ourselves with the throttle line that passes through point a only.

If we close the throttle an infinitesimal amount, the compressor operating point is forced off of the unstalled portion of the characteristic. If compressor behavior was such that the operating point could instantly change, the compressor operating point would "follow" the throttle line to the point where it intersects the stalled portion of the compressor characteristic. The compressor would then operate quasi-steadily at this point, shown as point b on the figure.

Unfortunately, compressor operating points cannot change instantly. Indeed, there is a definite time lag between unstalled and stalled operation. Furthermore, under some conditions, the compressor never reaches a stable operating point on the stalled characteristic. Due to operating conditions that are not yet completely understood but will be briefly discussed later, compressor performance beyond the unstalled portion of the characteristic is often defined by two related but very different instability phenomena. These are called rotating stall and surge. Although the bulk of this report is concerned with surge behavior, these two types of unstable compressor behavior are too interrelated to discuss one exclusive of the other, so both are discussed herein.

1.2 Rotating Stall and Surge

Rotating Stall

Rotating stall manifests itself as a volume or cell of stalled air flow that rotates about the compressor centerline at some fraction of the compressor rotor speed. This *stall cell* rotates in the same direction as the rotor rotation and can cause a significant amount of air flow blockage in the compressor. The basic mechanics of rotating stall inception are quite simple and were first detailed by Emmons et al. [1] in 1955.

Consider a single stage compressor rotor modeled as a linear row of compressor blades as shown in Figure 1.2. These blades are at a high angle of attack and are moving in the direction shown. If a flow disturbance occurs near blade *ii* which causes an increased angle of attack, such as exhaust gas ingestion or off-design inlet flow, the flow on the suction side of the blade separates. This causes a decrease in airflow through the blade passage, increasing the angle of attack of blade *i* and decreasing that of blade *iii*. This causes blade *i* to stall and at the same time inhibits stalling of blade *iii*. After blade *i* stalls, the next blade in the blade row stalls while the originally stalled blade (blade *ii*) tends to recover. This action occurs over and over again along the blade row, propagating in the direction shown in the figure. If the initial disturbance is strong and persists, a fully developed rotating stall cell may develop.

A fully developed rotating stall cell is defined as an area of extensive blade stalling that rotates around the compressor annulus. Over 50 percent of the annulus area can be taken up by a rotating stall cell. Moreover, multiple stall cells are possible. Air flow through a rotating stall cell is nearly zero, and is sometimes even reversed,

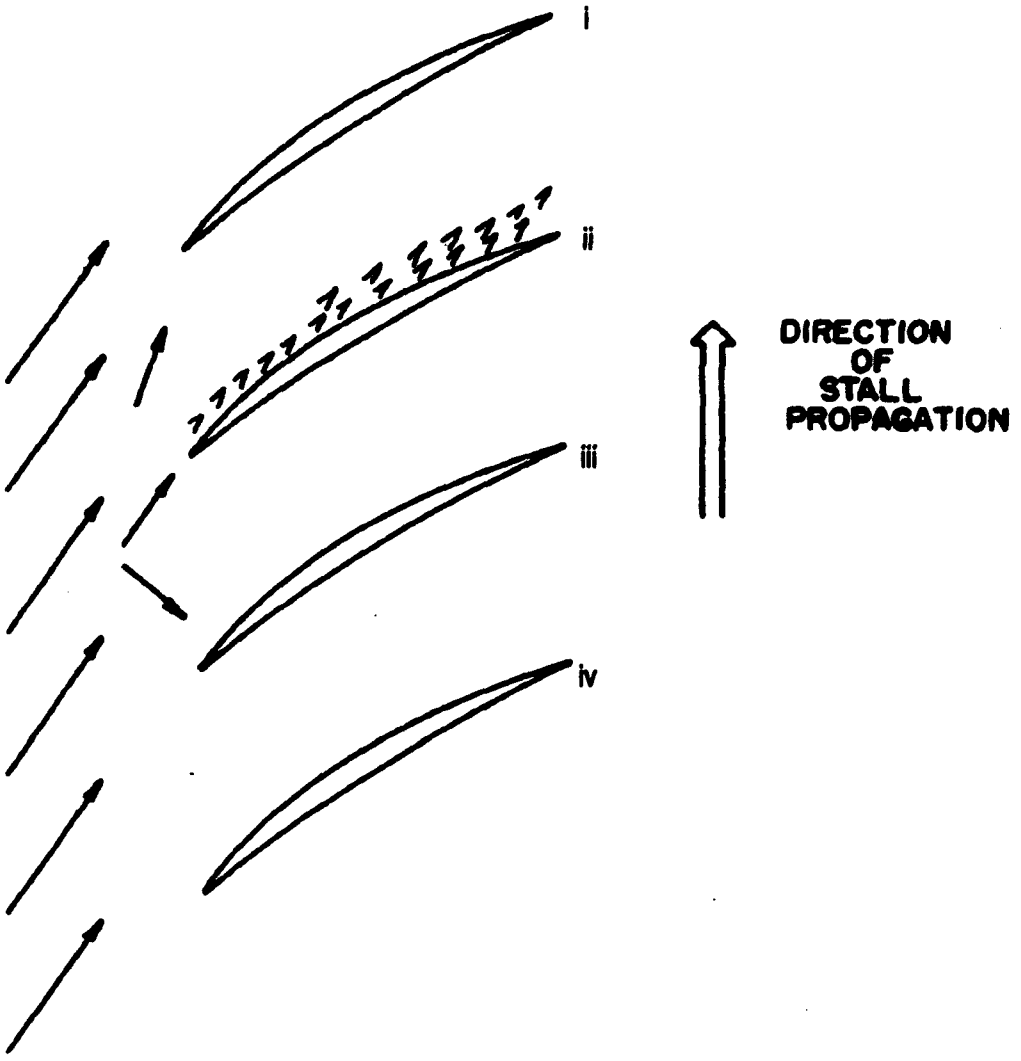

Figure 1.2 Rotating stall mechanism

accounting for the blockage mentioned earlier. Furthermore, the blade and case temperatures can become very high, so prolonged operation in rotating stall can seriously damage a compressor.

When an instability occurs that initiates rotating stall, the compressor can go into either progressive or abrupt rotating stall. Progressive stall occurs when the compressor operates on a continuous compressor characteristic. That is, when there is no abrupt boundary between stalled and unstalled performance. Abrupt stall occurs when the compressor characteristic is discontinuous and there is an abrupt boundary between stalled and unstalled performance.

The "typical" compressor characteristic shown in Figure 1.1 is conducive to abrupt stall, so in this case the compressor does not typically transition smoothly into stalled operation. Rather, the operating point of the compressor tends to oscillate around a point defined by the intersection of the stalled characteristic with throttle characteristic. Eventually, the operating point stabilizes at that intersection. Figure 1.3 shows a "typical" rotating stall inception, where the compressor operating point "spirals" in toward a quasi-steady operating point on the throttle/stall characteristic. The term quasi-steady is used to define rotating stall behavior because although the average compressor performance is often defined by a single operating point, the stall cell is still rotating about the compressor rotor causing significant fluctuations in pressure, mass flow, and temperature along the circumference. Thus, rotating stall is stable only in a one-dimensional sense.

Surge

The other possible compressor instability, surge, is characterized by large pressure and

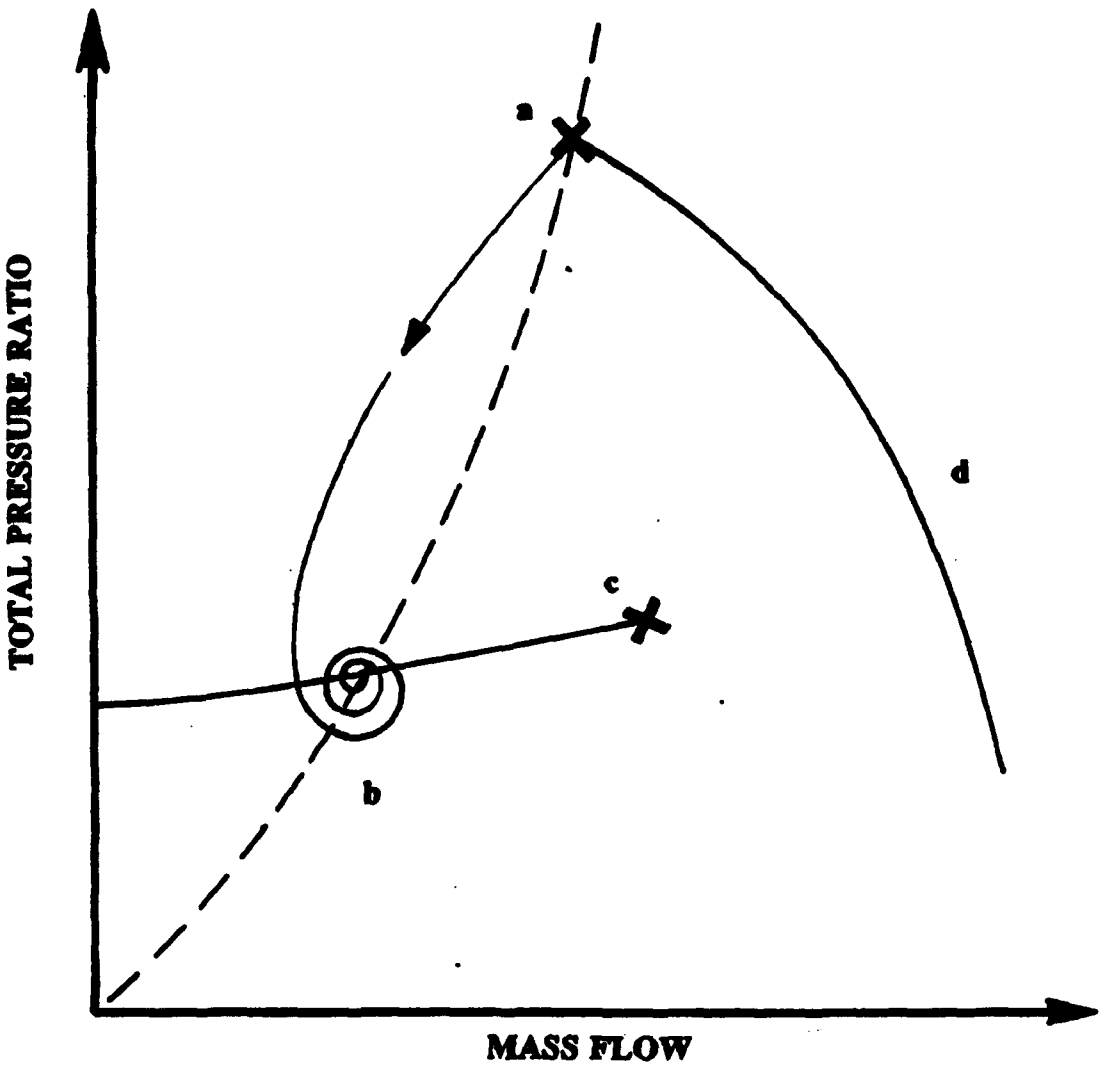

Figure 1.3 Rotating stall

mass flow fluctuations which tend to be cyclic in nature. During surge, compressor operation follows a cyclic path similar to that shown in Figures 1.4 and 1.5. Mass flow can drop significantly (Figure 1.4) or even reverse (Figure 1.5). Because of its low frequency and rhythmic behavior, compressor surge that occurs in an aircraft engine is often referred to as "banging." Indeed, surge can be a very violent occurrence, causing structural damage to the engine as well as reducing performance.

Unlike rotating stall, which is quasi-steady, surge is an unsteady phenomena. Surge tends to occur at higher speeds than rotating stall in multistage compressors. Further, the frequency of the surge cycles tends to be an order of magnitude lower than the rotational frequency associated with rotating stall.

Recoverability

Another important difference between surge and rotating stall is the ability of the compressor to recover from each. Experiments have shown that in many compressors, including the ten stage rig [2], surge is much easier to recover from than rotating stall. If the cause of the instability is removed, a machine that is experiencing surge will almost immediately shift back to steady, unstalled operation. This is not the case for rotating stall, where removing the cause of the initial instability is often insufficient to shift the compressor back into unstalled operation.

On the compressor characteristic shown in Figure 1.3, note that the operating path followed by the compressor as it enters rotating stall never crosses the unstalled characteristic. However in Figure 1.4, as the compressor surges, the operating path crosses the unstalled characteristic every cycle. It is because of this that the compressor

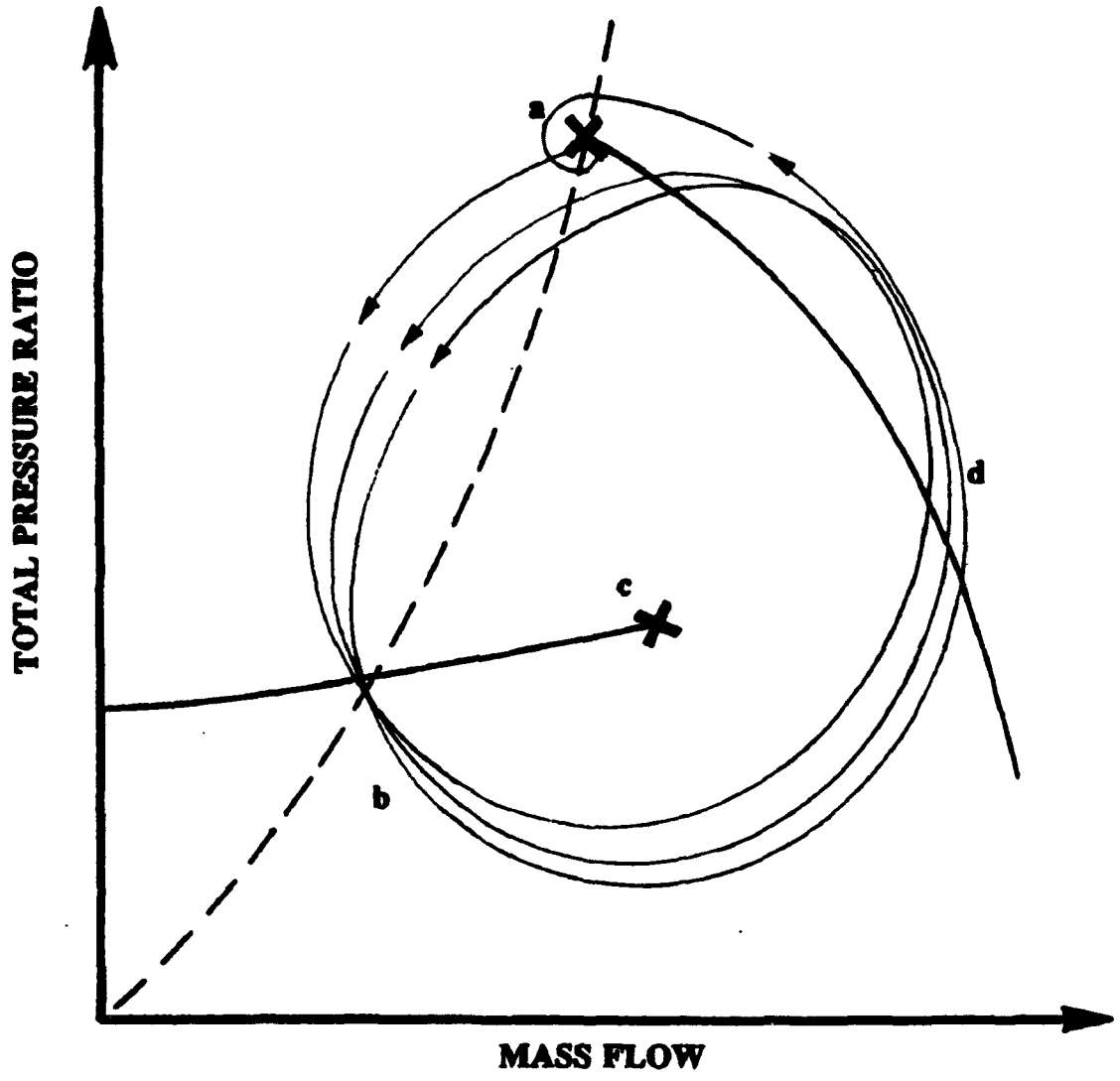

Figure 1.4 Surge

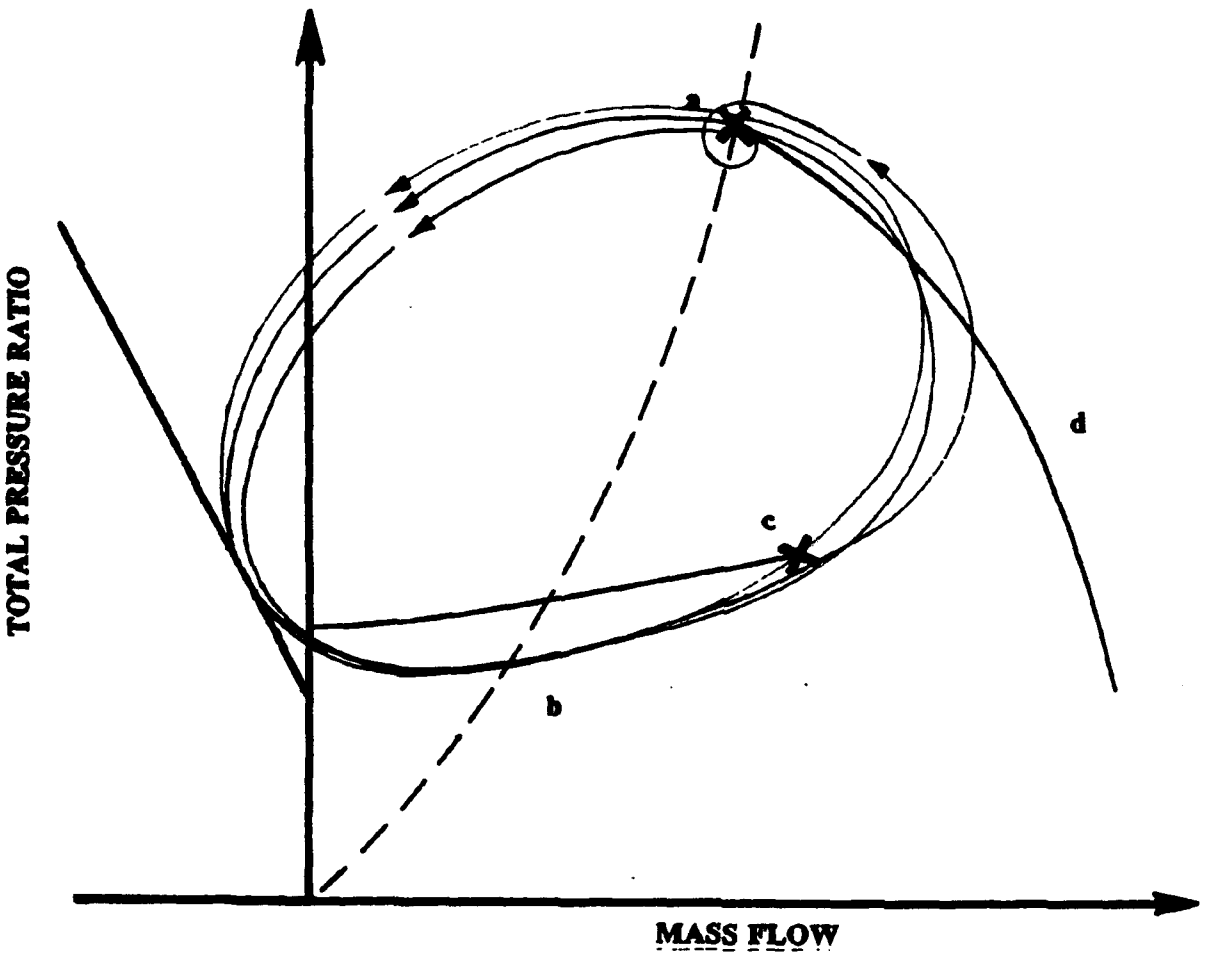

Figure 1.5 Surge, reverse flow

can more easily recover from surge than from rotating stall. When the cause of the surge is removed, the operation of the compressor continues to follow the surge operating path until it crosses the unstalled characteristic. Since the initiating disturbance no longer exists, the compressor recovers and begins operating on the unstalled characteristic once it crosses the characteristic.

The rotating stall operating path never crosses the unstalled characteristic, so the compressor must recover by different means. Usually, this is accomplished by somehow increasing the mass flow so that the compressor operating point is pushed past c, the near-recovery point. Recovery can also occur by reducing rotor speed and restarting the compressor. These sort of drastic corrective measures are even more necessary if the phenomenon known as *hysteresis* is present. In Figures 1.3 through 1.5, the stalled characteristic is seen to actually pass under and overlap the unstalled characteristic. This means that in the overlap region, there are two possible operating points for a given mass flow. This overlap is one symptom of hysteresis. As previously mentioned, one way of recovering from rotating stall is to increase the mass flow. By doing so, the compressor is forced off the stalled characteristic and onto the unstalled characteristic. If the compressor exhibits hysteresis, the operating point will remain on the stalled characteristic past point a in the figures, which means the mass flow must be increased even more than it was just before it stalled. Hysteresis associated with the ten-stage rig is discussed in greater detail by Copenhaver [2,3]. Suffice to say, surge is a more desirable condition than rotating stall from a recoverability point of view.

2.0 REVIEW OF LITERATURE

This section briefly describes some of the highlights of past research into compressor surge. The first two subsections discuss work concerning the surge/rotating stall boundary and compressor modeling work related to surge. The last subsection does not specifically concern surge, but covers research that was done using data from the same ten-stage compressor described in this report. Reviewing previous research on this compressor is important since this report is closely related to most of that work.

2.1 The Surge/Rotating Stall Boundary

Surge has been recognized as a problem in turbo-compression systems since the beginning of jet engine development. Among the more important studies done on this phenomenon was one conducted by Emmons, Pearson, and Grant [1]. Emmons, et al. investigated the relationship between compressor surge behavior and the Helmholtz resonance of the compression system. A model created to verify this theory predicted surge behavior similar to experimental results, with predicted surge frequencies of the same order of magnitude as those actually observed. Furthermore, Emmons, et al. documented the speed boundary between surge and rotating stall (the surge/rotating stall boundary), and characterized both as related but different phenomena.

The surge/rotating stall speed boundary was further explored by Greitzer [4,5] using data obtained from a three-stage, low-speed compressor rig. Greitzer developed a

nonlinear, lumped-parameter model to predict transient compressor response and used data from the three-stage rig to verify the model estimates. Figure 2.1 is a representation of the model, which used actuator disks in constant area pipes to simulate the behavior of the compressor and throttle. Since it was impossible to mathematically predict compressor pressure rise as a function of mass flow, the unstalled, stalled, and reverse flow pressure characteristics of the compressor had to be provided from experimental data. Similarly, the time lag between the onset of compressor instability and the establishment of fully developed rotating stall could not be explicitly calculated. Therefore, the time lag was estimated from the number of rotor revolutions that occurred between initial compressor instability and the development of quasi-steady rotating stall. This estimated lag was then used with a simple first order transient response model to simulate the time lag in compressor response.

While studying the surge/rotating stall boundary with the model and compressor data, Greitzer found that the location of the boundary depended heavily on the ratio of pressure forces to inertial forces in the compression system. This ratio, labeled B, comes from the equation:

$$B = \frac{U}{2a}\sqrt{\frac{V_p}{(A_c L_c)}}$$

which resulted from nondimensionalizing the governing equations. This "B parameter" is also related to the Helmholtz resonator frequency of the plenum volume, which was deliberately incorporated into the model. The model predicted that the compression system would exhibit surge for higher values of B, but would go into rotating

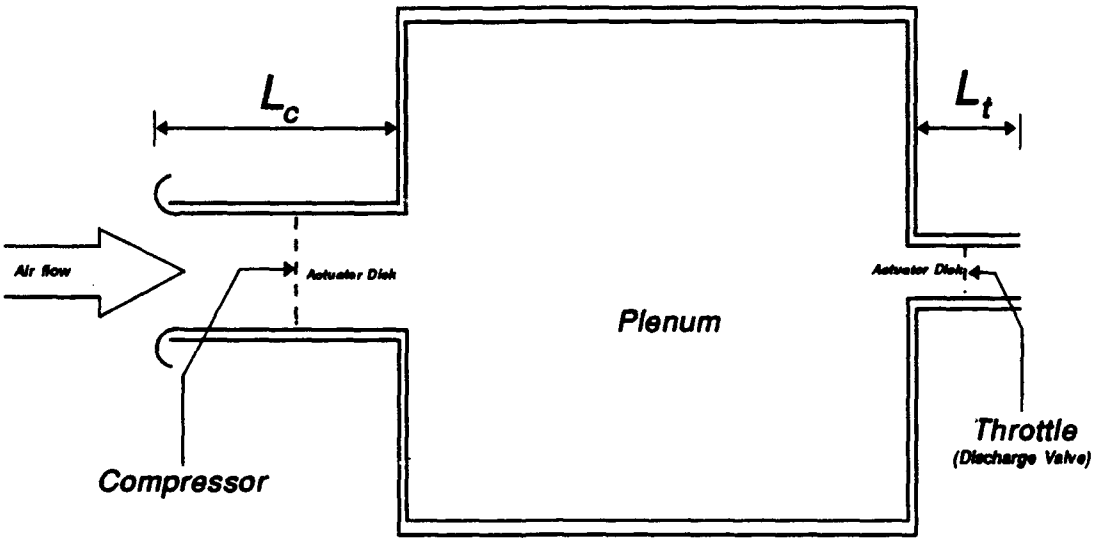

Figure 2.1 Greitzer's compressor model

stall for lower values. The data from the three-stage rig agreed well with the model predictions.

Small and Lewis [6] used Greitzer's model to estimate the instability behavior of their three-stage high-speed compressor rig. Using the B parameter, they attempted to shift the surge/rotating stall boundary in such a way that the compressor would stall at 100% speed with nominal IGV settings. They did this by altering the exit plenum volume in the compressor. The equation defining the B parameter shows a significant relationship between the exit plenum volume and the surge/rotating stall boundary. However, they found that the surge/rotating stall boundary shifted only slightly (a few percent) as the exit plenum volume was varied.

Hosny, Steenken, and others [7,8] also used the B parameter to shift the surge/ rotating stall boundary in the ten-stage, high-speed Energy Efficient Engine (E^3) core compressor. Earlier builds of this compressor exhibited rotating stall at speeds below 60%, but the researchers wanted to observe such stall behavior at higher speeds. Using the equation for the B parameter as a guide, they lowered the volume of the exit plenum in an attempt to raise the compressor speed defining the surge/rotating stall boundary. As expected, the boundary did shift to a higher speed, but it did not precisely follow B parameter equation. A plot produced in one the reports by Hosny and Steenken [8] showed that the surge/rotating stall boundary did not shift as much as the equation estimated it should have.

The work performed by Small et al. and Hosny et al. demonstrated that while the B parameter estimated the surge/rotating stall boundary behavior of low-speed compressors

(such as Greitzer's rig) rather well, it did not do so well in estimating such behavior in high-speed compressors. In an attempt to remedy this, Moore and Greitzer [9,10] developed a nonlinear, third-order, lumped-parameter compressor model which allowed for the simultaneous occurrence of surge and rotating stall. They showed that the length-to-diameter ratio of the compressor, in conjunction with the B parameter, was necessary to predict high-speed compressor behavior. This is important in multistage designs which tend to operate at high speeds and have increased compressor lengths.

2.2 Stage-by-Stage Compressor Model

While Moore and Greitzer were working with their lumped parameter model, Sugiyama [11] was also attempting to model instabilities in multistage, high-speed compression systems. Sugiyama's model was a stage-by-stage engine model which predicted instability behavior in an entire engine using individual stage characteristics instead of an overall compressor characteristic. Sugiyama's model was limited to short time periods (about 80 milliseconds) and had some instability problems, but was in general an excellent early attempt.

Later, Davis [12] developed an improved one-dimensional, stage-by-stage dynamic compressor model. Davis' model was a clear improvement over Sugiyama's model in that it allowed for longer simulation times and had a more stable numerical solver. Furthermore, the Davis model could simulate recovery from surge and rotating stall. Since the Davis model was limited to modeling the compressor rather than the entire engine, the results of the model could be compared to available compressor test data.

Davis validated the model by comparing the model estimates to three-stage compressor data provided by Greitzer and Moore [5],[10] and to ten-stage data provided by Hosny et al. [7,8]. Unfortunately, detailed characteristics for individual stages in the E^3 compressor were not available. Therefore, Davis synthesized characteristics for a nine-stage compressor using a stage-stacking model for the unstalled characteristics and estimations based on low-speed compressor data he had available for the stalled characteristics. The model predictions compared well with the E^3 data qualitatively, but quantitative comparison was not possible.

2.3 Ten-Stage Compressor Research

In addition to this report, a great deal of previous research has been done using data from this ten-stage compressor test. The first major research effort based on this compressor data was an Air Force technical report by Copenhaver [2] published in 1990. Besides describing the general behavior of the compressor during instability, Copenhaver developed the stall and unstalled compressor stage characteristics that are still being used in other research efforts. Copenhaver also validated the stage-by-stage model developed by Davis [12] using the 10-stage data.

In-stall hysteresis, which is the mass flow required to move from the initial in-stall operating point to the near-recovery point, was investigated by Copenhaver and Okiishi [3]. This compressor possessed an unusually large degree of in-stall hysteresis, which was related to the stalling problems associated with the engine from which this compressor design was based. Choking in the rear stages of the compressor was theorized to be one cause of this large degree of hysteresis.

Later, Boyer and O'Brien [14] used the compressor characteristics compiled by Copenhaver [2] to further explore the hysteresis and recoverability of this compressor. To this end, they used the Davis model [12] to simulate compressor stall and recovery. Using simulated interstage bleeds and increases in flow path area to relieve rear-stage choking, they determined that the recoverability of the compressor seemed to depend on the location of the bleed flow. Their efforts also further validated Davis' stage-by-stage model.

Gorrell [15] built on Copenhaver's work by continuing to explore the rotating stall

behavior of this compressor. By reviewing the discharge plenum data, Gorrell was able to determine the annular extent of the rotating stall cells. Significant transition regions and even areas of reversed flow were evident in those stall cells. More recently, Bloch [16] used the ten-stage data to verify a stage characteristic prediction method. This method used blade angles and flow geometry to predict the stage characteristics of a given compressor. The results of this method, as applied to the ten-stage compressor, were promising.

3.0 TEST COMPRESSOR DESCRIPTION

The data presented in this paper were obtained from a compressor test carried out at the Compressor Research Facility (CRF) at Wright Patterson AFB, Ohio. The test compressor design was based on a 10-stage axial-flow compressor core from a modern aircraft gas turbine engine. This compressor had a design pressure ratio of 8.3, a design corrected speed of 10913 rpm, and a design corrected mass flow of 24.69 kg/sec (54.44 lb/sec).

The compression system in the actual aircraft engine consisted of both a 3-stage low-pressure fan and a 10-stage high-pressure compressor along with the necessary ducting. The test compression section built from the engine did not include the fan, but it did include the inlet case section, the high-pressure compressor, the diffuser, and part of the combustor section. This test compression section is shown in Figure 3.1.

Inlet and discharge sections were designed and built so that the test compression section could be incorporated into the CRF test cell. The resulting test compressor is shown in Figure 3.2. While the bypass flow that occurs in the actual engine was not simulated, the flow path was designed to simulate air flow through the actual engine as much as possible. At the same time, the ability to vary both the flow path and the compressor geometry was made a requirement. To this end, the inlet guide vanes and the stators in the first two stages could be moved independently to provide variable blade stagger angles and thus variable flow conditions. Moreover, provisions for internal and external bleeds from the compressor core were also included in the design. It is noted

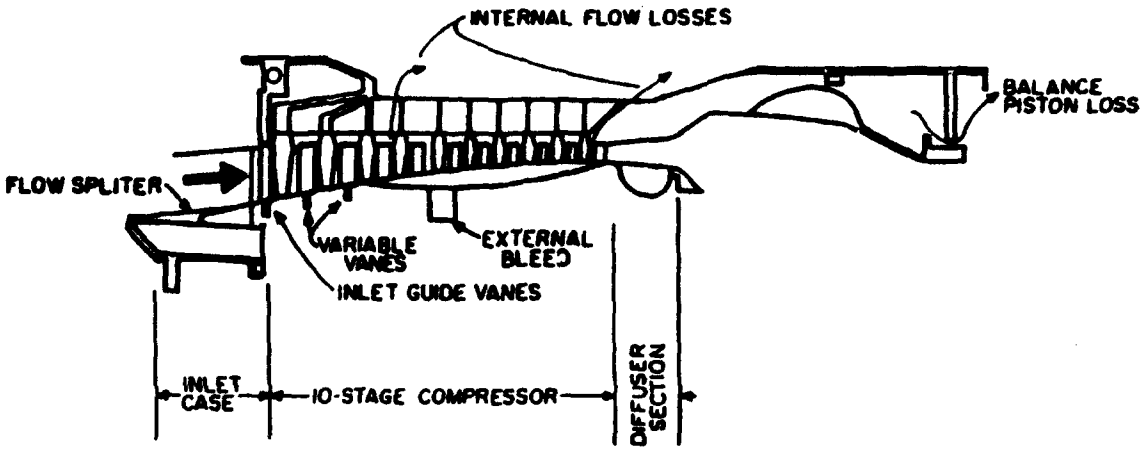

Figure 3.1 Test compressor compression section

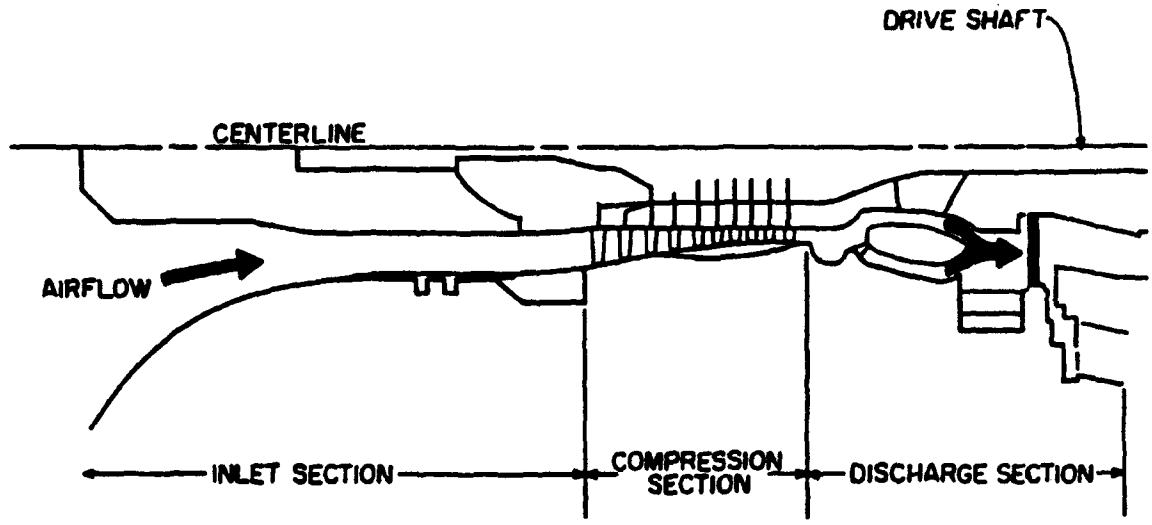

Figure 3.2 CRF 10-stage test compressor diagram

here that data presented in this report were obtained with all vanes and stators held at a constant, nominal angle. Also, the external bleed was closed off and the internal bleed was open in all of the data presented in this report.

The test compressor inlet section is shown in Figure 3.3. The inlet section was designed so that the airflow going into the compression section would be similar to the airflow going into the high-pressure compression section of an actual engine. Preswirl vanes helped simulate airflow angles that occur as a result of the fan in the actual engine.

Actual flow path simulation and variable geometry were also incorporated into the discharge section. Aside from the filler volume and the discharge valve, which simulated the combustor and turbine, respectively, the discharge section included variable volume hardware which allowed for testing at nominal and $\pm$ 20 percent nominal discharge volume. A view of the discharge section is shown in Figure 3.4. Unfortunately, the variable volume hardware made it impossible to simulate actual engine airflow through the discharge section, but this was judged a fair exchange for the ability to change the compressor discharge volume during the test.

Definition of the individual stages in this test compressor was done in a manner that goes against accepted convention. While compressor stages are conventionally defined as a rotor-stator combination, stages in this test compressor were defined as a stator-rotor combination (see Figure 3.5). This was required since instrumentation used to monitor interstage performance was typically mounted on the leading edge of the stator in each stage.

A brief description of the buildings, rooms, computer systems, and drive systems comprising the Compressor Research Facility is included in Appendix A.

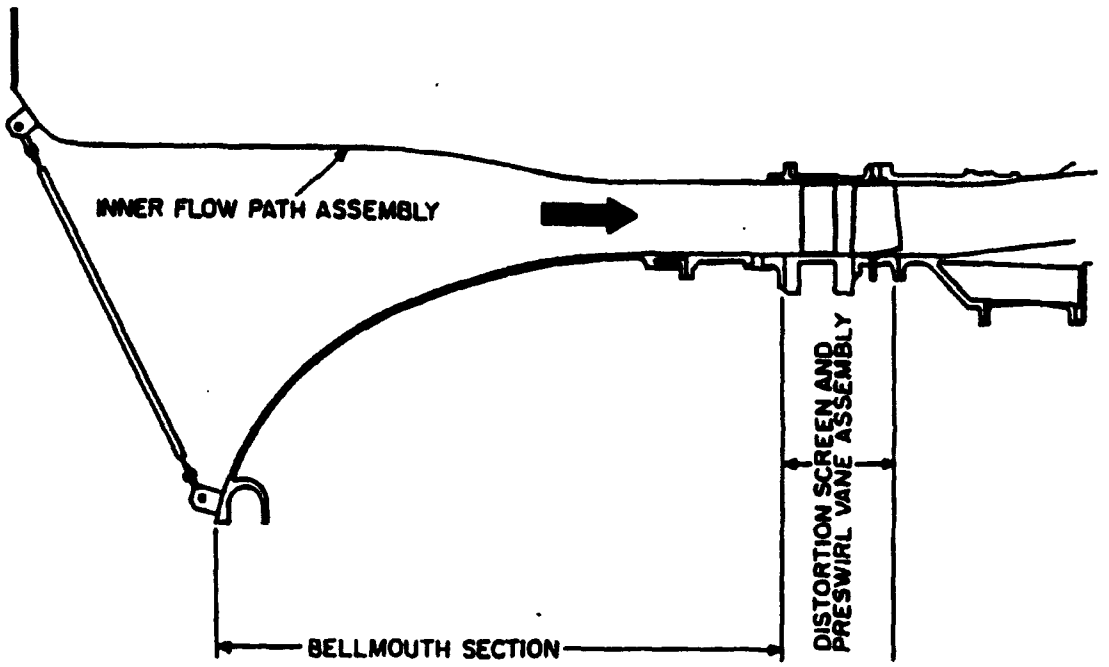

Figure 3.3 Test compressor inlet section

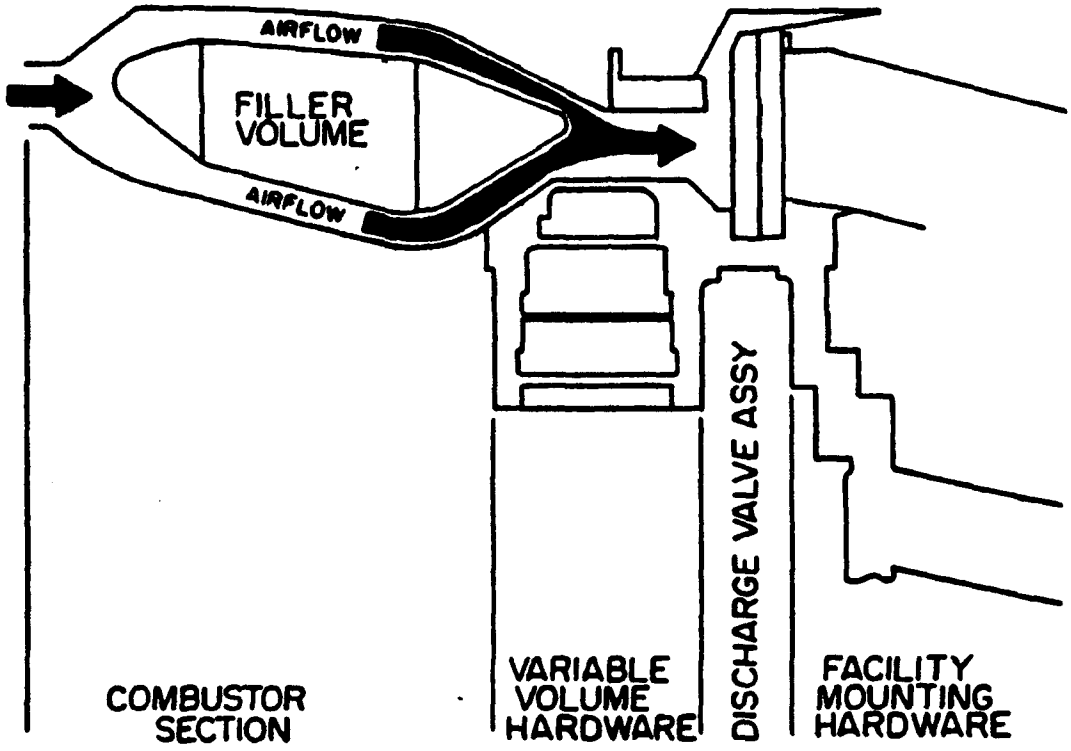

Figure 3.4 Test compressor discharge section

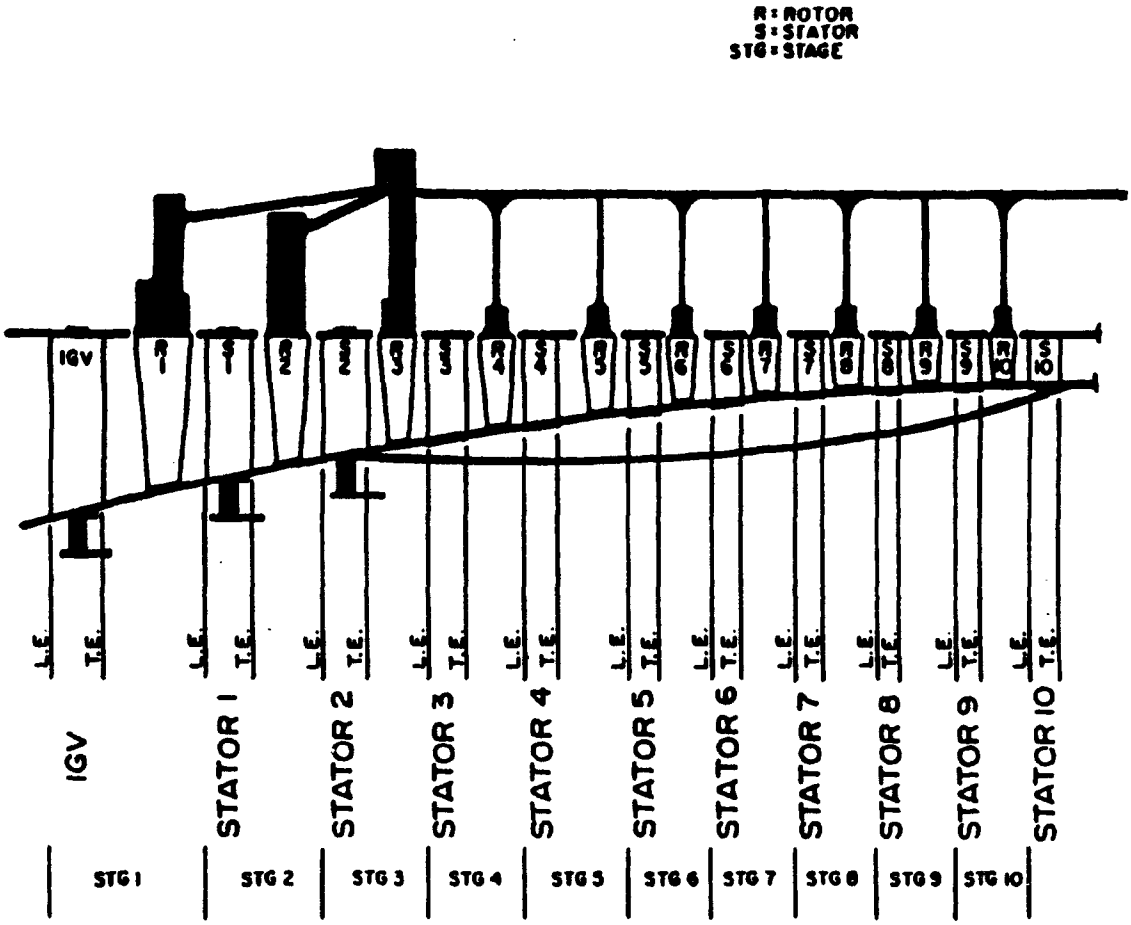

Figure 3.5 Test compressor stage definition and blade locations

4.0 COMPRESSOR INSTRUMENTATION

In order to document compressor performance and behavior, the test compressor was thoroughly instrumented to provide pressures, temperatures, and other performance values during testing. Much of this instrumentation and the data associated with it was not used in this report. Therefore, this section will deal only with the instrumentation used to provide data for this report. A more thorough explanation of the data acquisition methods used during the test is presented in Appendix B. A more detailed discussion of all instrumentation is provided by Copenhaver [2] and Copenhaver and Worland [17].

4.1 High-Response Pressure Measurements

During the compressor test, the data acquisition system was required to accurately record pressure fluctuations of 50 Hz or less. This requirement was set down so that rotating stall events, with fundamental frequencies of around 50 Hz, could be documented. To this end, high-response pressure measurements were acquired with frequency responses of 200 Hz. This was adequate to document the rotating stall events. The surge events presented in this report occurred at frequencies near 5 Hz, so the 200-Hz frequency response of the high-response data adequately documented the surge events as well.

Transient pressure data were obtained from six pressure transducers comprising four individual probes located in the compressor. Three of these probes were forward and aft facing pressure probes called Mach probes. The other remaining probe, which was

actually a simple pressure tap, measured static pressure. These four probes provided all of the transient pressure data presented in this report.

Sketches the two types of Mach probes used in the test are shown in Figures 4.1 and 4.2. Each Mach probe consisted of at least two impact tubes and one thermocouple. High-response pressure measurements were obtained through the impact tubes by pressure transducers located on the outside of the compressor case. Forward-facing and rearward-facing measurements were obtained through the angled impact tubes. The angle of the impact tubes allowed the dynamic (velocity) pressure component of the airflow to be monitored. Thus, the Mach probes were configured to measure the total pressure of the air at the measurement location. The value of having forward-facing and rearward-facing total pressure measurements will be demonstrated later in this report. A sketch of a static pressure "probe" is shown in Figure 4.3. As was the case with the Mach probes, pressure measurements were obtained through a tube by a high-response transducer located outside the compressor case. However, the tube used here was not angled as those on the Mach probes were, but was angled perpendicular to the air flow. In this way, only the static pressure was measured.

The positioning of the four probes in the test compressor is shown in Figure 4.4. Further, some important characteristics of each probe are listed in Table 4.1. Of the seven high-response pressure transducer outputs available from the four probes, only six were used. The rear-facing pressure measurements taken from the inlet Mach probe were found to be erroneous, so data provided by that transducer were not used. All high-response data were stored on analog tape during the compressor test for future recovery.

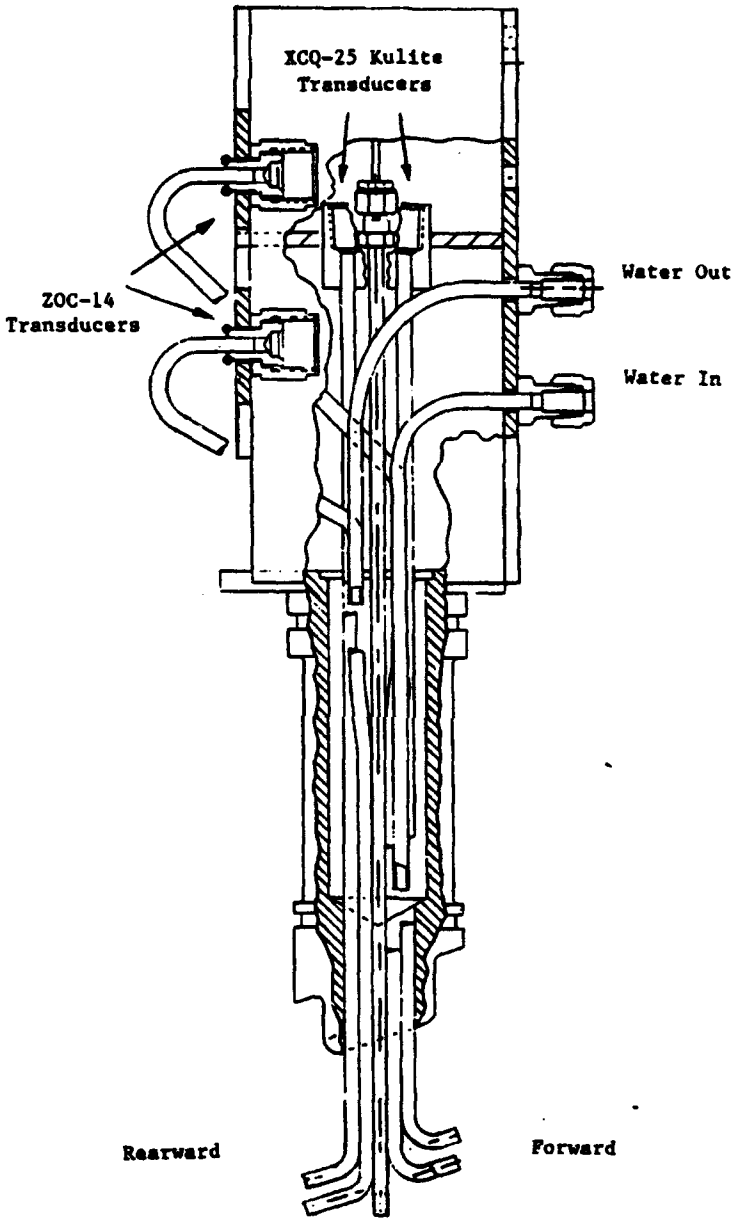

Figure 4.1 Inlet Mach probe

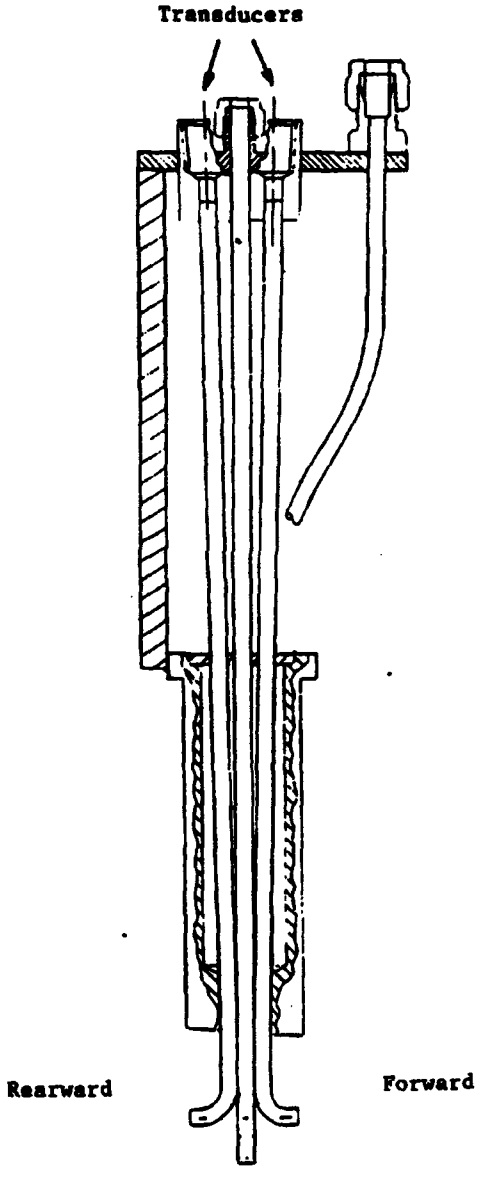

Figure 4.2 Discharge Mach probe

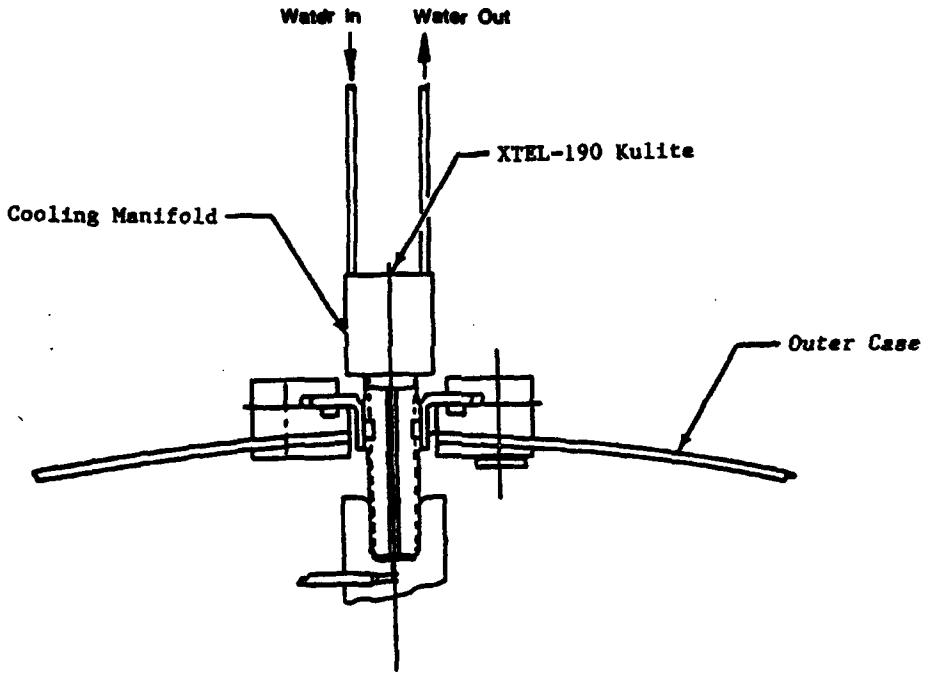

Figure 4.3 Static pressure probe

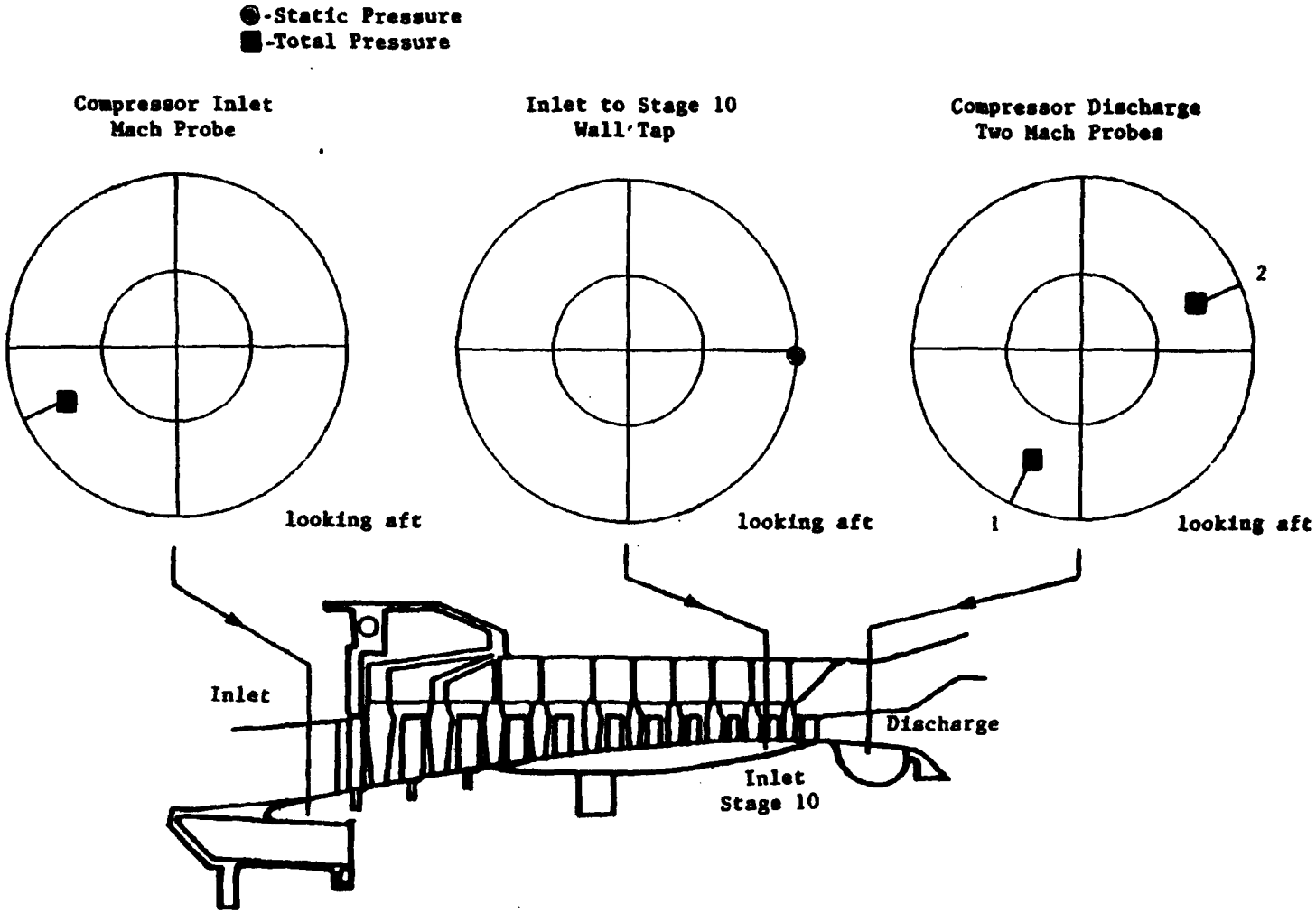

Figure 4.4 High-response pressure probe locations

Table 4.1 High-response Pressure Transducers

Pressure Transducer	Location/Probe	Transducer Type	Pressure Range
Number 1 Total Press.	Comp. Inlet, Forward-Facing Mach Probe	Kulite Model# XCQ-25	172 kPa (25 psi)
Number 2 Static Press.	Stg. 10 Inlet, O.D. Wall Tap	Kulite Model# XTEL-190	690 kPa (100 psi)
Number 3 Total Press.	Comp.Discharge Forward-Facing Mach Probe	Kulite Model# XCQ-150	1030 kPa (150 psi)
Number 4 Total Press.	Comp.Discharge Rearwd-Facing Mach Probe	Kulite Model# XCQ-150	1030 kPa (150 psi)
Number 5 Total Press.	Comp.Discharge Forward-Facing Mach Probe	Kulite Model# XCQ-150	1030 kPa (150 psi)
Number 6 Total Press.	Comp.Discharge Rearwd-Facing Mach Probe	Kulite Model# XCQ-150	1030 kPa (150 psi)

4.2 Time-averaged Measurements

Accurate steady-state measurements were required during the compressor test in order to facilitate several goals of the test program. One of these goals was the voltage-to-engineering unit conversion of the high-response transducer measurements, discussed in detail in Section 5 of this report. Time-averaged data acquisition was used to obtain the steady-state measurements needed to achieve these goals. The measurement uncertainty of the time-averaged data was much improved over the high-response data uncertainty because of the very accurate calibration standards used and the large number of samples that were averaged to make each measurement (see Appendix B). Time-averaged data acquisition was used to obtain the steady-state measurements because of the lesser degree of data uncertainty associated with it.

Sixty-nine pressure probes and thirty total temperature probes were used to collect the time-averaged data used in this report. All of these were placed at either the compressor inlet, the stage 10 inlet, or near the two discharge locations. Figures 4.5 and 4.6 show the time-averaged pressure and temperature probe locations in the test compressor. The locations of the high-response pressure probes are also shown in these figures for reference and can be related to the probe positions shown in Figure 4.4.

Total pressure and temperature measurements at the compressor inlet and discharge were taken by probes similar to the Mach probes used to obtain the high-response pressure measurements. Drawings of the inlet and discharge probes used by the time-averaged acquisition system are shown in Figure 4.7. These probes allowed simultaneous measurements to be taken at five specific radial positions. Each probe was

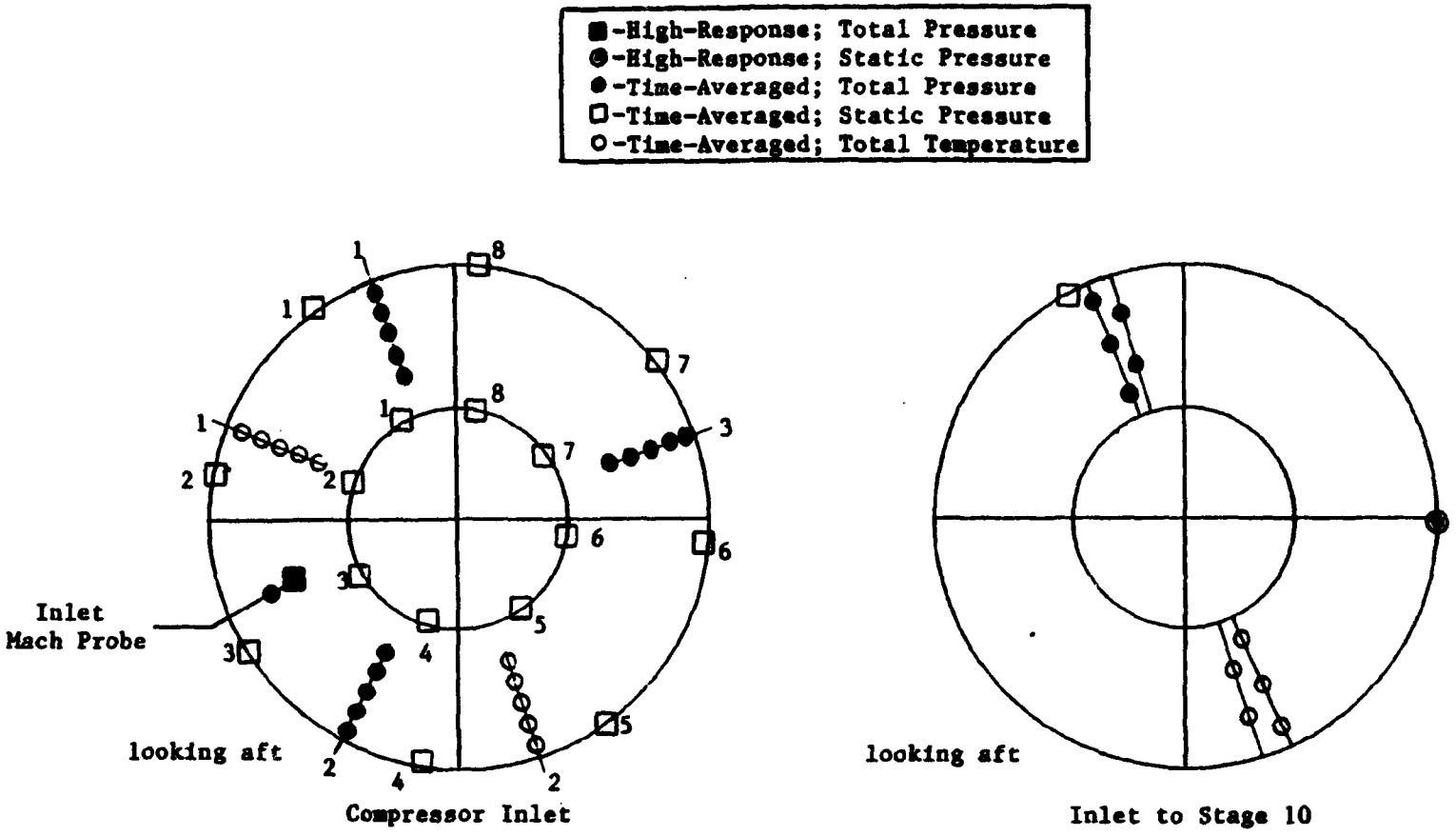

Figure 4.5 Time-averaged instrumentation locations

Figure 4.6 Time-averaged instrumentation locations

positioned on the outer diameter of the compressor case. Although the probe designs were identical, separate probes were used to obtain the total pressure and the total temperature measurements.

Time-averaged total pressure and temperature measurements at the inlet to stage 10 were taken with probes mounted on the leading edge of the ninth stator ring. For each set of radial measurements, two adjacent stators were used to mount the five different probes. Two locations on one stator and three on the other were instrumented for each set of measurements (see Figure 4.5).

The probes used to obtain the time-averaged static pressure measurements were virtually identical at all three measurement stations used in the test compressor. All time-averaged static pressure measurements were taken with probes mounted on the inner and outer diameters of the test compressor flow-path. The time-averaged and high-response static pressure probes have similar configurations, so except for the transducer the schematic drawing shown in Figure 4.3 is representative of both probe types.

One of the time-averaged total pressure measurements was obtained with the inlet Mach probe. The schematic of the inlet Mach probe shown in Figure 4.1 shows the second pair of impact tubes used to obtain two time-averaged total pressure measurements. As with the inlet high-response pressure measurement, only the forward-facing total pressure measurement was used in this report.

All time-averaged pressure measurements were taken with Scanivalve model ZOC-14 (Zero-Operate-Calibrate) pressure transducers. Total temperature measurements were taken with bead type thermocouples constructed from 0.152 mm (0.006 in) diameter

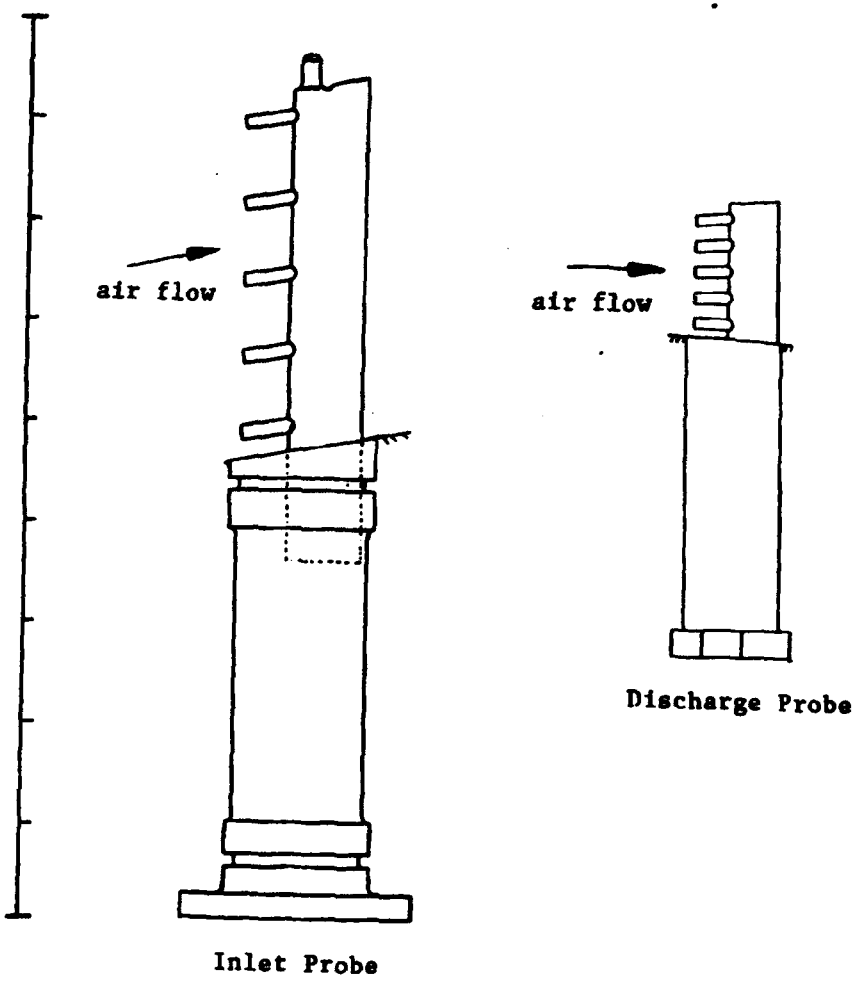

Figure 4.7 Time-averaged total pressure and temperature probe designs

chromel-alumel thermocouple wire. Total pressure measurements were obtained through the impact tubes with the actual transducers mounted on the outside of the compressor case. Total temperature measurements were obtained with the thermocouples placed just inside of the impact tubes on the total temperature probes. All time-averaged data acquisition was limited to a frequency response of 0.5 Hz. Time-averaged data were stored on digital tape for future recovery.

4.3 Other Measurements

Mass flow through the compressor was controlled by the discharge valve located just downstream of the variable volume hardware (see Section 3.0). Monitoring the discharge valve flow area was accomplished by the placement of three potentiometers along the perimeter of the discharge valve. Changes in potentiometer output voltage indicated changes in the position of the discharge valve. By knowing the area of the discharge valve when fully open, the flow area could be estimated based on output voltage. Discharge valve position data were recorded on analog tape with the high-response data.

The compressor flow rate was measured by a calibrated 48.3-cm (19-inch) throat-diameter flow venturi placed approximately 31 meters (25 pipe diameters) downstream of the compressor exit. Only time-averaged data were available from the venturi.

5.0 DATA REDUCTION AND INSTRUMENT CALIBRATION

Most of the data recorded from the 10-stage compressor test were not relevant to this report. For this reason, the first task was to determine which documented events would be of interest. When these were determined, the data recorded during these events were recovered. The high-response data, which were recorded on analog tape in the form of measured voltages, were of primary interest. To use the data, each recorded data set had to be digitized and calibrated. This process of data recovery, reduction, and calibration is described in the following three subsections.

5.1 Data Recovery

This report was limited to the presentation and discussion of compressor surge phenomena. Therefore, only surge events were of interest. During the 10-stage test, at least 24 instances of surge were observed (see Table 5.1). Of these, data were available for 22. Many of these surges occurred when the flow path geometry was off nominal, such as different stator or inlet guide vane angles. These were ignored since the effects of variable flow path geometry on surge behavior were not the subject of this report. After removing these from consideration, there remained 13 documented and recorded surge events at a variety of speeds and plenum volumes. One other surge event not

included in the table was too short to be considered useful and was not recovered[1]. Therefore, the final result was 12 useful and recoverable surge events. All of these occurred at either 81, 82 or 87 percent corrected speed.

[1] This event was interesting because it began as a surge but after one cycle ended up in rotating stall. In the past, this author has noted similar behavior in a different compressor, where the discharge valve was closed far enough to drive the compressor past surge and into rotating stall. It is possible that discharge valve closure during the 10-stage test caused the surge-rotating stall transition in the same way.

5.2 Data Reduction

High-response data for the 12 surge events were recorded by an FM tape recorder in analog form. In order to use this data on computer for both analytical and plotting purposes, it was necessary to convert the analog data into digital form. This was accomplished with the analog tape digitizing system (ATDS) built at the CRF.

The heart of the ATDS was the Masscomp 555/02 computer system. The computer controlled or communicated with all of the subsidiary hardware, including the analog tape player and anti-aliasing filters. The actual analog-to-digital conversion was performed by the computer as well. Once digitized, all data were written to computer hard disk for storage.

Conversion of data from analog to digital form requires some knowledge of the transient nature of the data. If there are pertinent high frequency components in the data, the sample rate during the conversion must be high enough to resolve them. However, high sample rates create large amounts of data which can quickly fill all available computer memory. Somewhere between these two requirements is an optimal sample rate.

Generally, it is desirable to have at least four sample points over one period or cycle. For example, if the frequency to be resolved is one cycle per second (1 Hertz), the digitization sample rate should be at least four samples per second. It was decided that 200 Hz would be the maximum frequency of interest in the high-response data, so a sample rate of 1000 samples per second was used. This provided a minimum of five samples per cycle at 200 Hz.

Once the sample rate was chosen, an anti-aliasing cut-off frequency had to be determined. Aliasing occurs when high frequency components in the raw analog data are digitized and appear in the digitized data as low frequency components. Aliasing is a pitfall of any digitization process, and is avoided only by using a sample rate at least twice as great as the highest expected frequency component. This is called the Nyquist rate. By filtering out any frequency components higher than one-half the sample rate, aliasing is avoided.

Under ideal circumstances an anti-aliasing cut-off frequency of 500 Hz would seem appropriate in this case. However, the nonlinear behavior of the low-pass filters used to remove the higher frequency components required deeper consideration. The low-pass filters used by the ATDS attenuate frequency components higher than the cut-off frequency but do not completely remove them. If a cut-off frequency of 500 Hz had been used, the filters would have allowed frequency components slightly higher than 500 Hz to pass. This would have caused aliasing. Therefore, a cut-off frequency of 400 Hz was used since this guaranteed a significant reduction in the signal strength of frequency components higher than 500 Hz.

Finally, 1 of the 12 analog data sets was digitized again at a higher sample rate. This "super digitized" set was produced to provide more data points for Fourier transform analysis of the rotating stall phenomena observed in the data after initial review. This data set was digitized using a sample rate of 10,000 samples per second. All other parameters were unchanged. A summary of the digitization parameters is given in Table 5.2.

Table 5.1 Observed and Usable Surge Events

Volume	Total Number of Surge Events	Minus Surge Events with no data	Minus Surge Events w/stator angle change	Minus Surge Events w/IGV angle change	Minus Surge Events w/dist. screen remvd.	Minus Surge Events w/bleed on	Total Number of Usable Surge Events
80% Nominal	9	9	5	3	3	3	3
Nominal	14	12	12	12	10	8	8
120% Nominal	1	1	1	1	1	1	1

Table 5.2 Digitization Parameters

Digitization Parameters	All Twelve Surge Events	One Surge Event
Sample Rate	1000 $^{samples}/_{sec}$	10000 $^{samples}/_{sec}$
Maximum Frequency of Interest	200 Hz	200 Hz
Anti-Aliasing Frequency	400 Hz	400 Hz

5.3 Calibration

Before the high-response instrumentation was installed in the test compressor, bench calibrations were performed on all the high-response transducers. The original intention was to use this calibration data to convert the output voltages into engineering units after the test. However, day-to-day observations demonstrated that the transducer output voltages changed under the same known pressures over several weeks. This voltage drift made the bench calibrations less accurate. After reviewing similar data from this test, Gorrell [15] found that drifts of approximately 7 kPa (~1 psi) for the total pressures and 2 kPa (0.3 psi) for the static pressures had occurred. Because of this voltage drift phenomenon, calibration of the high-response data was accomplished by using time-averaged data. Bias errors associated with the total and static steady-state, time-averaged measurements were approximately ± 3.5 kPa (~0.5 psi), which were smaller than the errors associated with the voltage drift.

During steady-state compressor operation, high-response and time-averaged measurements were taken periodically and simultaneously to establish steady-state operating points. At these points, both time-averaged engineering unit measurements and high-response voltage measurements were recorded. If a specific time-averaged instrument was in the same immediate location as a high-response instrument measuring the same property, the two instrument readings could be related. This is what was done to calibrate the high-response data.

High-response data taken in the compressor discharge could not be identically matched to time-averaged data since the related time-averaged instrumentation was 2.5

cm (~1 in) upstream of the high-response instrumentation. It was necessary in this case to estimate the conditions at the high-response instrumentation location based on the time-averaged measurements and some sort of flow model. Isentropic flow was assumed between the two locations, since it was a bladeless duct with a small area change, and the static conditions 2.5 cm downstream of the time-averaged instrumentation were estimated assuming isentropic expansion. Total pressure was unchanged (isentropic) between the two locations.

Time-averaged and high-response data taken on the same day as the occurrence of specific surge events were found and chosen as calibration points. The high-response voltage data were digitized at 1000 samples per second for 500 milliseconds. This produced 500 high-response voltage measurements which were averaged to determine a mean voltage. Maintaining a 95% confidence interval for the mean, the worst case difference between the upper and lower confidence limits was 3.5 kPa (~0.5 psi). Generally, the difference was on the order of 0.7 kPa (~0.1 psi).

Linear fits using the method of least squares were calculated using the averaged high-response measurements and the time-averaged data to determine calibration equations. Usually, three or four time-averaged/high-response data point pairs were obtained for the process, and the resulting equations came very close to matching these points. Each set of equations included calibration data for seven different high-response measurements.

Several of the 12 surge events occurred on the same days, which allowed one set of calibration equations to be used for more than one surge event. Each of the 12 surge events occurred on one of 5 test days. Furthermore, the voltage drift of the high-response

instruments used did not exceed 0.5% over any particular day. Therefore, precision was only minimally affected if the same calibration data were used to calibrate two or more different sets of surge data which occurred on the same day. A total of 5 sets of calibration equations were used to calibrate all 12 surge events.

The calibration equations were also effected by precision errors associated with the time-averaged and high-response data. An example of this effect is shown in Figure 5.1. In this figure, calibration lines using the worst case precision errors are plotted to form a calibration error band. The nominal calibration line was used to calibrate voltage data from probe number three on the second of the five test days. This is one of the worst cases out of all the calibration data used in this report. In this particular case, errors on the order of 4 kPa (~0.6 psi) were possible. In general, most measurement errors were smaller than this. For a more complete discussion of the precision and uncertainty calculations associated with the measurements, the reader is referred to Appendix B.

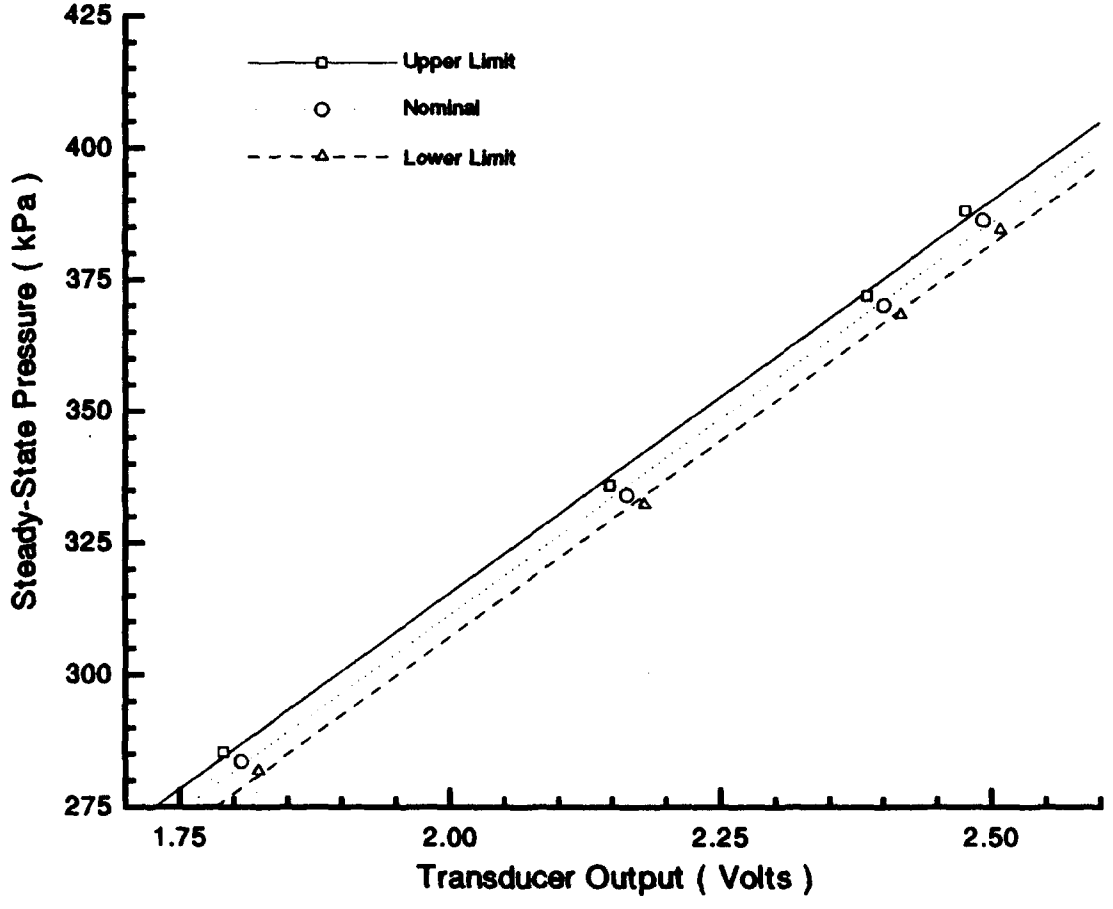

Figure 5.1 Example calibration error band

6.0 Data Analysis

The calibrated surge data are presented in this section. Table 6.1 lists the 12 surge events and some of their basic characteristics. The 7 sets of time resolved data were plotted for each of the 12 surge events. A complete compilation of these plots is given in Appendix C. One of the most important observations made concerning this data is the apparent lack of a relationship between the surge/rotating stall boundary and the plenum volume. The possible reasons for this lack of a relationship are as yet unclear. The surge/rotating stall boundary is the subject of an investigation detailed in Section 6.2.

6.1 Overview

A single cycle from 1 of the 12 documented surges is shown in Figure 6.1. It was apparent from this figure that the general nature of surge in this compressor was typical of surge behavior observed in other compressors. An instability brought on by some irregularity in normal operation of the compressor resulted in the break-down of compressor ability to maintain a pressure rise. This break-down caused a rapid depressurization of the discharge plenum immediately upstream of the compressor. The compressor pressure ratio fell until the compressor was able to recover. At the point of recovery, the compressor began to repressurize the plenum until the pressure reached an amount nearly equal to the original value before the plenum depressurized. Unless the cause of the instability was removed, the plenum depressurized again. This cycle of depressurization, often called blowdown, followed by repressurization repeated itself until

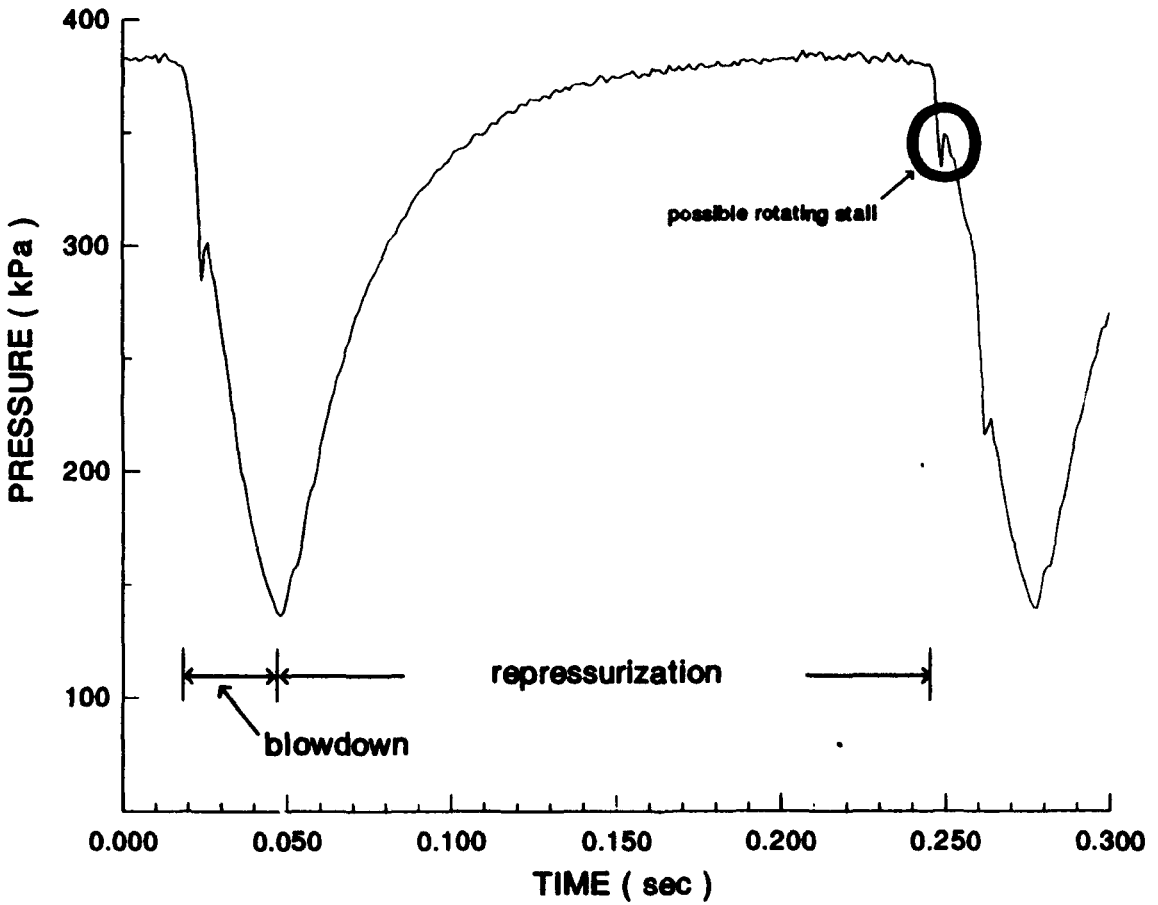

Figure 6.1 Typical surge cycle

the cause of the instability was removed. In Figure 6.1, the rapid blowdown of the discharge plenum followed by a slower repressurization period is clearly evident.

When the forward-facing and rearward-facing pressure probe data from the discharge were compared, it became apparent that flow reversal had occurred for brief periods during surge. Figure 6.2 shows forward and rearward pressure data from a discharge Mach probe during surge. The dynamic pressure component was perceived only by the forward-facing probe during steady-state operation, so the forward-facing probe normally measured total pressure and the rearward-facing probe normally represented static pressure. This is shown in Figure 6.2, where the higher total pressure (forward-facing) is plotted with the lower static pressure (rearward-facing) just before the first blowdown. However, for brief instances during surge, the rearward-facing probe measured a higher pressure than the forward-facing one, as the figure shows. During these periods, the total pressure was measured by the rearward-facing probe and the static pressure by the forward-facing one because the dynamic pressure component was briefly being perceived by the rearward-facing probe. This indicated flow reversal.

Given the static and total pressure, it is possible to estimate the flow Mach number at the discharge probe location. In Figure 6.3, the flow Mach number based on the average forward and rearward pressure measurements in the discharge during surge (81% speed, 100% volume) is shown. The negative Mach numbers indicate reverse flow. Although not shown, the pressure data from the other four surge events at the same speed and volume provided for Mach numbers of similar magnitude. The other seven sets of surge event data also showed evidence of reverse flow, so the fact that flow reversal

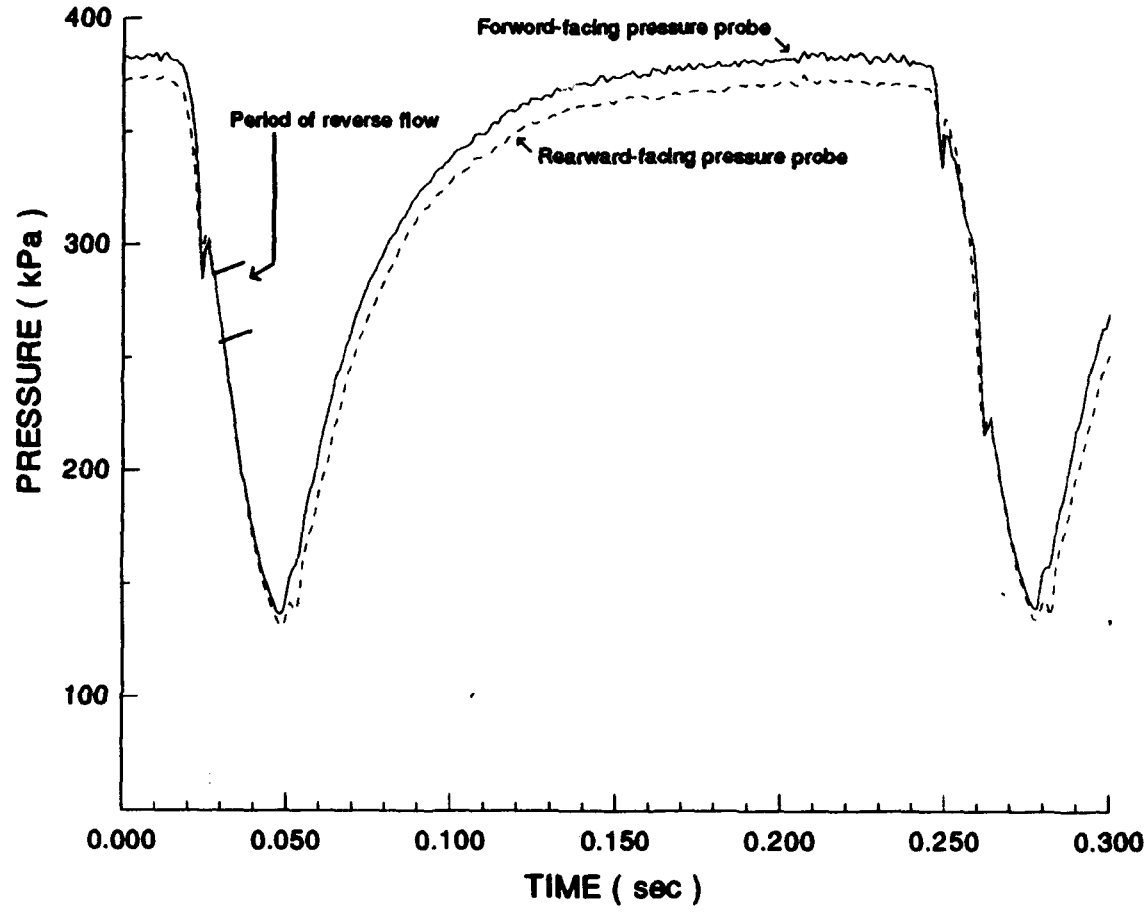

Figure 6.2 Forward-facing and aft-facing probe pressure measurements

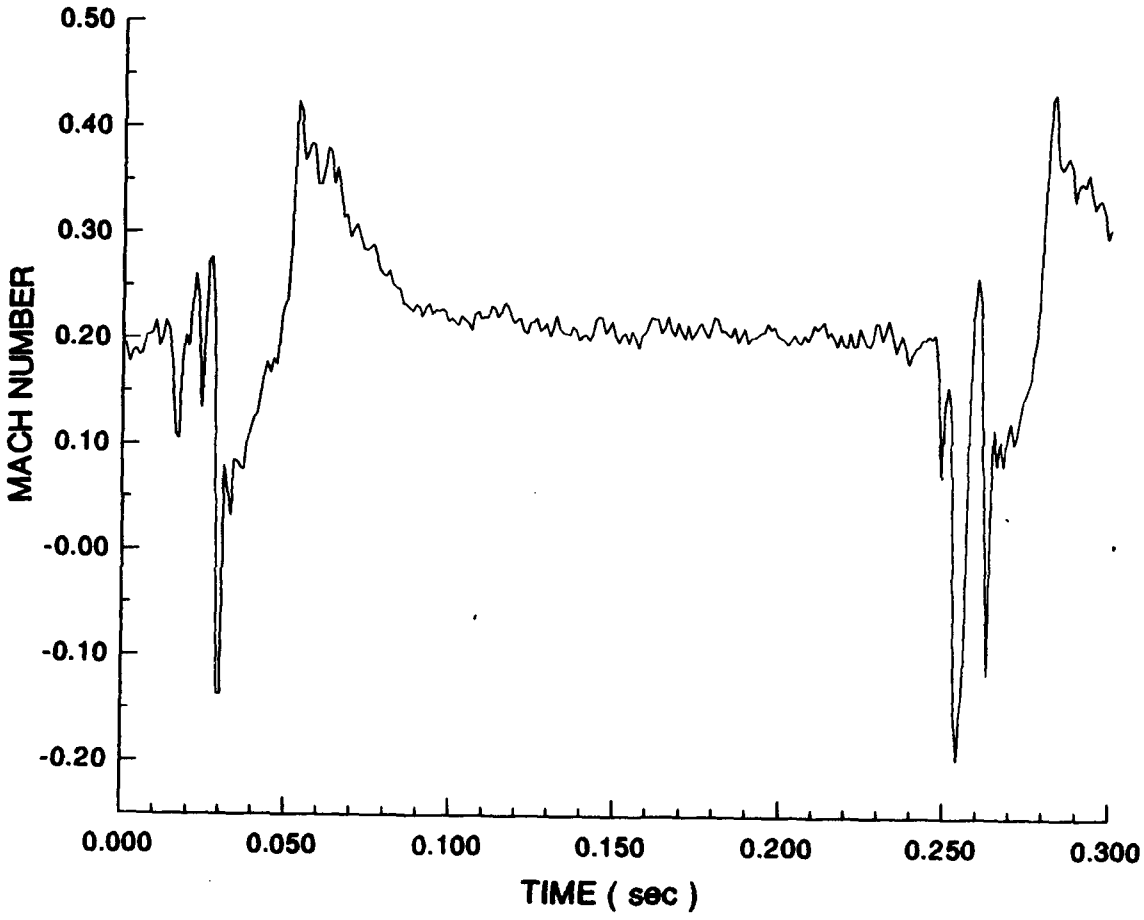

Figure 6.3 Mach number estimate in the compressor discharge

occurred is supported by data from all 12 surge events.

High-response mass flow data were not available for this research effort, so plots of pressure as a function of mass flow during surge, like the plots shown in Figures 1.4 and 1.5, could not be created. However, since the discharge flow Mach number was available from the pressure data, pressure versus Mach number plots could be generated. One such plot, based on data from Figures 6.2 and 6.3, is shown in Figure 6.4. By relating the Mach number to the mass flow and comparing this figure to Figure 1.5, the movement of the compressor operating point from unstalled to stalled operation and back again is clearly evident. Although interesting, this type of plot was not particularly useful in this research effort, so similar plots of the other 11 surge events were not generated.

During the reverse flow periods, what appeared to be rotating stall cells were observed in all 12 surge events. One of these is identified in Figure 6.1. The annular length of these cells stretched at least from the discharge pressure probes to the inlet to stage 10. This fact is demonstrated in Figure 6.5, where pressure data from the compressor discharge are compared to pressure data from the stage 10 inlet. The two data collection locations are nearly in line with one another, and it is clear that the cell passed both locations at almost the same time. The other static pressure probe located in the discharge also recorded the cell passage, but it is out of phase with the other two probes. Using the surge data, an attempt was made to isolate the rotating stall pattern from the surge. This was done by subtracting a representative blowdown from actual blowdown data. The representative blowdown was created by obtaining points along a blowdown trace recorded by the pressure probes in the discharge. The points were

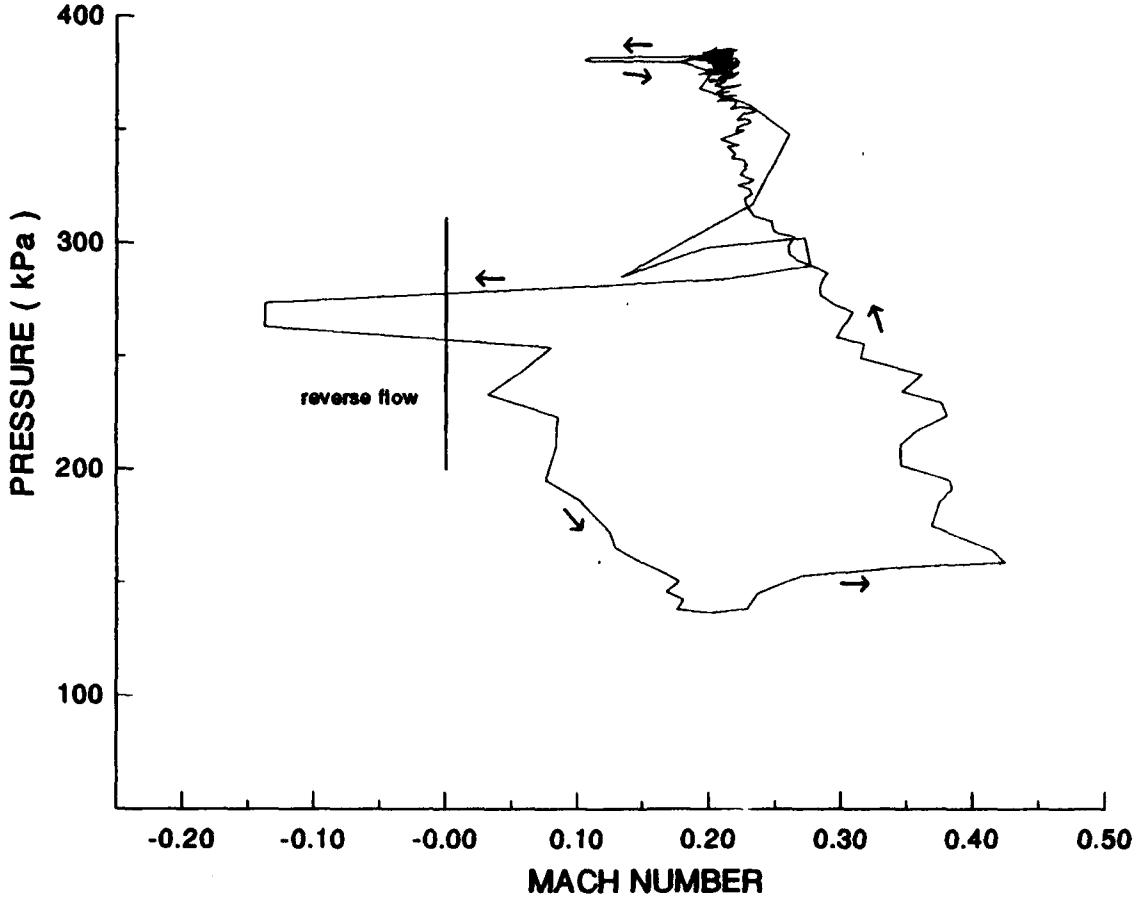

Figure 6.4 Pressure as a function of Mach number in the compressor discharge

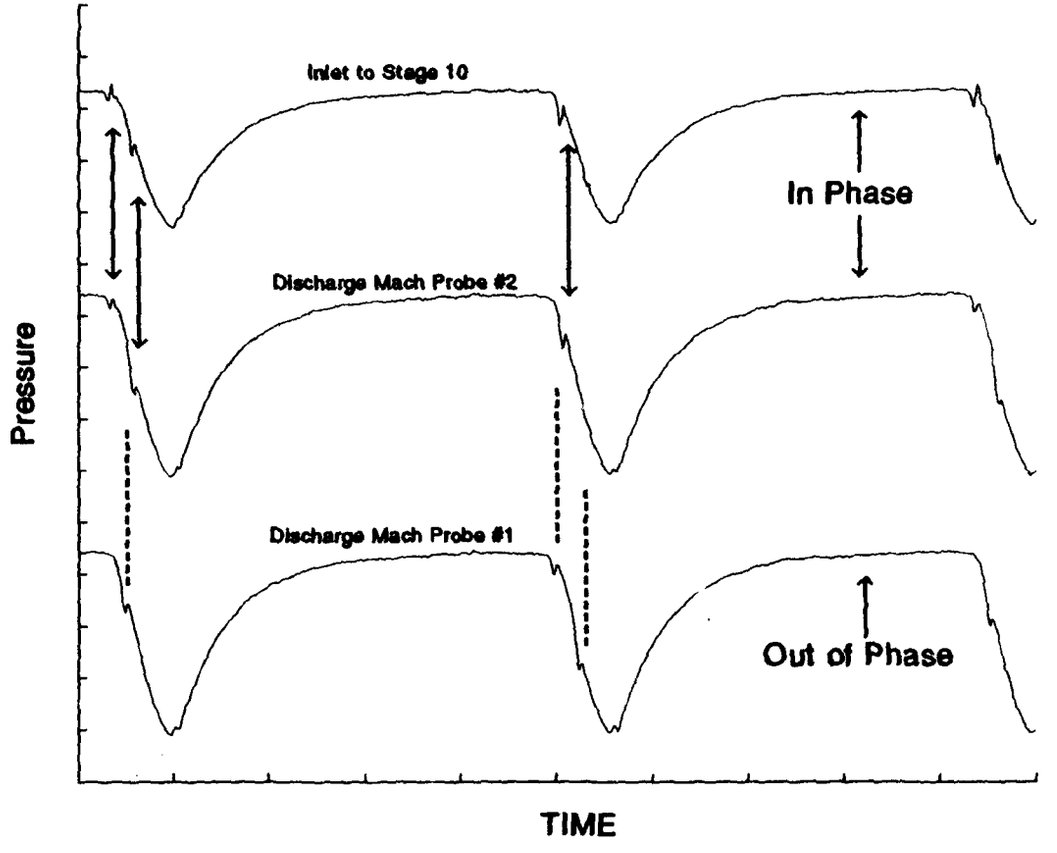

Figure 6.5 Rotating stall phase relationship: stage 10 inlet and discharge pressure probes

chosen from blowdown regions where the rotating stall was absent, so that the representative blowdown would be free of rotating stall components. Since pure surge is generally an axisymmetric phenomenon, the points obtained from probes facing the same direction were combined and a curve fit was calculated. The curve fit was used as a representative blowdown.

To adjust the magnitude of the static and total pressure readings once the blowdown was subtracted, average in-stall pressure measurements taken at 79.5% compressor speed were used as reference pressures. Clearly, using these pressures as references is not an altogether correct practice, but in-stall data above 79.5% does not exist. For this reason, the data resulting from this process should be considered qualitative and not quantitative. The results of this process using one set of probes are shown in Figure 6.6. The general shape of the stall cell resembles the rotating stall plots produced by Copenhaver [2] using lower speed data from this compressor. This was interesting because it seemed to support the premise that these pressure abnormalities were indeed rotating stall cells.

In several cases the stall cell rotated about the compressor twice during a blowdown. Therefore, sufficient data existed to estimate the rotating stall frequency had the compressor not recovered from surge. The estimated stall frequencies for each surge are shown in Table 6.1. It is clear that the stall frequency did not change as the volume was changed, but the frequency did increase as the compressor speed was increased.

All 12 surges were induced by reducing the mass flow, accomplished by slowly closing the discharge valve. Since surge could cause significant structural damage, the compressor was not allowed to surge for very long. Therefore, once the compressor was

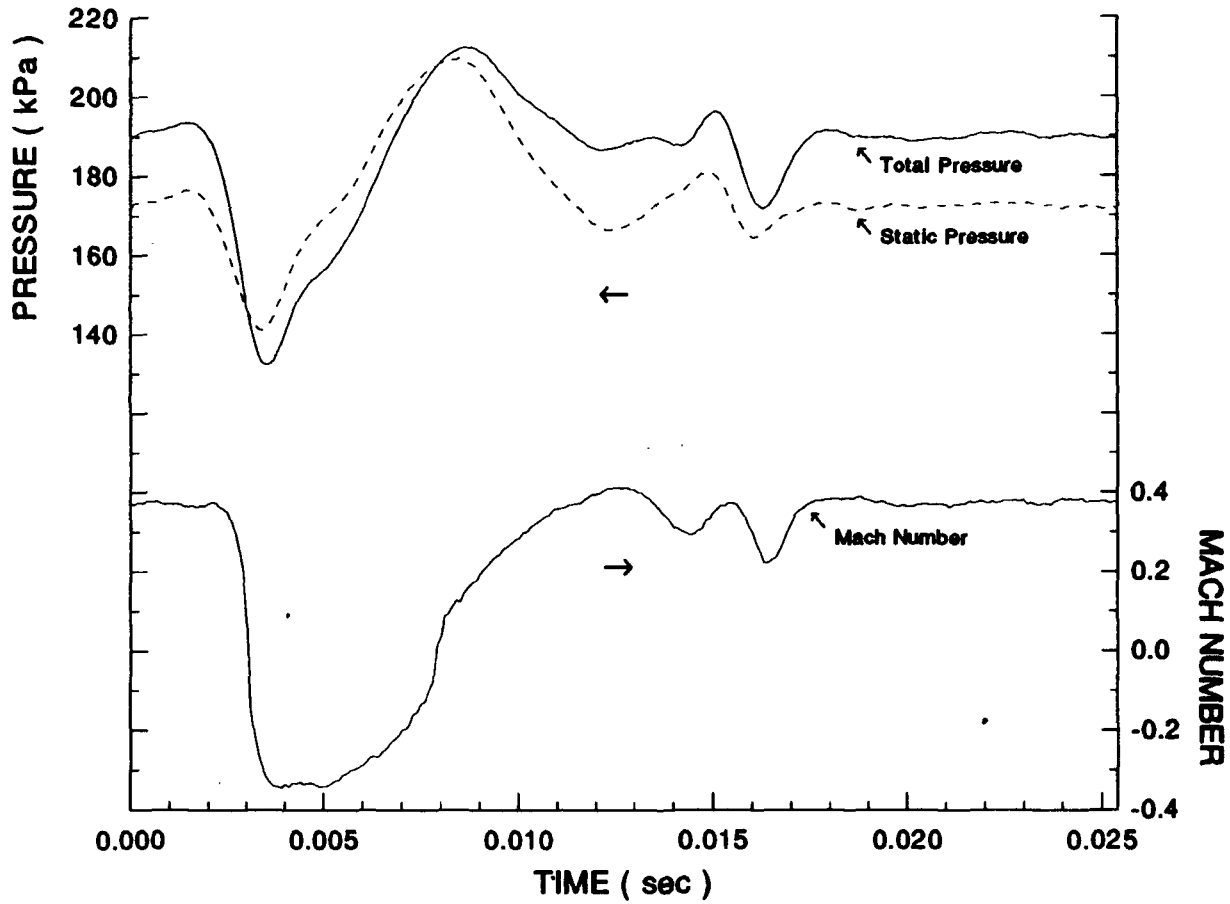

Figure 6.6 Rotating stall isolation attempt

Table 6.1 Surge event characteristics

Compressor Speed	Plenum Volume	Surge Number	Length	Number of Cycles	Throttle Area at Stall	Throttle Closure Rate	Apparent Surge Frequency	Average Surge Frequency	Rotating Stall Frequency	Volume Averages		
										App. S. F.	Ave. S. F.	R.S. Freq.
81%	100%	1	~0.7 sec	3	90 sq cm	0.5 %/sec	4.4 cps	4.4 cps	77 cps	4.3 cps	4.6 cps	75 cps
		2	~1.7 sec	7	90 sq cm	1.0 %/sec	4.6 cps	4.9 cps	71 cps			
		3	~0.5 sec	3	87 sq cm	5.0 %/sec	4.9 cps	5.2 cps	77 cps			
		4	~1.0 sec	5	90 sq cm	1.0 %/sec	4.8 cps	4.7 cps	77 cps			
		5	~1.3 sec	5	103 sq cm	0.5 %/sec	3.3 cps	4.0 cps	71 cps			
	120%	6	~0.9 sec	4	94 sq cm	0.5 %/sec	4.1 cps	4.3 cps	77 cps	4.1 cps	4.3 cps	77 cps
	80%	7	~0.7 sec	6	90 sq cm	0.5 %/sec	4.8 cps	5.1 cps	77 cps	4.8 cps	5.1 cps	77 cps
82%	100%	8	~0.7 sec	3	94 sq cm	0.5 %/sec	4.4 cps	4.4 cps	83 cps	4.5 cps	4.5 cps	83 cps
		9	~0.6 sec	3	94 sq cm	0.5 %/sec	4.6 cps	4.5 cps	83 cps			
	80%	10	~1.3 sec	6	116 sq cm	0.5 %/sec	3.4 cps	4.4 cps	83 cps	3.4 cps	4.4 cps	83 cps
87%	100%	11	~1.0 sec	5	97 sq cm	0.5 %/sec	4.7 cps	5.4 cps	100 cps	4.7 cps	5.4 cps	100 cps
	80%	12	~1.3 sec	9	120 sq cm	0.5 %/sec	6.5 cps	7.1 cps	100 cps	6.5 cps	7.1 cps	100 cps

seen to be surging, the discharge valve was usually opened quickly. Figure 6.7 shows the time history of the discharge valve flow area during a surge event. The line is only slightly negatively sloped most of the period, until the point where the discharge valve was rapidly opened.

Also shown in Figure 6.7 is the time history of the discharge pressure. In this figure, it is clear that the discharge valve was still being closed after surging had started. It was observed that the time length, or period, between surge cycles continued to decrease as the discharge valve was being closed. This behavior is clear after careful examination of Figure 6.7. The time period between surge cycles decreased because the plenum repressurized faster when the outflow was less. This becomes clear if one imagines trying to inflate a balloon with a large tear in it versus inflating one with a tiny tear instead.

Although this behavior was not unexpected, it was important to realize that surge was not occurring under constant conditions because of this phenomenon. Surge cycles from the beginning of a surge event could not be compared to cycles at the end on an equivalent basis. This fact made it difficult to attach significance to an average surge frequency based on summing all of the surge cycles during a surge event. However, it was possible to compare surge data from the beginning of one surge event to data from the beginning of another surge event because the discharge valve area that initiated surge was fairly consistent for all three volumes at a given speed. This allowed for the calculation of surge frequencies based on the periods of the first surge cycles.

Table 6.1 includes the surge frequencies calculated in two different ways. The average surge frequency is calculated by averaging the periods of all the surge cycles

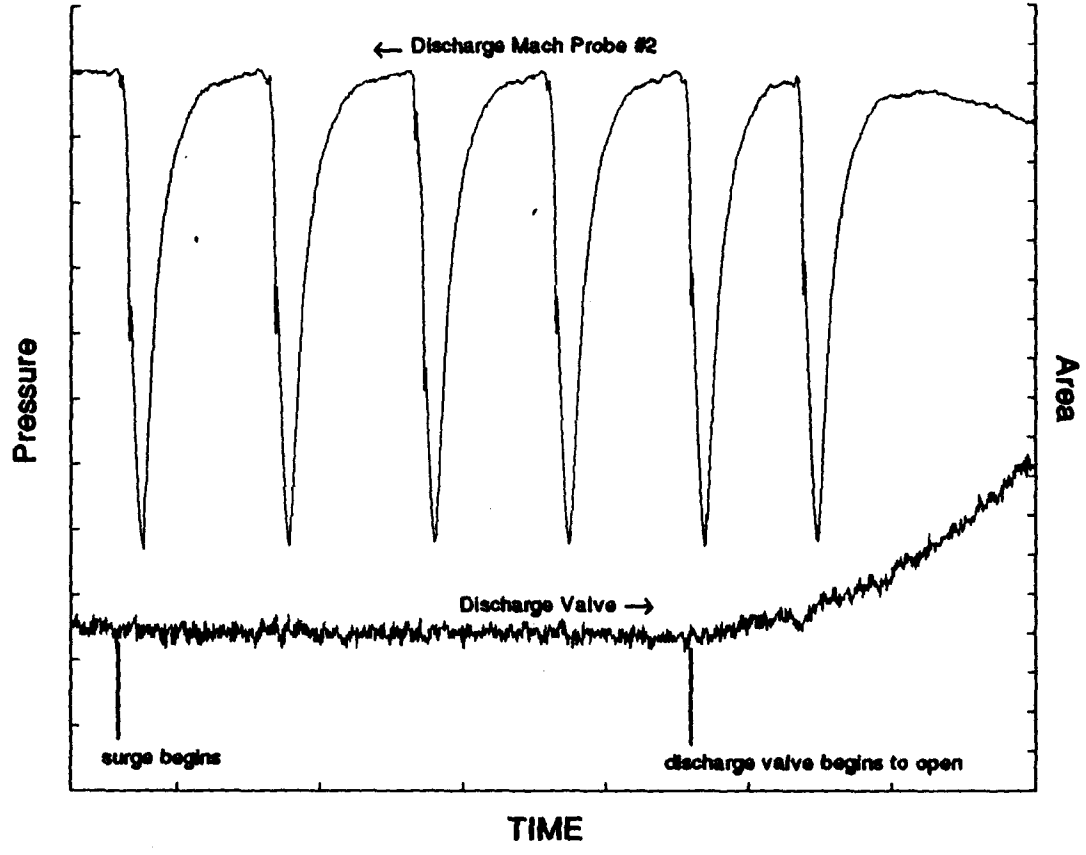

Figure 6.7 Discharge valve time history

during the surge event. The apparent surge frequency is an estimate based on the first cycle only. In both methods, the period is the time between the low pressure points, or the troughs. It was found that determining the time period trough-to-trough was much easier and more consistent than trying to determine the peak-to-peak period.

After reviewing the surge frequency data, a relationship between the surge frequency and the plenum volume seemed to emerge. Most theories, including the compressor model discussed in the next section, predict an increase in surge frequency with decreasing plenum volume. Indeed, at 81% speed, the surge frequency seemed to increase as the plenum volume decreased. However, at 82% speed the opposite trend seemed to occur: as the volume decreased so did the frequency. This apparent contradiction is probably due to the lack of available data. For example, at 81% speed and 120% volume, the one surge event recorded had only four complete cycles. Four cycles is insufficient for a good estimate of the average surge frequency. Further, the apparent surge frequency at this speed and volume is based on only one cycle, since only one instance of surge occurred under those conditions. So even though the surge frequency probably increased with decreasing volume, a lack of data made it difficult to prove this conclusively.

Pressure data from the compressor inlet was also available for study. Figure 6.8 shows a typical time history of the inlet and discharge total pressures during surge as recorded by forward-facing Mach probes. Unfortunately, the rearward-facing Mach probe at the inlet worked only intermittently and did not provide useful data. The passage of pressure waves through the inlet during each surge cycle is evident by the pressure spikes

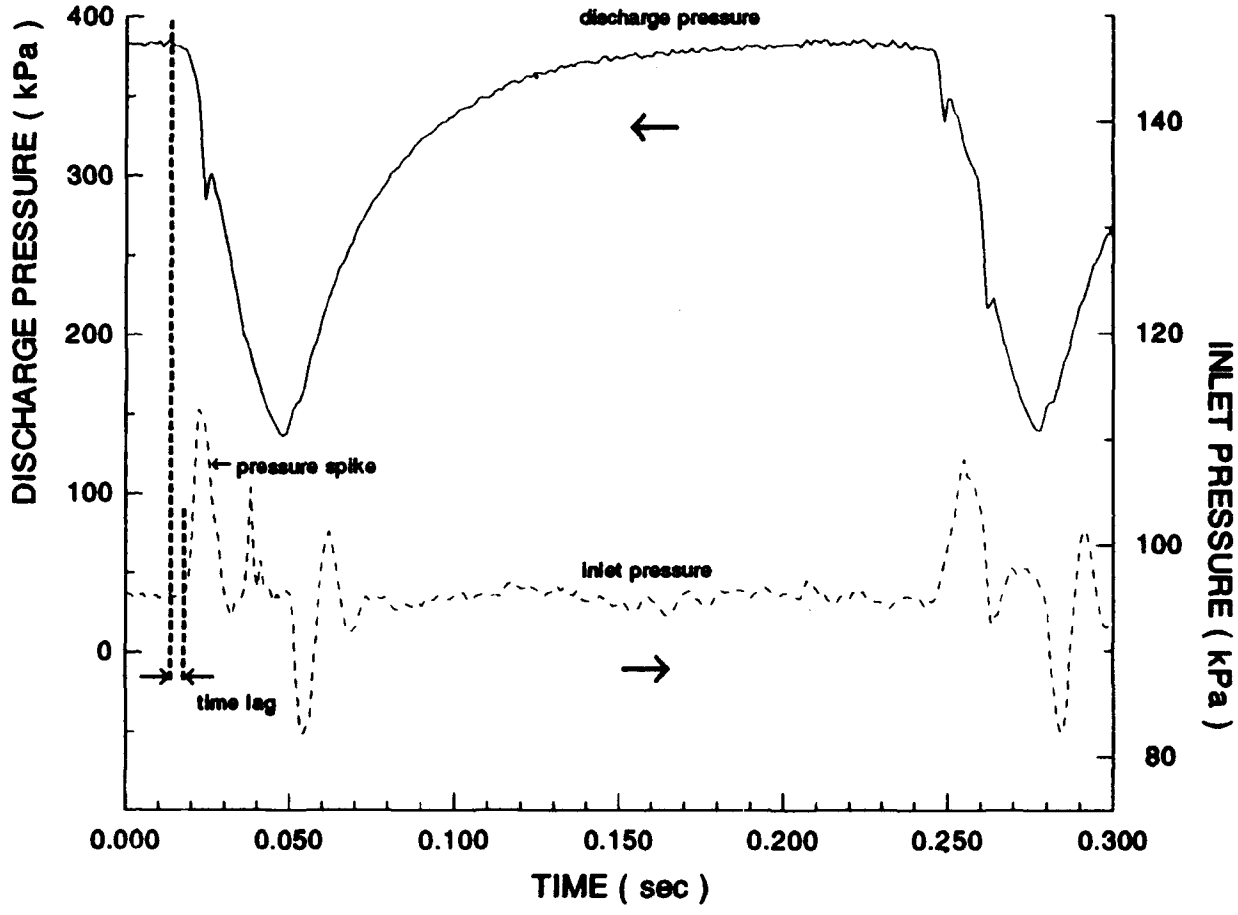

Figure 6.8 Inlet and discharge pressure comparison

in the figure. There is a definite time lag between these pressure spikes and beginning of blowdown registered by the discharge Mach probe. It was possible to use this time lag in conjunction with steady-state temperature and pressure data to estimate the approximate location in the compressor where the initial stall that caused the surge occurred. In all 12 cases (81% to 87% speed), the initial stall seemed to originate in the last 3 or 4 stages of the compressor. This agreed well with earlier research efforts concerning this compressor including Copenhaver's [2] work, which showed that stalls near 78.5% compressor speed originated in the seventh stage.

Further study of lower speed data from this compressor showed that 78.5% speed was the highest speed at which rotating stalls were recorded in this compressor[2]. Under nominal through-flow conditions, this maximum speed for stall did not change when the plenum volume was varied. Further, it was apparent from the surge data presented herein that the minimum speed for surge, 80.4% (~81%) corrected speed, also did not change when the plenum volume was varied. Thus, the speed boundary between surge and rotating stall, shown in Figure 6.9, did not change when the plenum volume was increased or decreased.

[2] This does not include the surge-to-rotating stall transition mentioned earlier in this report (see footnote [1]).

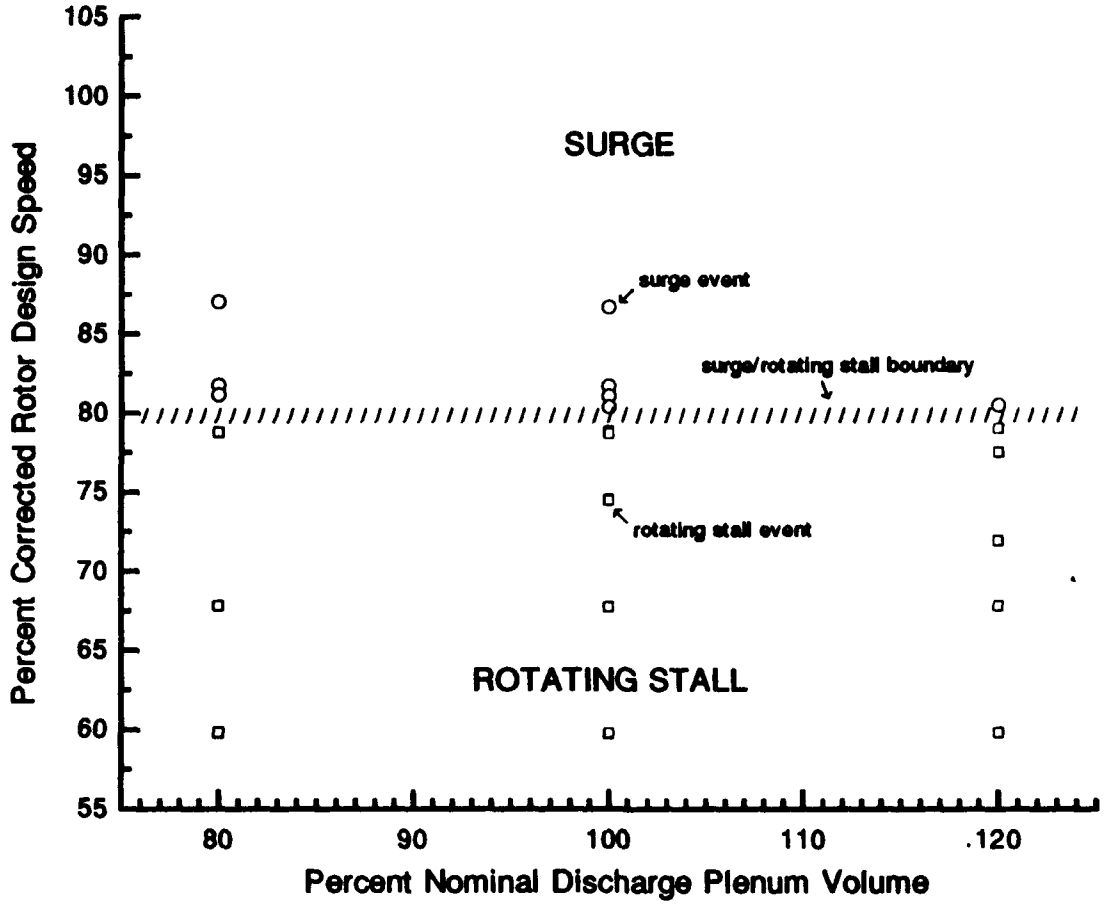

Figure 6.9 Surge/rotating stall boundary

6.2 Surge/Rotating Stall Boundary Investigation

All compression systems that exhibit both surge and rotating stall over portions of their operating range have what is called a surge/rotating stall boundary (henceforth to be called the S/RS boundary). This is typically defined as a speed boundary that separates the compressor stall regions where either surge or rotating stall occur. When a given compressor operates beyond the stall line with constant geometry and discharge volume, surge occurs at compressor speeds above the S/RS boundary and rotating stall at speeds below it.

The compressor speed defining the S/RS boundary is unique to a particular compressor. Some of the factors that determine this boundary are blade geometry, the size and length of the compressor, and the number of stages, but the factor that receives the most attention herein is the compressor discharge volume. Most dynamic compressor models, including the ones to be discussed later in this section, show a relationship between the discharge volume and the S/RS boundary. This has much to do with conservation of energy within the system. When pressurized, the discharge volume behaves much like a capacitor in an electrical system, storing mechanical potential energy in the form of pressurized air. If the volume is large, the amount of potential energy stored is greater than if the volume were smaller. It has been found that the more energy there is in the system, the greater the likelihood that surge will occur. Therefore, larger discharge volumes tend to cause surge instead of rotating stall.

The 10-stage compressor tested at the CRF exhibited both surge and rotating stall during unstable operation. As expected, rotating stall tended to occur at lower compressor

speeds while surge occurred at higher speeds. However, discharge volume changes did not seem to affect the S/RS boundary. In Section 6.1, it was shown that the boundary remained near 80% corrected rotor speed despite discharge volume changes of ± 20% nominal. The surge frequency should also have changed, but as mentioned in the previous section, the surge frequency changed very little (if at all). Possible reasons for this lack of a volume - S/RS boundary relationship are investigated in this section.

In the process of investigating the S/RS boundary behavior, a dynamic compressor model is used. After comparing the estimated (or simulated) and actual behavior, a lack of agreement between the two is apparent. The possibility that more volume was apparent to the compressor than previously thought is explored in detail, and several theories, which attempt to account for this, are formulated. Several other hypotheses which might explain the S/RS boundary behavior are presented at the end of this section, but none of these are investigated in detail.

6.2.1 Pre-test S/RS boundary prediction: the NBM parameter

Before the test, the builder of the test compressor (Pratt & Whitney) made an estimate of the surge/rotating stall boundary. This was done to aid in the design of the variable volume hardware. Based on this surge/rotating stall boundary estimate, the maximum test plenum volume was determined. The maximum temperature allowed [18] put limitations on the minimum volume, but the boundary estimate helped the designers choose a factor of safety. Although 70% nominal volume was possible based on temperature limitations, 80% nominal volume was thought to be compatible with the overall test objective.

To make the boundary estimate, the manufacturer used a dimensionless parameter related to Greitzer's B parameter [4,5]. The NBM parameter [19], was defined in the following manner:

$$NBM = \frac{PRa}{2u_c}\sqrt{\frac{V_p}{A_c L_c}}$$

where:

PR = pressure ratio <u>at stall</u>
u_c = axial flow velocity,
a = speed of sound
A_c = compressor flow-through area
V_p = plenum volume
L_c = effective length of equivalent duct for compressor

Using this relationship in conjunction with their previous experience with similar compressors, P&W made the surge/rotating stall boundary estimate shown in Figure 6.10. At any point on the S/RS boundary prediction, NBM ≈ 7. Obviously, the prediction failed to agree with the actual boundary. This disagreement was the first indication that the S/RS boundary behavior of this compressor required further investigation.

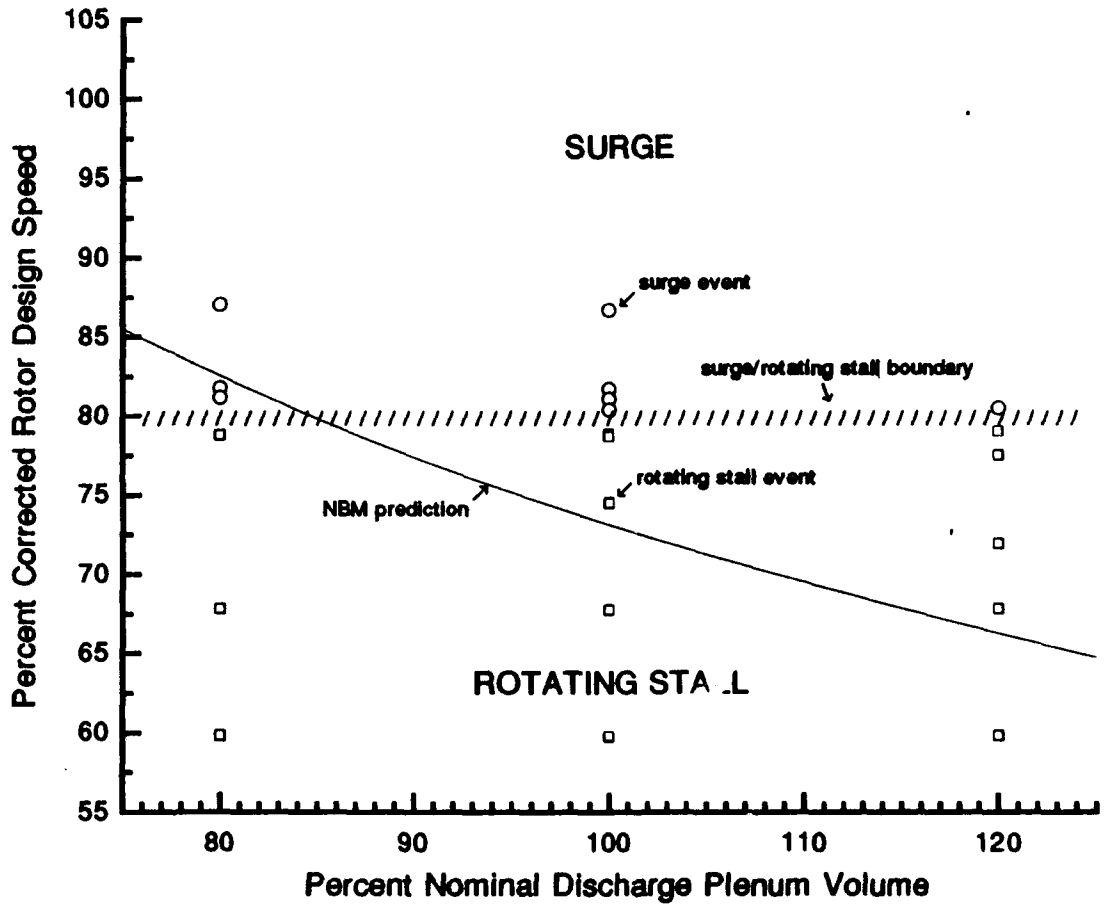

Figure 6.10 Pre-test S/RS boundary estimate

6.2.2 Stage-by-stage model

During the early 1990's, a stage-by-stage post-stall compressor model was developed at Arnold Engineering and Development Center (AEDC) based on the work of Dr. Milt Davis of Sverdrup Technology Inc. [20]. This model was designed to deal with the multiple stages and high pressure ratios associated with modern compressors. The Dynamic Turbine Engine Compressor Code, or DYNTECC, was and still is the state-of-the-art in computer based dynamic compressor modeling.

DYNTECC models the compressor as a series of control volumes, much like the configuration shown in Figure 6.11. Individual compressor stages as well as ducting segments are modeled as elemental control volumes. Mass flows, pressures, bleeds, blade forces, etc., are related to one another in each control volume through conservation of mass, momentum, and energy principles. Pressure and temperature characteristics for each stage are required for the model to determine the blade forces and shaft work.

To account for the transient response of the compressor, the blade forces are lagged using the first-order lag equation:

$$\tau_D \frac{dFX}{dt} + FX = FX_{ss}$$

and a specified time constant, τ_D. The value of τ_D depended upon what portion of the compressor characteristic the compressor was operating on. At stall inception (post-stall) up to some minimum mass flow coefficient, the model would use one value for τ_D. During pre-recovery (or near-recovery in the case of rotating stall), τ_D would take on a different value from some minimum to some maximum mass flow coefficient value.

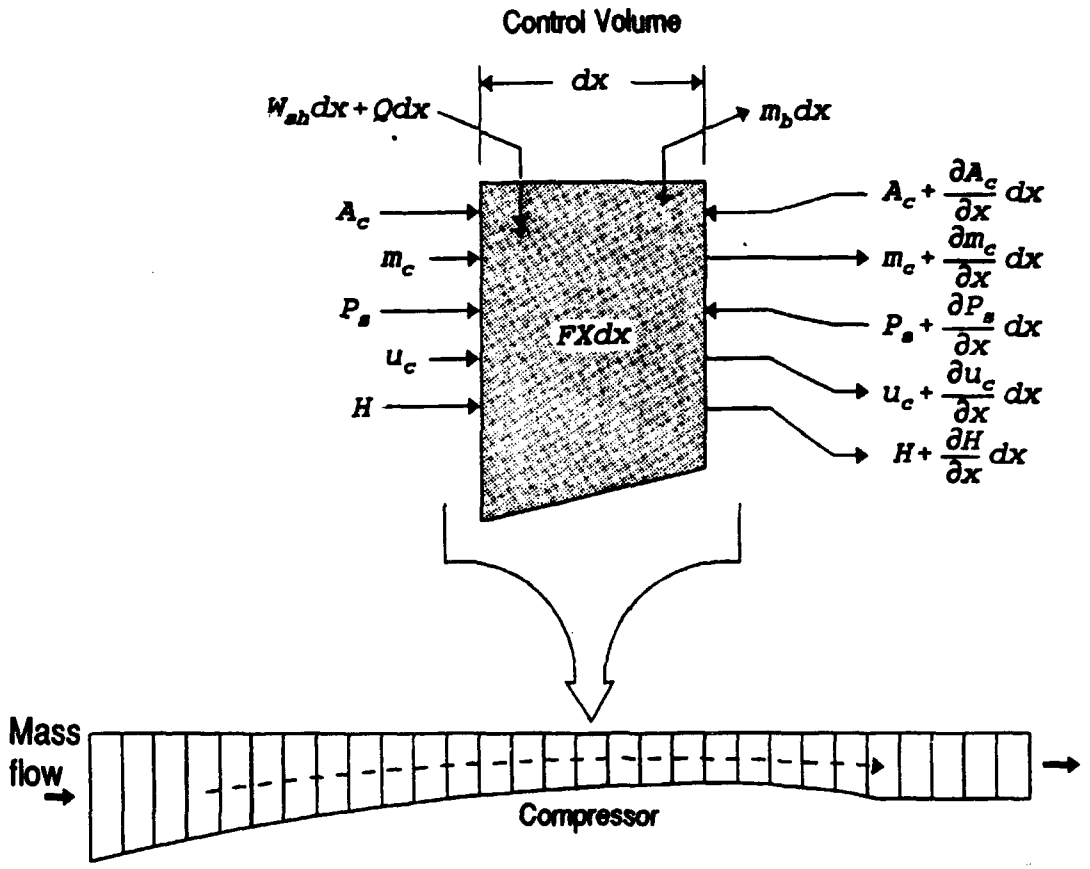

Figure 6.11 Control volume for stage-by-stage model (DYNTECC)

Multipliers included in the input to the model controlled the mass flow coefficient ranges. For the post-stall τ_D value, the multipliers were based on the near-stall point on the unstalled characteristic. In the case of the pre-recovery τ_D value, the multipliers were based on the near-recovery point on the stalled characteristic. The value of the maximum flow coefficient multiplier for the pre-recovery τ_D value dictated the degree of hysteresis in that particular stage. In the case of these model simulations, pre-recovery lag was applied up to a flow coefficient value 1.2 times the near-recovery point value on the stalled characteristics of all 10 stages. This flow coefficient value was based on the observed hysteresis of the compressor.

The reverse flow characteristics could also be manipulated in this model. Since no reverse flow characteristics exist for this compressor, deciding what these characteristics should look like is up to the researcher. For this report, the reverse flow characteristics estimated by Bloch [16] were used. The multipliers for slope and offset in the model input reflect these estimates. All of the specific values for τ_D and the various multipliers used in this DYNTECC model are shown in Table 6.2.

As previously mentioned, this model uses the individual stage characteristics to simulate overall compressor behavior. For compressor speeds where specific characteristics do not exist, the model uses an interpolation routine to estimate the appropriate characteristics. This routine uses the characteristics from a higher speed and a lower speed to make the estimate. In the case of this compressor, characteristics for 78.5% speed and 82% speed were made available. The characteristics for 82% speed are shown in Figure 6.12. Since most of the transient data recovered were for speeds near

Table 6.2 DYNTECC input values

Stage-by-stage Model Inputs	Value	Variable Names
Percent design mass flow	37.70 / 41.65	PWCDES
Percent design rotor speed	78.5 / 81	SPEEDHPC
τ_D, Post-stall	0.012 sec	TLAGHPCT
τ_D, Pre-recovery	0.033 sec	TLAGHPCB
Post-stall τ_D control; Initial	1.0	PHIHPCTR
Post-stall τ_D control; Final	0.120 Stages 1-3 0.235 Stages 4-7	PHIHPCTL
Pre-recovery τ_D control; Initial	1.2	PHIHPCBR
Pre-recovery τ_D control; Final	0.0	PHIHPCBL
Reverse flow characteristic slope for each stage (Pressure only)	4,2,2,1.8,2.5 3.5,2.5,2.5,2,2	HPCROTAT
Reverse flow characteristic offset multiplier (Pressure coefficient)	1.0 Stages 1-3 0.65 Stages 4-7	PDROPHPC
Reverse flow characteristic offset multiplier (Temperature coefficient)	1.0	TDROPHPC

81%, the model estimated the characteristics at that speed when comparisons between the model and actual data were made. The actual characteristics used were compiled by Boyer and O'Brien [14] and Copenhaver [2].

Most of the work involved in setting-up the 10-stage compressor model using DYNTECC had already been accomplished by previous researchers, but it was still necessary to adapt the model to this research effort. Parts of the computer code were altered to modify the output for the plotting software used, but no significant modifications were made to DYNTECC. Once set-up, DYNTECC was used to help accomplish two research goals. The first of these was to determine if the model could be made to simulate the behavior of the test compressor using the actual compressor geometry and operating conditions as inputs. If this could not be accomplished, the second goal was to find a discharge volume which would allow the model to simulate actual compressor behavior with all other operating conditions held constant. The first goal was not met: the model did not simulate actual behavior using nominal input data. However, the second goal was accomplished. The efforts made and results from both simulation attempts are described next.

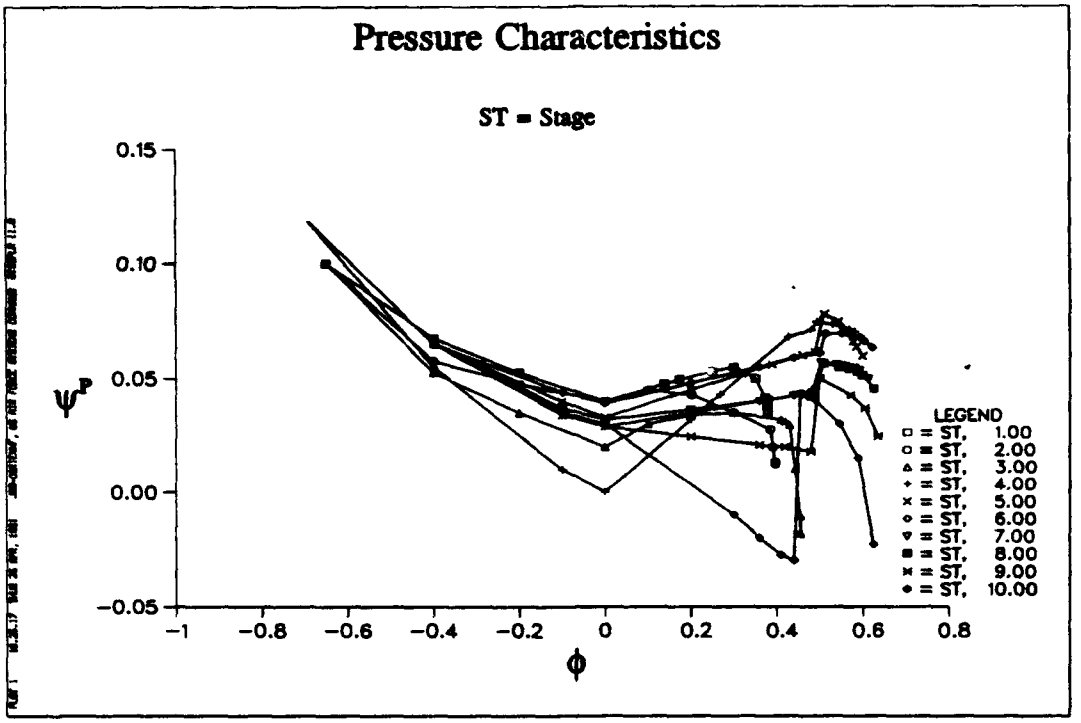

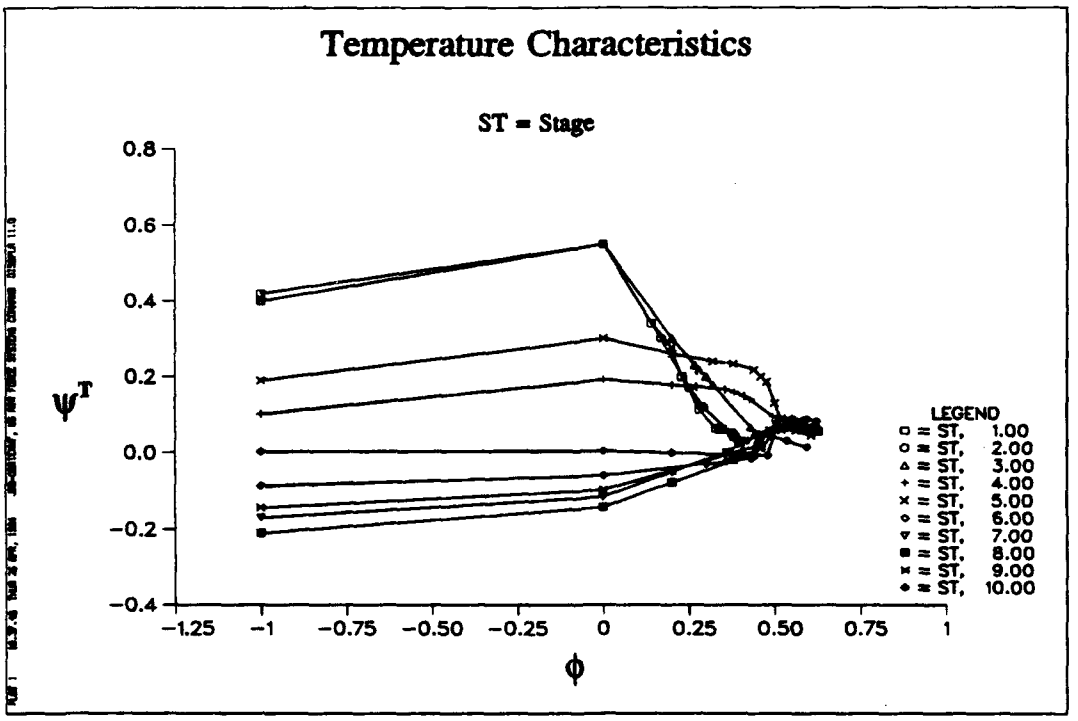

Figure 6.12 Ten-stage compressor characteristics; 82% speed

Model simulation using actual geometry and operating conditions as inputs

The model was calibrated at 100% nominal discharge volume so that the S/RS boundary appeared between 79% and 81% compressor speed. The compressor time constants, τ_D, were instrumental in accomplishing this. By trial and error, values for τ_D were found which caused the simulation to stall at 79% speed and surge at 81% speed with nominal discharge volume. These were 0.012 sec (post-stall) and 0.033 sec (pre-recovery). However, it was not possible to set the S/RS boundary and simulate the actual surge frequency. In fact, there were no values for τ_D which caused the simulation to exhibit the actual surge frequency at 100% discharge volume and 81% compressor speed. The possible significance of this will be discussed later. Once the values for τ_D were found, they were kept constant in all simulations despite changes to the other variables.

Discharge plenum volume in the model was varied by increasing or decreasing the size of several elemental control volumes in the rearward section. Since the elemental control volumes were sometimes altered a great deal, care was taken so that the stability criterion was not violated by any of the volumes. The model time-step, Δt, was to be kept constant in all cases, so the time required for a sound wave to travel from one side of a control volume to another had to be greater than or equal to Δt. This meant that the length of any particular elemental control volume could not be less than some set amount.

The behavior simulated by the model using 80%, 100% and 120% nominal discharge volume at 79% and 81% compressor speed was compared to actual test data. These six cases are shown in Table 6.3. In all but one case, the type of instability the model simulated matched the type actually observed. However, at 120% volume and 79%

speed, the model simulated surge while rotating stall occurred in actuality. More importantly, the surge frequencies from the simulations were much higher than those from the actual test data. At this point, it was clear that the model failed to simulate actual compressor behavior using actual geometry and operating conditions.

Model simulation using larger-than-nominal discharge plenum volume

Next, the model was run with increasingly larger discharge volumes at a constant compressor speed of 81%. As expected the surge frequency decreased as the volume was increased. Figure 6.13 shows this trend, where surge frequency is plotted against discharge plenum volume. Near 160% nominal discharge volume the surge frequencies from the simulation nearly matched the surge frequencies observed from the test data. Thus, the model produced surge frequencies near actual frequencies only by using larger volumes than those presumably tested. Hence, it seemed possible that the discharge volumes used during the test were actually larger than designed.

In all simulations discussed so far, the compressor time constants were held constant. Therefore, when the model was run using 160% volume at 81% speed, the simulation did not match actual compressor behavior, even though the frequencies were nearly the same. This was because the simulation did not stall at 79% speed as the compressor did in reality. In fact, when using 160% simulated volume the model did not exhibit rotating stall unless the simulated compressor speed was considerably below 79%. This was the result of using the same τ_D values in all cases.

In order to simulate actual compressor behavior using larger volumes, it was necessary to recalibrate the model. This was done by a trial-and-error process where different volume and τ_D values were used. After picking some values for the volume, values for τ_D were found which caused the simulation to surge at 81% speed and rotating stall at 79% speed. Then the simulation surge frequency was compared to the actual surge frequency at 100% nominal volume. Eventually, a simulation volume was found

Table 6.3 Model and actual data comparison

	80% Volume		Nominal Volume		120% Volume	
	Model	Actual	Model	Actual	Model	Actual
81% Speed	Surge ~7½ cps	Surge ~5 cps	Surge ~7 cps	Surge ~4½ cps	Surge ~6 cps	Surge ~4¼ cps
79% Speed	Stall	Stall	Stall	Stall	Surge ~5½ cps	Stall

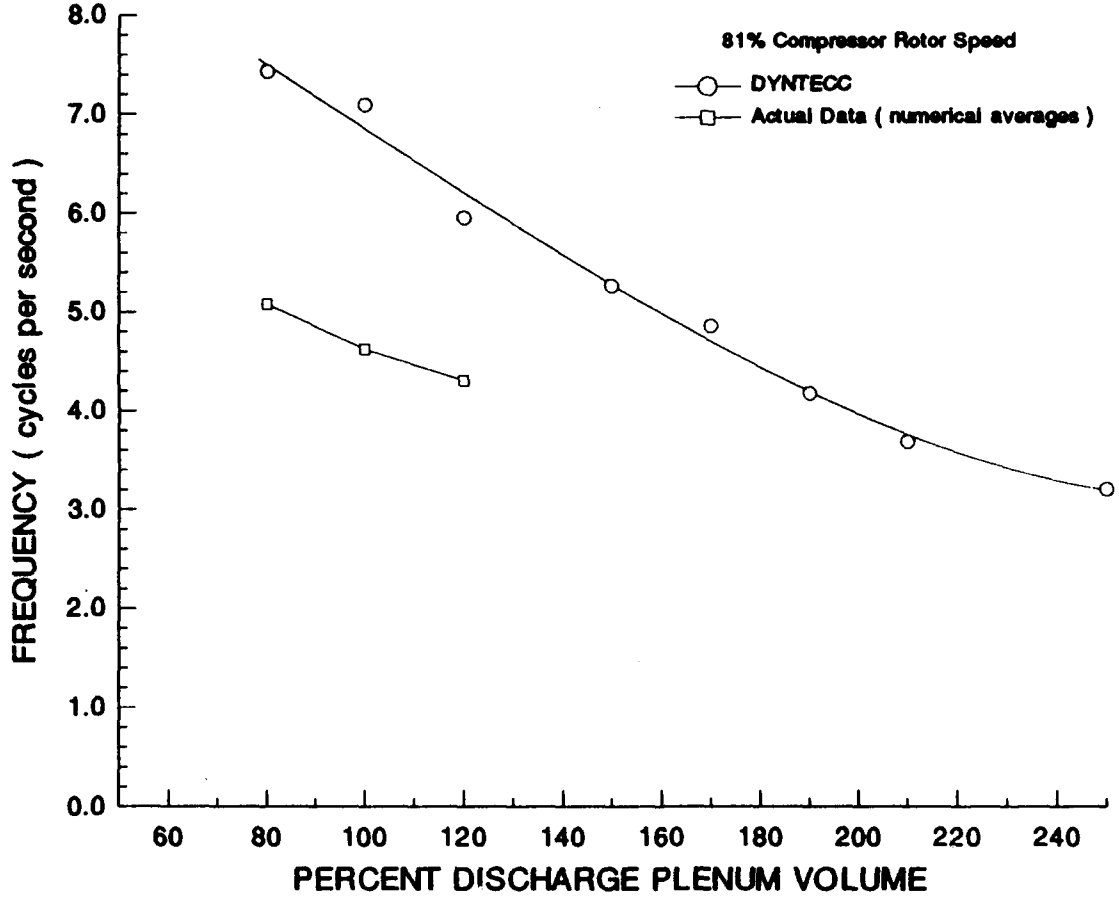

Figure 6.13 Surge frequency comparisons

where both the surge frequency and S/RS boundary matched actual test data.

Using 190% simulated volume, the model exhibited simulated surge behavior very similar to that actually observed at 100% test volume. The corresponding values of τ_D were 0.012 seconds (post-stall) and 0.017 seconds (pre-recovery). In Figure 6.14, simulation results are compared to actual test data. Both pressure transients shown are from the compressor discharge. As the figure shows, the simulation and actual pressure transients nearly overlap. If the model is a correct representation of the compressor, the simulation results seem to suggest that the compressor was affected by more volume than was present in the discharge plenum.

Assuming that there was more volume than designed, the compressor would then have been expected to exhibit the same surge frequency as the simulation. Moreover, the changes in volume would have been smaller (by percentage) than desired. Instead of ±20% nominal, the volume changes would have been nearly ±10%, assuming that the actual nominal volume was in fact 190% of the design value. Smaller changes in volume would have produced smaller changes in the S/RS boundary, causing the actual boundary curve to appear "flatter." Indeed, the S/RS boundary curve based on the actual data appeared to be a flat line, which could be explained if the higher volume hypothesis was correct. There is also the possibility that some flow phenomenon occurred which caused the plenum volume to appear larger to the compressor than it really was. In fact, this was probably the case, since an error as large as 190% in the design of the plenum volume is very unlikely. In any event, if there was more volume "in play" than expected, then it had to come from somewhere. Therefore, to prove or disprove the higher volume

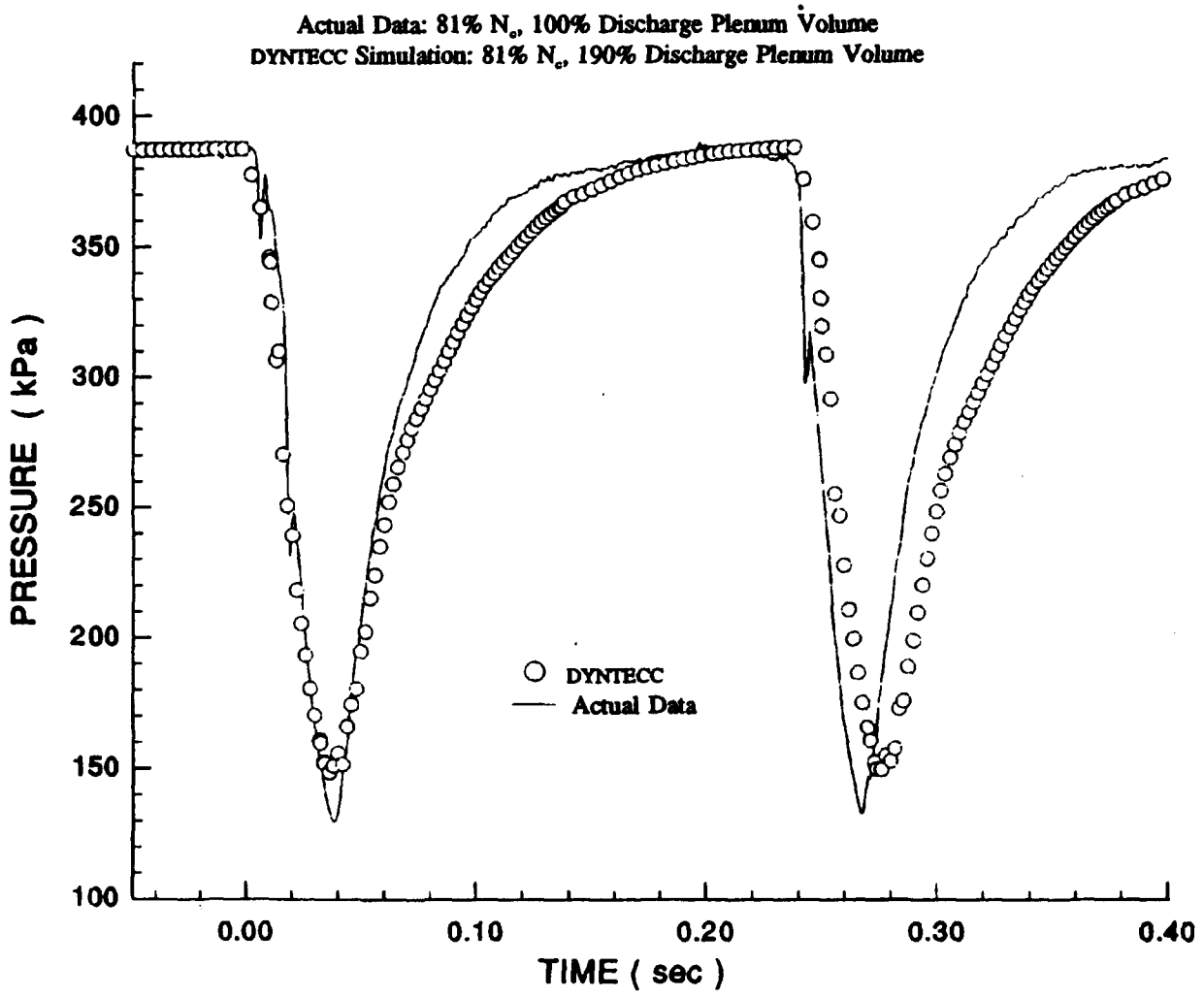

Figure 6.14 DYNTECC simulation and actual data comparison

hypothesis, several possible sources of actual and effective extra volume were considered.

6.2.3 Unchoked Flow through the Discharge Valve

During the compressor test and in both models previously discussed, the discharge volume was defined as all the flow volume between the exit of the last stator row and the inlet of the discharge valve. Limiting the volume size to the discharge valve was justified so long as it remained choked. Both models assumed a choked throttle (discharge valve), and in most cases this is true. However, the large pressure drop associated with surge in 10-stage test compressor may have caused brief periods of unchoked flow in the discharge valve. During those periods, the total discharge volume may have included some of the volume behind the discharge valve. This may have caused the surge frequency to decrease or even have caused surge to occur where rotating stall was expected.

There are several items which support the possibility of unchoked flow. The volume downstream of the discharge valve, which was made up of the discharge ducting and mass flow measurement venturi, had a Helmholtz (or organ pipe) frequency of 5 to 10 Hz. This was nearly the same as the observed surge frequency, which suggests that the discharge duct volume was affecting surge behavior. Furthermore, the minimum pressures during surge blowdowns were on the order of 130 kPa, nearly atmospheric. Such low pressures could cause the discharge valve to become unchoked, or even cause reverse flow if the discharge ducting does not depressurize as fast as the plenum. Evidence of unchoked flow through the discharge valve exists in surge data from the E^3 compressor test [7], so the phenomenon is not without precedent. Certainly, unchoking the discharge valve could provide the excess volume which the compressor model

simulations suggest existed.

In order for the valve to unchoke, the pressure in the discharge plenum (P_p) must reach some minimum value, such that the relation:

$$\frac{P_d}{P_p} \geq 0.5283$$

is valid[3]. For instance, if the static pressure in the discharge ducting was atmospheric (~ 101.3 kPa), then the when the pressure in the discharge plenum dropped below ~192 kPa, the mass flow through the valve would have become unchoked. Since there was no pressure instrumentation immediately downstream of the discharge valve, there is no way to know exactly what the pressure in the duct, P_d, really was. However, it seems certain that when the effects of friction and flow constriction at the venturi are considered, the pressure near the discharge valve must be higher than the pressure at the exit of the venturi, which was nearly atmospheric. Referring to the discharge plenum pressure data in Appendix C, near atmospheric pressure in the discharge ducting would have caused the valve to become unchoked for brief periods during blowdown and repressurization. Discharge duct pressures higher than atmospheric would have caused the valve to become unchoked for even longer periods.

An attempt was made to estimate the pressure difference between the venturi inlet and the discharge valve exit by determining the pressure loses due to friction in the discharge duct. Assuming the duct walls were smooth and using the nominal dimensions of the duct system, the effects of friction were found to be nearly negligible due to the relatively low flow velocities (Mach# < 0.1) near stall. For this reason, the pressures near the

[3] For a sharp-edged orifice, the choking pressure ratio may be greater.

discharge valve exit were assumed to be nearly equal to those at the venturi inlet.

Time-averaged data taken near stall at 81% speed indicated that the pressure and mass flow at the venturi inlet were ~110 kPa and ~10 kg/sec, respectively. However, high-response data obtained before and during surge indicated that the discharge valve area, and hence the mass flow, was less than the near-stall time-averaged value. Because of this discrepancy, an effort was made to estimate the duct pressure and discharge valve Mach number at stall inception based on the high-response data. A simple one-dimensional model based on continuity principles and assuming isentropic flow conditions was used to estimate the duct pressure and valve Mach number based on discharge plenum data. Since the flow velocities in the duct were low except in the discharge valve, total and static pressures were assumed to be approximately equal in all cases. This model was coded in FORTRAN for use on a computer.

High-response pre-stall pressure data were used as model input data in order to estimate the steady-state flow conditions in the discharge duct just before surge. Further, a sinusoidal pressure variation approximating surge, shown in Figure 6.15, was used to provide input conditions to the model in order estimate the transient flow conditions in the discharge duct during surge. The resulting duct pressure and Mach number estimates are shown in Figure 6.16.

The approximate amount of time the discharge valve was unchoked during surge was determined by assuming that the model estimates for the pre-stall and average post-stall duct pressures were correct. According to the model, duct pressure varied between 104 and 107 kPa. Based on this pressure range and the ideal choking pressure ratio, the

discharge valve became unchoked whenever the discharge plenum pressure dropped below between 197 to 203 kPa during surge. Pressure data from the seven surge events that occurred at 81% speed were compared to this minimum pressure range. The average length of time that the valve was unchoked based on all seven surge events was 23 milliseconds per cycle, which was an average of 11.1 percent of the surge cycle period.

There was also a variation in the length of time the valve remained unchoked depending on the plenum volume. At 80%, 100%, 120% plenum volumes, the unchoked time lengths were 21, 23, and 28 milliseconds, respectively. This is a reflection of how long it took the compressor to repressurize the plenum in each case, and more importantly, demonstrates that the plenum volume had at least a small effect on the surge behavior.

Whether or not the estimated 23 milliseconds of unchoked flow during each cycle had any effect on the instability behavior of the compressor remains an unanswered question. Even if some of the discharge duct volume did contribute to the overall discharge volume, it is difficult to determine exactly how much. Without a region of choked flow, defining the boundaries of the volume to be included in any sort of surge behavior estimate becomes arbitrary. It is also important to remember that the calculations made above are based on several assumptions which may or may not be correct. For instance, the static pressure in the exit flow of the discharge valve was assumed to be nearly equal to the static pressure immediately behind the valve. In reality, the static pressure in the flow is probably lower, which would cause the valve to remain choked for a longer period of time. However, it was possible to form an hypothesis concerning the S/RS boundary

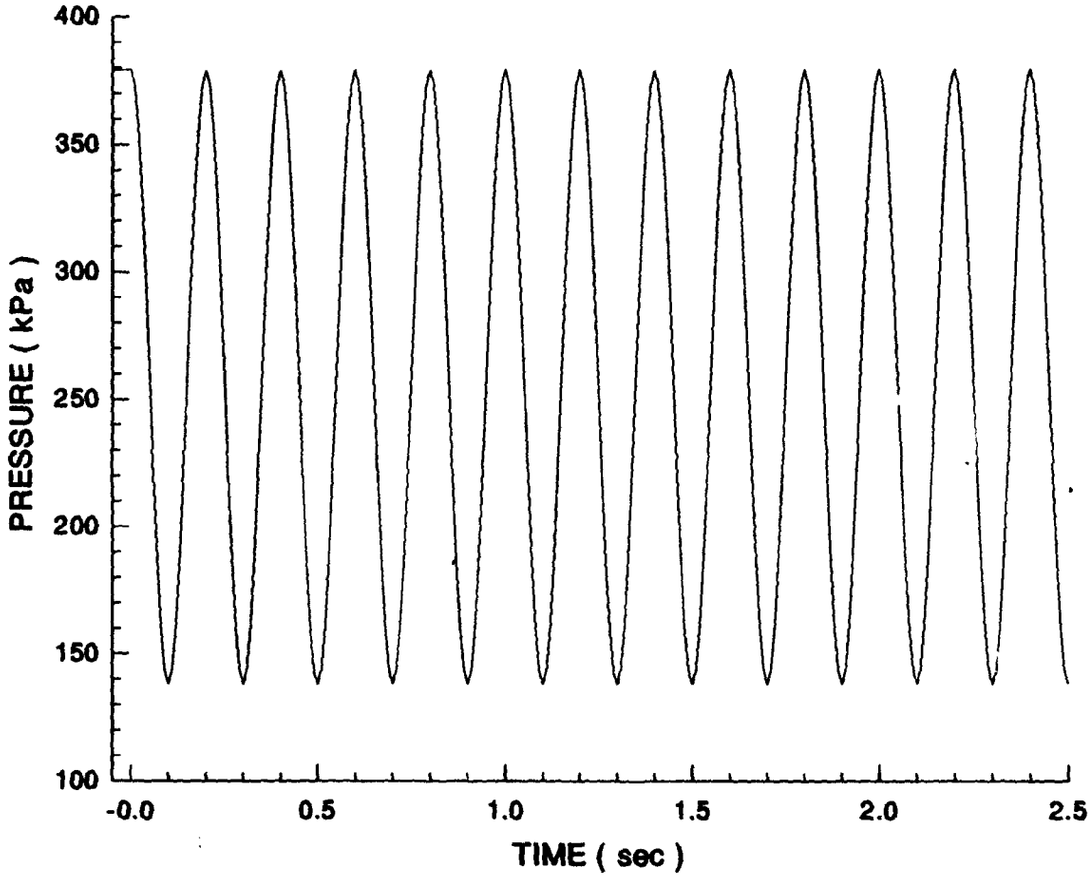

Figure 6.15 Duct volume model sinusoidal input; simulated surge

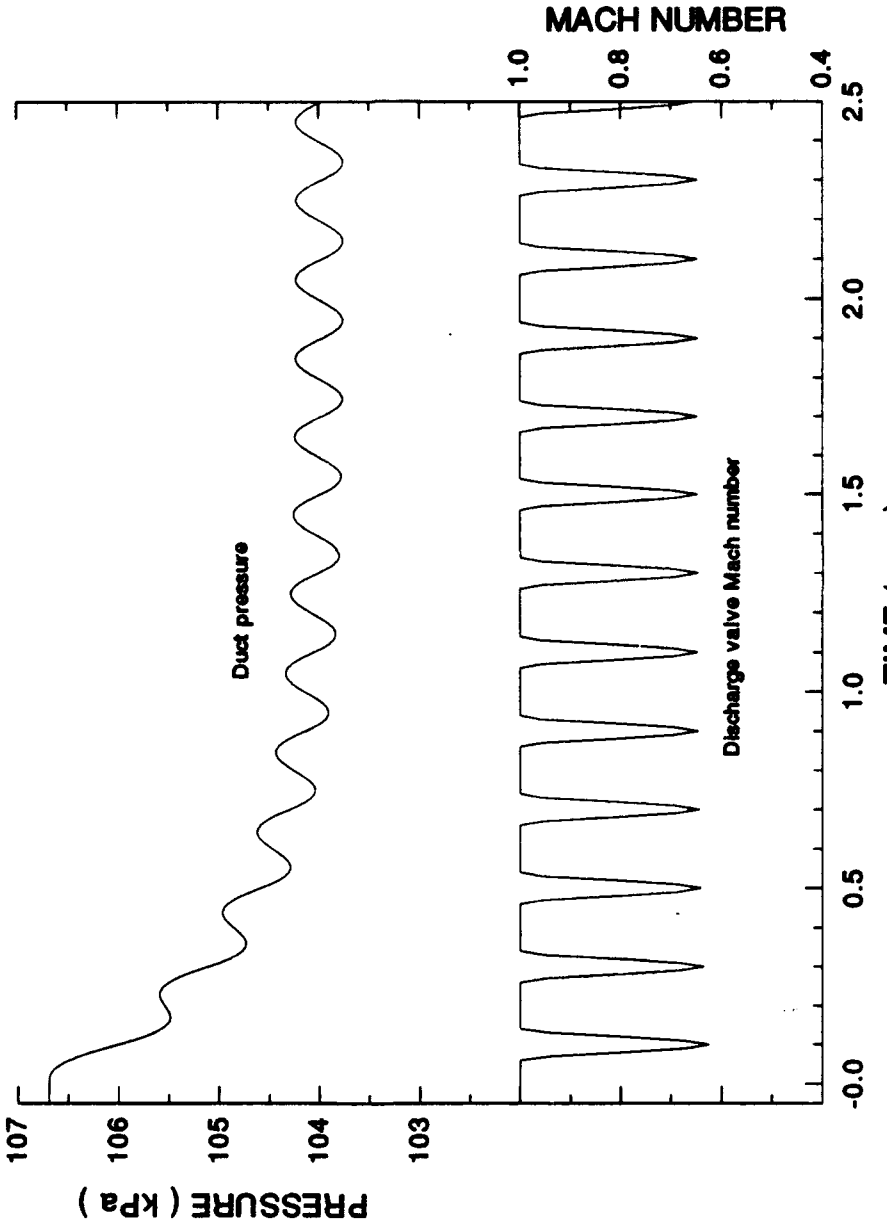

Figure 6.16 Duct volume model output

assuming that the valve does become unchoked for a significant length of time.

Unchoked discharge valve hypothesis

When the compressor went into either surge or rotating stall, the initial behavior of both phenomena were identical. In both cases, the plenum depressurized rapidly as a result of compressor inability to maintain a pressure rise across itself. Surge and rotating stall behavior were nearly indistinguishable until the plenum began to repressurize. At this point, if the compressor recovered and began to operate on the unstalled pressure characteristic (see Figure 1.4), another surge cycle began. If the compressor was unable to recover (Figure 1.3), the compressor appeared to "almost surge" but then failed to reach peak pressure and slipped into rotating stall.

Since the behavior of the two phenomena are similar until repressurization, it is reasonable to assume that there was no difference between surge and rotating stall until the compressor began to repressurize. The amount of volume in the discharge plenum was, therefore, irrelevant at first. Assuming that the character of the instability (surge or rotating stall) was determined just as the compressor began to repressurize, the total discharge volume became important only at this point.

As the compressor tried to recover, it began to repressurize the volume behind it. If the discharge valve was choked, the compressor communicated only with the volume up to the discharge valve, which was the plenum volume. However, if the valve was unchoked, the compressor communicated with the volume in the plenum and in the discharge ducting. The total volume including the ducting was, of course, much larger than the plenum volume alone. If the valve was unchoked, ±20% changes in plenum

volume would have been almost insignificant compared to the total volume. In fact, these comparatively small changes in volume would have been nearly unnoticed by the compressor. The effect: little apparent variation in instability behavior based on plenum volume changes.

Once the compressor began to surge or stall based on the combined volume, it was "locked" into that behavior. This was so because when the discharge valve again became choked, the compressor had already either recovered or not recovered. Therefore, the plenum volume alone was not a factor in determining whether the compressor surged or went into rotating stall. However, the plenum volume did help determine the surge frequency, since the compressor had to repressurize only the plenum volume once the valve again became choked.

According to a lumped-parameter model run by Gamache [21], a rotating stall event can be initiated during the near zero flow portion of a surge cycle by means of a forcing function. Zero mass flow occurs just before the minimum blowdown pressure, which is almost precisely where the hypothesis says the delineation between surge and rotating stall was made. So perhaps it is true that the character of a compressor instability event, whether it is surge or rotating stall, is definable at a minimum of two locations on the compressor characteristic: near stall and near zero flow.

It remains to be seen if this hypothesis can be proved. Since there was no pressure data available immediately behind the discharge valve, it was impossible to say for certain that the discharge valve was indeed unchoked for the estimated period of time. Extremely brief periods of unchoked flow would probably not have affected compressor instability

behavior, so it is critical to this hypothesis that the valve be unchoked for some unspecified minimum amount of time. Further, there was no way to be sure at what point compressor instability behavior was irrevocably defined. Therefore, this hypothesis remains interesting but none-the-less unproven.

6.2.4 Combustor insert filler volume

In the actual engine, the volume immediately behind the compressor discharge is taken up by the combustor. Unfortunately, it was difficult to design variable volume hardware which would allow the combustor volume to vary without upsetting the flow path. To solve this problem, the test engineers made the assumption that flow velocity inside the combustor itself was low, which allowed them to replace the volume inside the combustor with an open plenum volume just aft of the combustor location. At low flow velocities, it would not matter where the volume was located. Therefore, the variable volume hardware could be placed in this alternate location without upsetting the flow path.

The combustor flow path was maintained by the incorporation of a hollow insert (filler volume) as shown in Figure 3.4. Four 6.35-mm holes were drilled through the insert walls to allow air to circulate between the filler volume and the discharge plenum volume. These holes were included so that during steady-state operation the pressure inside the insert could equalize with the pressure in the discharge plenum. This reduced the risk of pressure induced stresses which could cause deformation or damage.

Although interaction between the volumes was desirable during steady-state operation, it was not during transient operation. The small, 6.35-mm hole size was originally chosen

so that during transient operation, the volume inside the insert would not interact with the discharge plenum volume. To verify this, a simple flow model was written to see if the air mass inside the combustor could have significantly contributed to the overall compressor mass flow during a pressure transient. The model, which was coded in FORTRAN for computer use, was fundamentally the same model used to estimate flow behavior in the discharge ducting.

The same sinusoidal surge representation and initial conditions used in the discharge duct model were used for the filler volume model. Unlike the duct volume model, where the direction and amount of mass flow through the flow openings were not necessarily the same or equal, the geometry of the insert guaranteed that the mass flows through the four holes would be equal and in the same direction at all times. Thus the flow areas of all four holes were summed so that the model could treat all four holes as a single opening. For the purposes of comparison, the model was also run using a step drop in pressure as an input. This was done to determine how long the filler volume would take to blow down with a constant imposed plenum pressure as opposed to a varying one. For consistency, the minimum pressure in the step pressure drop was set equal to the average pressure of the sinusoidal surge representation.

The results from the model are shown in Figures 6.17 and 6.18. In Figure 6.17, filler volume pressure and mass flow are shown as a function of time. As expected, the pressure fell exponentially toward some minimum value and the mean mass flow approached zero during the simulated surge. Even at its peak value, the mean filler volume mass flow was far smaller than the total mass flow. According to the model, the

mean mass flow out of the filler volume never exceeded 0.2% of the total mass flow. This is shown in Figure 6.18. The blowdown period observed during simulated surge was also long (>15 seconds) when compared to that observed during the step drop in pressure. The typical time length of a recorded transient from this test was less than 2 seconds, so little air was likely to have escaped from the filler volume during that time. It is unlikely that this small amount of air contributed significantly to the instability behavior of the test compressor, so it was possible to conclude that the filler volume had little or no effect on the S/RS boundary in this compressor based on these results.

6.2.5 Other possible sources of extra discharge volume

The possibility of other sources of volume in and around the compressor discharge was investigated by closely examining the design drawings and querying those personnel who actually worked with the test compressor. Neither the drawings nor the experiences of those questioned could account for any significant amount of extra discharge volume. A certain amount of volume related to the seals and connections to the discharge ducting existed, but these were clearly negligible. There were no other sources of extra discharge volume other than the filler volume and discharge ducting as already discussed in Sections 6.2.4 and 6.2.5.

6.2.6 Choked flow in the rear stages of the compressor

Earlier in this report, the stage-by-stage compressor model DYNTECC was used to demonstrate the possibility of extra volume affecting the S/RS boundary behavior of this compressor. One of the basic assumptions which allowed this model to be used was that neither sonic nor supersonic flow occurred anywhere in the model except at the discharge.

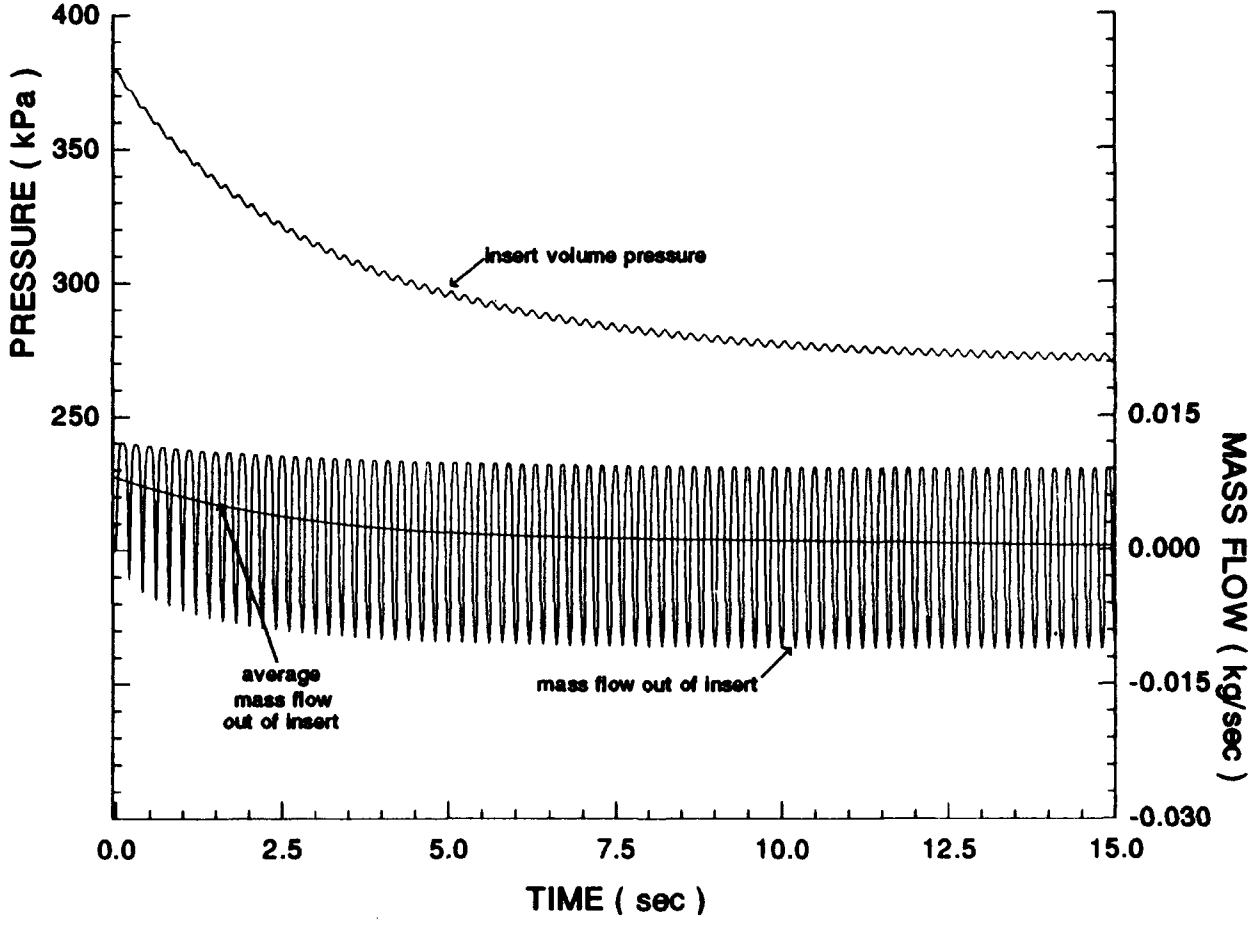

Figure 6.17 Insert volume dynamic behavior estimate

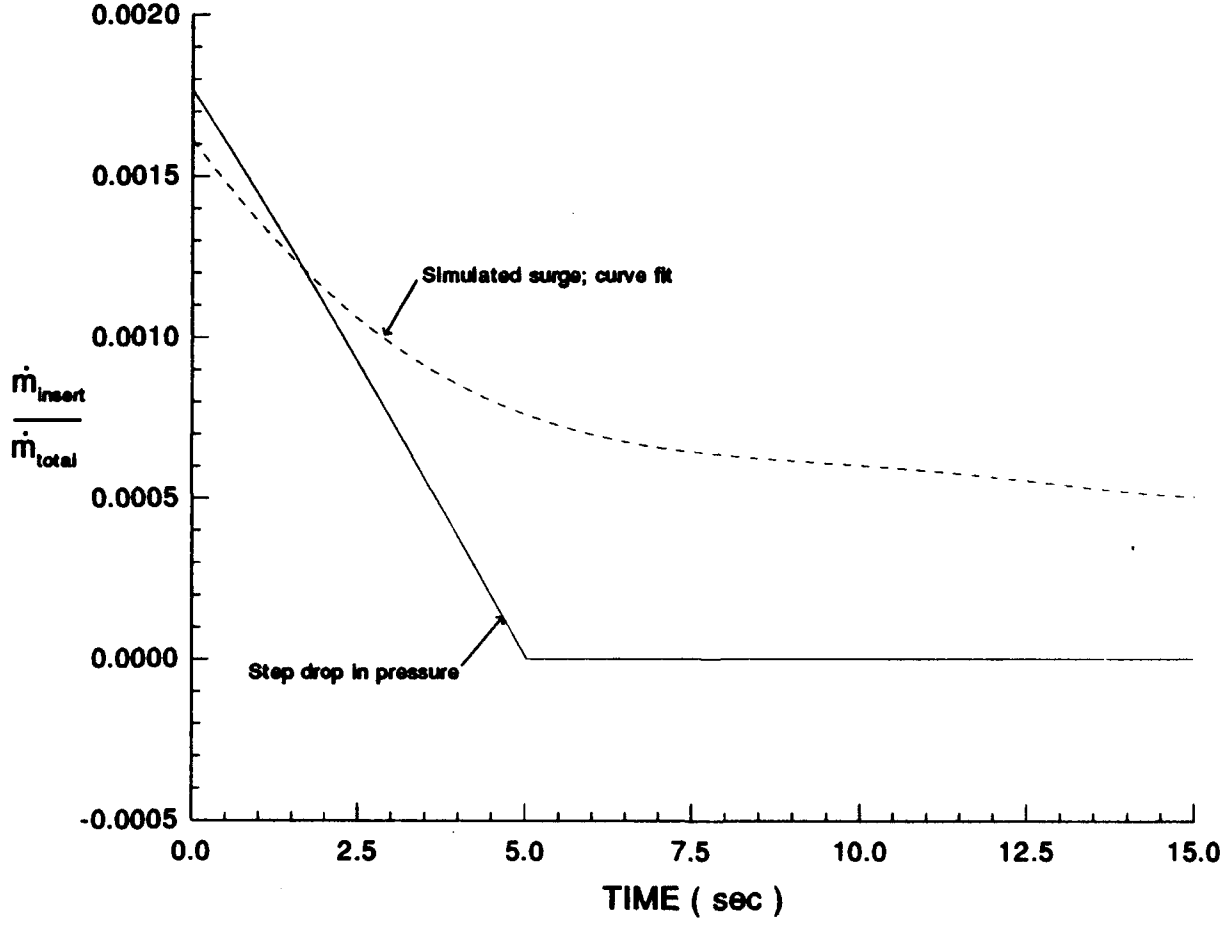

Figure 6.18 Insert volume mass flow ratio

In fact, if the input geometry were such that sonic flow occurred, the model would have failed utterly.

In his technical report, Copenhaver [2] suggested that the unblocked portion of the tenth stage rotor was probably choked during rotating stall. In the model, this is accounted for in the tenth stage characteristics. When the surge data used in this report were reviewed, the possibility of choked flow in the exit stator row was also discovered. Due to the stator-rotor stage definition used during the compilation of the stage characteristics, the flow conditions in the exit stator row may not have been included in the tenth stage characteristics. Furthermore, DYNTECC does not model flow through blade rows, so it is possible that instances choked flow occurred in the exit stator row of the actual compressor that were not accounted for in the model.

Even if the tenth stage characteristics included exit stator flow conditions, another assumption made in order to use the DYNTECC model could also be invalidated by the possibility of choked exit stator flow. When compiling the stage characteristics for use with the DYNTECC model, it was necessary to assume that the stall characteristics for 78.5% speed could be substituted for those at 81% speed. Since the compressor surged at 81% speed, and the researchers responsible for the compressor did not want to risk causing damage to the compressor or the facility, steady-state data were not obtained under those operating conditions. If the exit stators did choke during surge but not during rotating stall, this could have caused the 78.5% and 81% speed stall characteristics to differ greatly. This would invalidate the assumption of similar stall characteristics at 78.5% and 81% speed.

To explore the possibility of choked flow in the stators during surge, a simple isentropic flow model was devised. Using the high-response static and total pressure data from the compressor discharge, the Mach number in the exit stator row was estimated. The flow area through the stator row was critical in these estimates. Since the flow area depends entirely upon the flow angle through the exit stator row, three different values for the flow area were run. These three different values represented the effect three different flow angles had on the flow area in the stator row. Boundary layer effects were ignored in these calculations, so the effective areas are smaller than those used in this model. This would cause the stators to become choked more often than the model predicted. Some of the model results are shown in Figure 6.19 and Table 6.4.

According to the model, flow through the stators may have been choked for time periods of up to 16 milliseconds. These possible periods of choked flow always occurred during the repressurization phase of a surge cycle. Shorter time periods were expected in those cases where the plenum volume was smaller, since it takes less time to repressurize smaller volumes. The apparent disagreement with this trend at 120% volume is probably not significant; only three surge cycles at that speed and volume were available for averaging. Although these data are interesting in a qualitative sense, it is important not to attach too much significance to these calculations. Unfortunately, there was insufficient data available to determine the flow angle in the exit stator row, so there was no way to prove that the stators were choked or unchoked during any of the documented surge or rotating stall events.

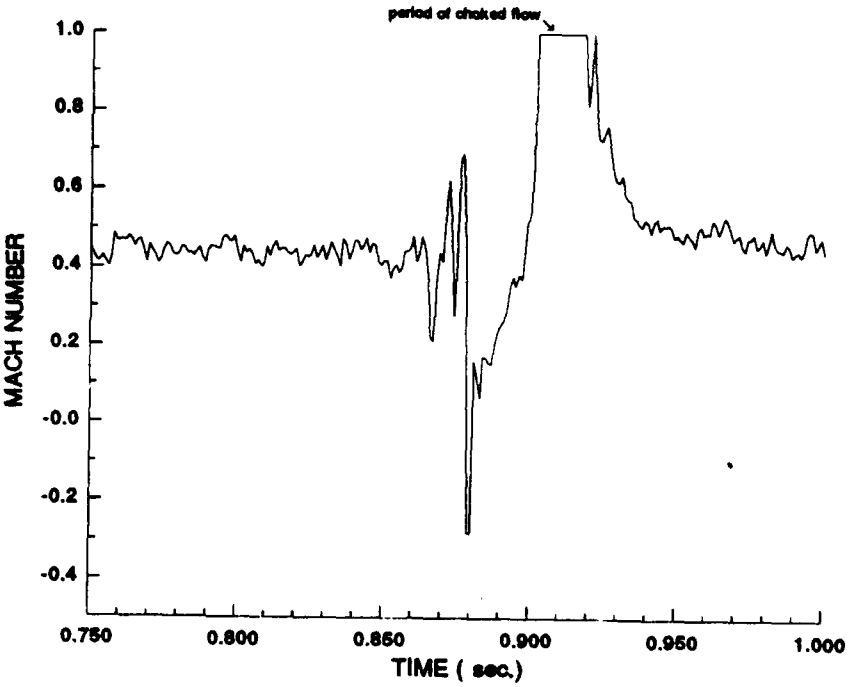

Figure 6.19 Estimated Mach number in exit stator row during surge, 81% speed, 100% plenum volume, 37° flow angle

Table 6.4 Estimated time periods of choked stator flow during surge, 81% speed

	-10° Flow Angle (37°)	Nominal Flow Angle (47°)	+10° Flow Angle (57°)
80% Volume	4 msec	0	0
100% Volume	16 msec	2 msec	0
120% Volume	7 msec	2 msec	0

6.2.7 Other possible reasons for S/RS boundary behavior

Several other possible reasons for the unexpected S/RS boundary behavior abound. One item that could have had a significant affect on the instability behavior of this compressor, but was almost completely ignored in this report, was the upstream volume. The DYNTECC model included upstream volume up to the bellmouth, but there was a large amount of volume in front of the bellmouth, including the flow conditioning barrel, that went ignored. In the case of the B parameter calculations, virtually none of the volume in front of the compressor was considered. Only volume up to ~0.20 meter in front of the inlet guide vanes was included in the form of the effective compressor length, L_c. Exactly how much of the upstream volume should have been used in the instability behavior estimates was not clear. It was decided that much of the forward volume could be ignored since the flow velocities upstream of the bellmouth were relatively low. It is the feeling of this researcher that omitting much of the upstream volume was justified, but it is certainly possible that much more of the upstream volume should have been considered in both the stage-by-stage model and in the B parameter calculations. Determining how much of this volume to use is a recommendation for future research.

As previously mentioned, the simple, lumped-parameter model used to estimate the S/RS boundary does not account for the compressibility of air across the compressor itself. It is, therefore, possible that had this been somehow included, the estimated behavior would have matched the observed behavior. This is doubtful, since the S/RS boundary didn't seem to move at all. It seems likely that even including compressibility the lumped-parameter model would have predicted some shift in the S/RS boundary,

although this is not necessarily so.

After completing this research effort, it was apparent that the S/RS boundary behavior could not be predicted with existing theories unless certain assumptions concerning the flow volume were made. Therefore, it seems likely that assumptions concerning the flow volume are the reason for the disagreement between observed and predicted S/RS boundary behavior.

7.0 SUMMARY AND CONCLUSIONS

This report presented some of the surge data associated with a 10-stage core compressor test conducted at the CRF. Of the at least 24 documented instances of surge observed during this test, 12 were used in this report. Pressure data from three different axial locations in the compressor were used to help characterize the surge events. It was clear from this data that the surge/rotating stall boundary did not move significantly when the discharge plenum volume was changed ±20%. Possible reasons for this lack of movement were discussed, and the results suggest that care must be taken when applying current theories to the CRF compressor.

The following are observations and conclusions concerning the general character of the 12 surge events used in this research effort:

1. The 12 surge events documented in this report are examples of classic surge. The rapid blowdown and slower repressurization periods observed in each surge cycle are typical of this type of surge. Further, the surge frequencies of ~5 to ~7 cps are small compared to the rotating stall frequencies of ~50 to ~100 cps, which were also typical.

2. Periods of reverse flow during the blowdown period of each surge cycle were evident. Data obtained from pressure instrumentation in the compressor discharge demonstrate this conclusively.

3. Plots of discharge pressure as a function of time showed that rotating stall occurred simultaneously with surge during the blowdown periods of all 12 surge events. If they

had continued past the blowdown period to become fully developed, the stall cells would have exhibited passage frequencies of 70 to 100 cps, which are completely reasonable for the speeds at which they occurred.

4. The compressor was tested using three different discharge plenum volume values: 80%, 100% and 120% nominal volume. The surge frequency may have changed slightly when the plenum volume was changed. There is insufficient data to prove this, and even if such a change occurred, it was very slight indeed (from –4.3 to –4.8 cps at 81% speed).

The following are observations and theories concerning the behavior of the surge/rotating stall boundary:

1. Theory predicts a shift in the surge/rotating stall boundary when the plenum volume is altered, but the test compressor showed no such shift. Indeed, the surge/rotating stall speed boundary seemed to remain constant despite plenum volume changes.

2. Six theories which attempt to explain the constant surge/rotating stall boundary were formulated and investigated in this report. Table 7.1 lists these theories and the results of the investigations concerning their merit. No theory was proved to be the cause of the surge/rotating stall boundary behavior. However, the unchoked discharge valve theory was found to be the most reasonable explanation. After reviewing the research conducted with other high-pressure test compressors, such as the E^3, it seems possible that this sort of behavior is not unique to this compressor. If true, this theory and explanation differentiates the surge behavior of low- and high-pressure compression systems.

Table 7.1 Surge/rotating stall boundary behavior theories

Theory	Possible Affect on Instability Behavior	Proven or Disproved	Actual Affect
Unchoked flow through discharge valve allowed extra volume to be perceived by the compression system	Increase in likelihood of surge instead of rotating stall; reduction in surge frequency	Neither (Unchoked flow did occur, but possibly for only very brief periods)	Unknown
Choked flow through exit stators limited mass flow through compressor	May alter the stage characteristics used by DYNTECC to simulate S/RS boundary behavior	Neither	Unknown
Combustor filler volume contributed to the overall discharge volume despite being designed not to do so	Increase in likelihood of surge instead of rotating stall; reduction in surge frequency	Disproved	None
More of the inlet volume should have been considered in the compressor models and S/RS boundary predictions	Unclear; probable increase in likelihood of surge instead of rotating stall; reduction in surge frequency	Neither (Not researched)	Unknown
Extra volume from seal areas and ducting connections contributed to the discharge volume	Increase in likelihood of surge instead of rotating stall; reduction in surge frequency	Disproved (No extra volume from seals or connections)	None
Inclusion of compressibility effects into S/RS boundary-prediction methods may cause the predictions to agree with the test data; perhaps there was supposed to be no shift in the S/RS boundary	Unknown	Neither (Not researched)	Unknown

3. Two of the theories presented in Table 7.1 were not researched, but were formulated as a result of this research effort. They are also listed among the recommendations as topics for future research.

8.0 RECOMMENDATIONS

Much information concerning the surge behavior of a high-speed, multi-stage compressor has been presented in this report. More such information should be generated to help continue the investigation of both the surge/rotating stall boundary behavior of this compressor and of the surge behavior of high-speed compressors in general. Certainly, a follow-on test of this or a similar compressor is recommended, with some of the following improvements included.

1. High-response pressure and temperature instrumentation should be placed at the entrance and exit of the discharge valve. Similar instrumentation should be placed at the entrance and exit of both the exit stator row and the tenth stage. This would allow researchers to determine if choking is occurring at the two locations.

2. Surges of longer duration should be induced and recorded. Further, the discharge valve area should be held constant for a significant portion of those surge events. The fundamental problem with doing this is that stresses in the rotor may become too extreme if the compressor remains in surge for too long. However, a longer surge event with constant discharge valve area would allow a more confident estimate of the surge frequency to be made. Comparing individual surge events with one another and with model generated data would also be easier.

3. More steady-state, high-response data should be recorded in conjunction with the time-averaged data points. During this test, researchers sometimes turned off the analog tape recorders during steady-state data points in an effort to conserve tape. Unfortunately,

this made calibration of the high-response instrumentation more difficult. Without the time-averaged data, calibration of the high-response instruments depends on either the bench calibrations or the individual monitor points, both of which are less accurate than using the time-averaged data. It was fortunate that this researcher found sufficient time-averaged/high-response data overlap to calibrate the high-response instruments, but these calibration points sometimes numbered only three or four points in a day. More calibration points are desirable. The more calibration points there are, the more accurate the calibration equations become.

Even if more surge data are not obtained for this compressor, there are several items which should receive more attention if research concerning the surge/rotating stall boundary of this compressor continues.

1. Consideration should be given to including more inlet volume in both the lumped-parameter and the stage-by-stage models. The additional volume may help account for the surge behavior of this compressor.

2. The ability to model choked flow in the compressor blade passages should somehow be incorporated into DYNTECC.

REFERENCES

1. Emmons, H. W., C. E. Pearson and H. P. Grant. *Compressor Surge and Stall Propagation.* Transactions of the ASME 77 (May 1955): 455-469.

2. Copenhaver, W.W. *Stage Effects on Stalling and Recovery of a High-Speed 10-Stage Axial Flow Compressor.* Air Force Technical Report, WRDC-TR-90-2054. June, 1990.

3. Copenhaver, W.W. and Okiishi, T.H. *Rotating Stall and Recoverability of a High-Speed Ten-Stage Axial-Flow Compressor.* AIAA-89-2687. July 1989.

4. Greitzer, E.M. *Surge and Rotating Stall in Axial Flow Compressors. Part I: Theoretical Compression System Model.* Transactions of the ASME, Journal of Engineering for Power 98 (April 1976): 190-198.

5. Greitzer, E.M. *Surge and Rotating Stall in Axial Flow Compressors. Part II: Experimental Results and Comparisons with Theory.* Transactions of the ASME, Journal of Engineering for Power 98 (April 1976): 199-217.

6. Small, C. J. and J. T. Lewis. *High Speed Compressor Rig as a Stall Recovery Research Tool.* Presented at the AIAA/SAE/ASME/ASEE 21st Joint Propulsion Conference, AIAA-85-1428. June 1985.

7. Hosny, W. M., C. H. Lenhardt, H. T. Liu, R. C. Lovell, and W. G. Steenken. *Energy Efficient Engine (ICLS/IOC) High Pressure Compressor Component Performance Report.* NASA CR-174955. August 1985.

8. Hosny, W.M. and W.G. Steenken. *Aerodynamic Instability Performance of an Advanced High-Pressure-Ratio Compression Component.* Presented at the AIAA/ASME/SAE/ASEE 22nd Joint Propulsion Conference, AIAA-86-1619. June 1986.

9. Moore, F. K. and E. M. Greitzer. *A Theory of Post-Stall Transients in Axial Compression Systems: Part I - Development of Equations.* ASME Paper No. 85-GT-171. March 1985.

10. Greitzer, E. M. and F. K. Moore. *A Theory of Post-Stall Transients in Axial Compression Systems: Part II - Application.* ASME Paper No. 85-GT-172. March 1985.

11. Sugiyama, Yokichi. *Surge Transient Simulation in Turbo-jet Engine.* Ph.D. Dissertation, University of Cincinnati. 1984.

12. Davis, Milton W. *A Stage-By-Stage Post-Stall Compression System Modeling Technique: Methodology, Validation, and Application.* Ph.D. Dissertation, Virginia Polytechnic Institute and State University. 1986.

13. Davis, M. W. and W. F. O'Brien. *A Stage-by-stage Post-stall Compression System Modeling Technique.* Presented at the AIAA/ASME/SAE/ASEE 23rd Joint Propulsion Conference. AIAA-89-2088. June 1987.

14. Boyer, K. M. and W. F. O'Brien. *Model Predictions for Improved Recoverability of a Multistage Axial-Flow Compressor.* Presented at the AIAA/ASME/SAE /ASEE Joint Propulsion Conference. AIAA-89-2687. July 1989.

15. Gorrell, Steven E. *An Experimental Study of Exit Flow Patterns in a Multistage Compressor in Rotating Stall.* Air Force Technical Report, WRDC-TR-90-2083. November 1990.

16. Bloch, G.S. *A Wide-Range Axial-Flow Compressor Stage Performance Model.* Air Force Technical Report, WL-TR-91-2125. April 1992.

17. Copenhaver, W. W. and C. J. Worland. *Acquisition of Unsteady Pressure Measurements from a High-Speed Multi-Stage Compressor.* ASME Paper No. 88-GT-189. June 1988.

18. Lewis, Jim. Telephone conversation with United Technologies engineer. Febuary, 1993.

19. Small, Clay. Telephone conversations with United Technologies engineer. November, 1990.

20. Davis, Milton W. Various meetings and technical dialogues with Sverdrup Technology Inc. engineer, 1990-1992.

21. Gamache, R.N. *Axial Compressor Reversed Flow Performance.* Ph.D. Dissertation, Massachusetts Institute of Technology. May 1985.

22. Abernathy, R. B. and J. W. Thompson Jr. *Handbook of Uncertainty in Gas Turbine Measurements.* AEDC-TR-73-1, February 1973.

APPENDIX A: Compressor Research Facility Description

Appendix A briefly describes the layout and operation of the CRF. Figure A.1 shows the buildings that comprise the CRF while Figure A.2 shows a schematic of the test chamber.

The data presented in this report were obtained during a compressor test carried out at the Compressor Research Facility (CRF) at Wright-Patterson AFB. A rough layout of this facility is shown in Figure A.1. The operations building contained the test chamber, signal conditioning equipment, and compressor drive motors. The electrical power conditioning building contained such equipment while the test building contained the computer and test compressor control systems.

The test was controlled from the facility control room located in the test building. Commands to carry out all test procedures were sent from the control room via a monitor computer, located in the computer room, to four control computers located in the signal conditioning room. The control computers provided input to the electrical power conditioning equipment which powered the drive motors. The control computers also controlled services that support variable geometry devices on the test compressor.

The test compressor was driven by 22.37-MW (30,000 hp) synchronous electric drive motor. The test compressor speed range was provided through two speed increasing gear boxes. A speed range of 3,000 to 15,000 RPM was required for this test compressor. Within this range, the compressor speed was changed by varying the frequency of the current supplied to the drive motor. Frequency variation of the supplied current was accomplished by the electrical power conditioning equipment.

The test compressor was mounted inside a 6.1-m (20.0 ft) diameter test chamber, shown in Figure A.2. Atmospheric air passed through filtering equipment, five inlet valves, and a series of flow conditioning elements before it was finally drawn into the test compressor. Air was discharged from the test compressor into the atmosphere through

the throttling valve, the facility discharge collector, and discharge ducting (see Figure A.2). Exit flow from the test compressor was monitored by a 48.26-cm (19 in) throat diameter venturi positioned in the discharge ducting approximately 30.48 m (100 ft) downstream of the compressor exit.

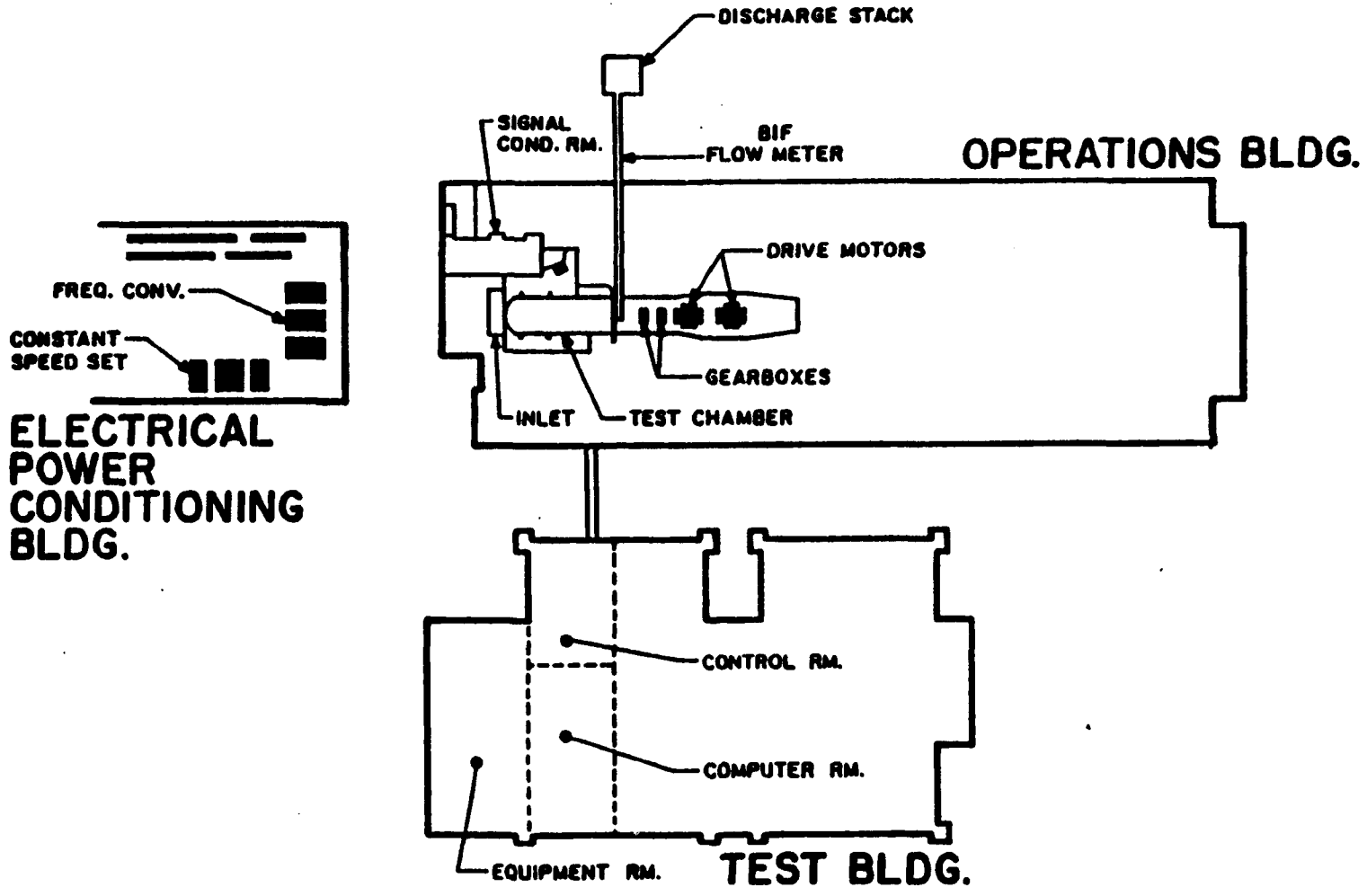

Figure A.1 Compressor Research Facility layout

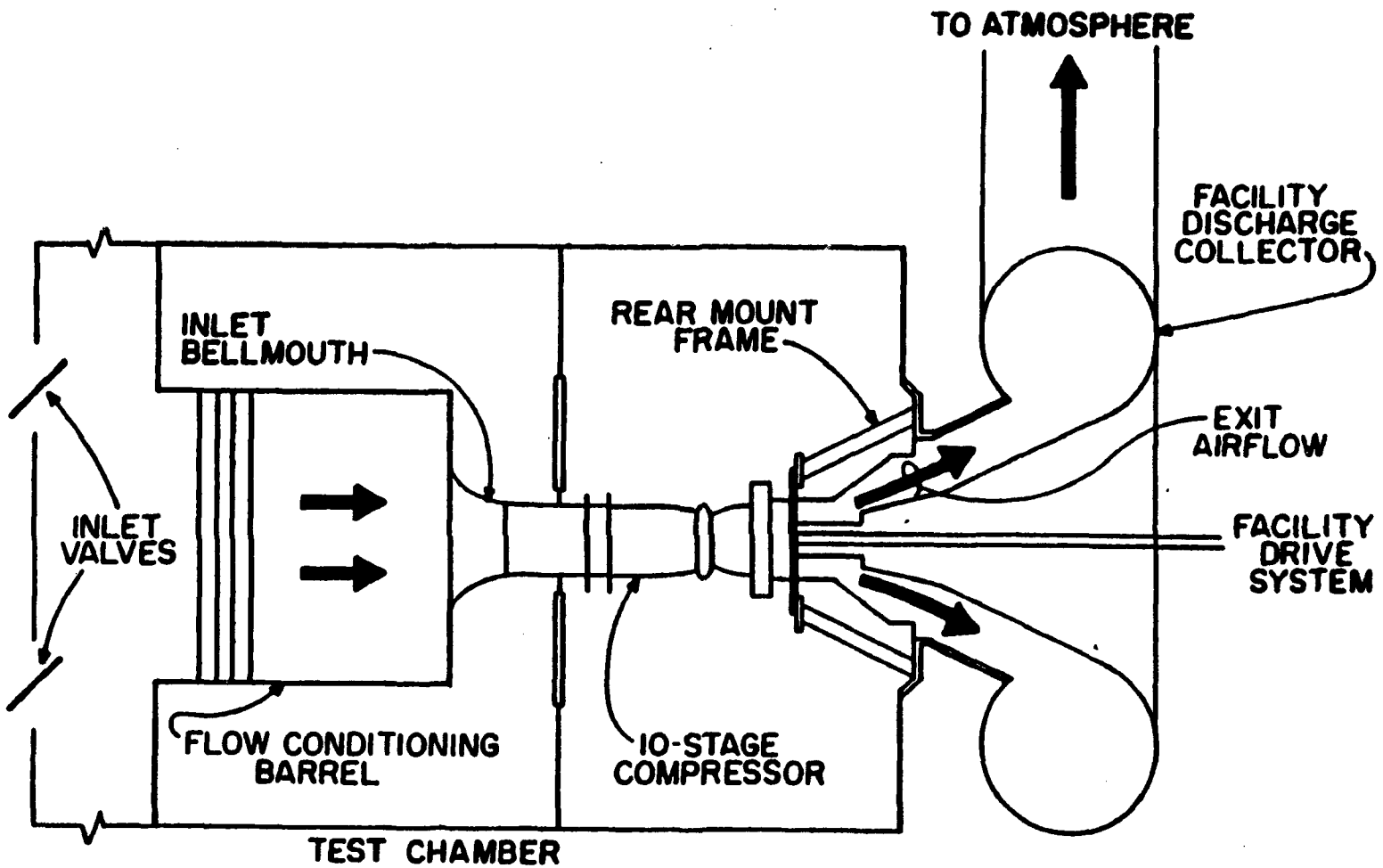

Figure A.2 Test compressor installation in test chamber

APPENDIX B: Data Acquisition

Appendix B details the high-response and time-averaged data acquisition methods used to gather data during the compressor test. Measurement uncertainty is also discussed. Figures B.1 and B.2 show schematics of the high-response and time-averaged systems, respectively.

During the CRF compressor test, three methods of pressure data acquisition were employed: high-response, close-coupled, and time-averaged data acquisition. These three methods acquired data with frequency responses of 200 Hz, 70 Hz, and 0.5 Hz respectively. Since only high-response and time-averaged data are presented in this report, close-coupled data acquisition will not be covered in detail here. For details on the closed-coupled data acquisition system, see References 2 and 3.

High-Response Data

During the compressor test, 52 channels were designated as high-response pressure measurement channels. Each channel had a nominal frequency response of 200 Hz, which was adequate to document the fluctuating pressures expected. Only pressure fluctuations with fundamental frequencies of less than 50 Hz were anticipated to be of importance. This is higher than the fundamental frequencies documented during the surge events discussed in this report. Only 6 of the 52 available high-response pressure measurement channels were used in this report.

The pressure transducers used to obtain the high-response pressure measurements were Kulite model# XCQ-25's (inlet), XCQ-150's (discharge) and XTEL-190's (inlet stage 10). Each of these transducers, with the exception of those at the inlet, was contained in a special cooling jacket. Cooling was required to assure survivability and stability of the transducers in the test environment. Transducer ranges were based on the maximum pressures expected during testing, which occurred at 87 percent corrected rotor speed, the maximum compressor speed tested. For the configuration and placement of the high-response pressure transducers used in this report see Section 3.1.

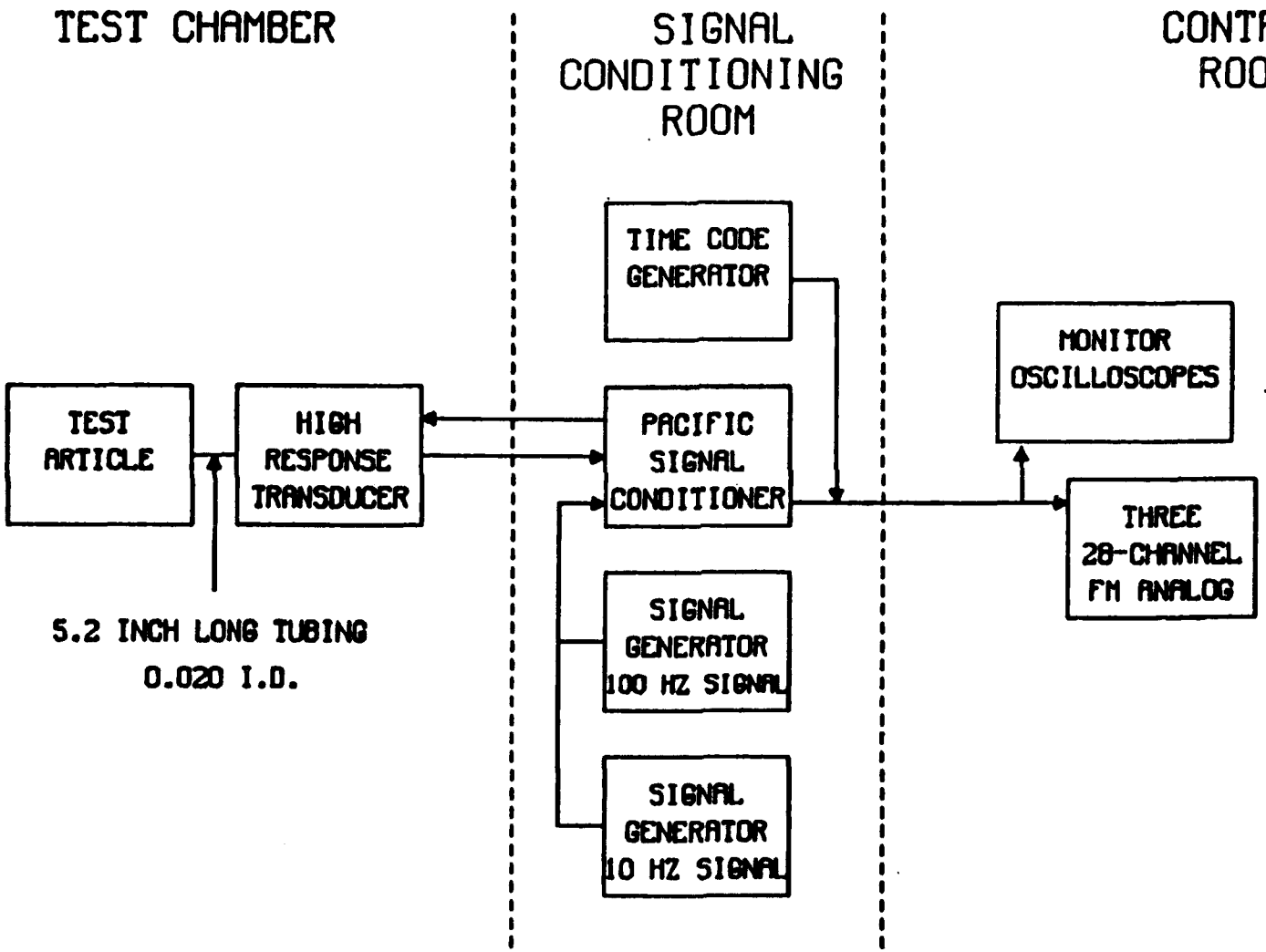

Figure B.1 High-response data acquisition system schematic

A schematic of the high-response data acquisition system is shown in Figure B.1. In this system, Pacific Model #8255 signal conditioners provided excitation voltages to the pressure transducers and handled transducer output signal filtering and amplification during testing. Furthermore, the conditioners provided ac/dc coupling for the voltage signals from the transducers. Preset cut-off filter frequencies of 10 Hz, 100 Hz, 1 kHz, and wide band were available with these conditioners. The transducer output signals were attenuated by a two pole Bessel filter with a -3-db attenuation at the cut-off frequency chosen. The cut-off frequency for this test was set at 1 kHz to assure the desired frequency response of 200 Hz would be obtained. Transducer output was dc coupled, so that the dc component could be used in calibration procedures to determine actual pressures at the measurement locations (see Section 5). Care was taken to avoid saturation of the amplifiers and the recording equipment since the dc components of the transducer output signals were being retained.

The high-response pressure measurements were recorded on three Datatype model #2808, 28-channel recorders configured for frequency modulation (FM) recording. Each pressure channel was assigned to a track (channel) on the recorder and recorded on analog tape. Signals from each channel were recorded at a center frequency of 75.6 kHz. Frequency deviation was adjusted to allow for a maximum input signal level of 5 volts. Recording speed was set at 38.1 cm/sec (15 in/sec) which allowed for a data frequency response of 10 kHz. This is well above the required 200 Hz response. Channels that required phase correlation for post-test comparison were recorded on either all odd or all even track (channel) numbers. All high-response data presented in this report were

recorded on odd track numbers except for stage 9 static pressure data. Also recorded on analog tape were data signals indicating discharge valve position. These signals were provided by a potentiometer used to monitor the discharge valve. Like the high-response pressure transducer signals, the dc component of the potentiometer signal was retained to allow for post-test calibration.

Along with the data signals mentioned above, three other signals were recorded on the analog tapes. One track on the recorder was designated for recording of IRIG A time code, which allowed for timing resolution of 0.1 millisecond. Another track was designated for recording of the tape drive servo signal which is used to set playback speed. This is done so that any speed fluctuations in tape speed will be duplicated in playback. A third track was used to record a standard wave signal, which can be used to verify phase alignment when data recorded on two different tapes (but recorded at the same time) are compared.

Effort was made to verify that the pressure transducers remained stable on a day-to-day basis. At selected times during testing the test compressor was brought to a fixed operating point. At this "checkpoint" the dc levels of the high-response pressure transducers were noted and compared to dc levels of the previous test period. Differences in day-to-day dc levels were thereby noted. Transducer instability due to dc drift was not significant during this test. However, the daily "checkpoints" did help locate pressure transducers that were not functioning properly. The high-response transducers used in the test were fragile and not really suited to the test environment, so malfunction was not uncommon. Faulty transducers of this type were often noted and replaced where possible.

A more detailed discussion of the high-response data acquisition system used during the compressor test is presented in a paper written by Copenhaver and Worland [13].

Time-Averaged Data

Four hundred and one channels were set aside for time-averaged measurements during the compressor test. Time-averaged pressure and temperature data were taken to characterize the steady (unstalled) and quasi-steady (rotating stall) performance of the test compressor. Time averaged data were obtained in digital form during the test and recorded on digital tape. This allowed for easier conversion to engineering units during post-processing. Close-coupled data, which are not presented in this report, were obtained using the same instrumentation as the time-averaged data. These two acquisition techniques differed only in their respective data acquisition rates and number of scans made per measurement.

Time-averaged data were obtained by taking a specified number of individual samples over a specific time period and then calculating the arithmetic average. The calculated average, a voltage, was then stored and used to calculate the pressure or temperature at the measurement location. In this test, 30 individual samples were taken over a time period of 195 ms. The time-averaged sample rate (frequency response) was dictated by the maximum rate at which analog signals could be digitized and by the tube length between the pressure port and the transducer. This limited the frequency response of the time-averaged acquisition system to about 0.5 Hz. The use of 30 samples to calculate the average was based on limitations imposed by the statistical method employed to calculate measurement uncertainty.

A schematic of the time-averaged data acquisition system is shown in Figure B.2. The pressure transducers used by this system were Scanivalve model ZOC-14's (Zero-Operate-Calibrate). These were a "more rugged" type of transducer than those used by the high-response system and, therefore, more suited to this test environment. However, it was still necessary to control the temperature of the ZOC transducers in order help guarantee calibration, zero offset, and sensitivity stability. This was accomplished by a closed loop cooling system with cooling water maintained at 21.1° C (70° F). Pressure transducer signals were conditioned by Preston (model 8300-XWBRC) amplifiers. Each amplifier was capable of outputting a 10-volt signal, and each was equipped with a three-pole Butterworth-Thomson filter with selectable cutoff frequencies of 10 Hz, 40 Hz, 120 Hz, 400 Hz, and 1200 Hz. The analog-to-digital (A to D) converter saturated at 5 volts, so appropriate gains were selected for each channel to ensure that the maximum output from the amplifier was as close to 5 volts as possible. The cutoff frequency chosen for the test was 10 Hz (for time-averaged acquisition). This frequency was the lowest possible filter setting and reduced the level of 60 Hz noise in the transducer signals. After conditioning, the transducer signals were sampled by the A to D converter to provide the 30 individual samples necessary for calculation of the time-averaged measurements. The time-averaged measurements were then processed by the Data Acquisition Computer (DAC) and recorded on digital tape via the Main Computer (IBM 4341).

Performance mapping of the test compressor was accomplished by using the time-averaged data acquisition system to provide steady-state and quasi-steady-state data points

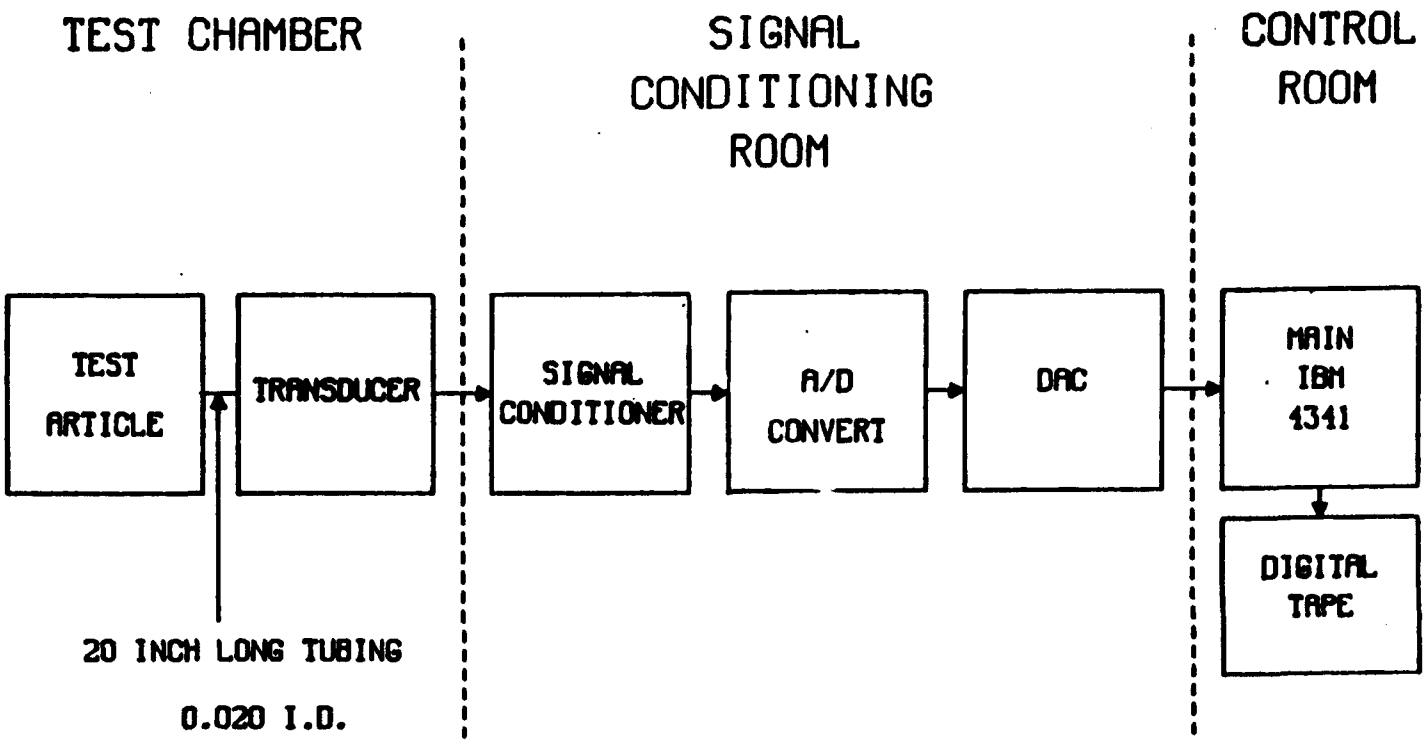

Figure B.2 Time-averaged data acquisition system schematic

for the map. At each data point, a time-averaged measurement from each relevant transducer was taken. The data obtained at each steady-state data point were then used to determine the operating characteristics of the compressor at that operating point. This information was in turn used to create a performance map of the compressor. Three minutes waiting time between each set of time-averaged measurements was the minimum time delay allowed. This was done to assure steady-state or quasi-steady-state equilibrium had been reached after each operating condition change.

In this report, time-averaged data in the form of overall compressor and individual stage characteristics was used in the mathematical models. Time-averaged data were also used to convert high-response transducer data into engineering units. The development of the stage characteristics used in this report was accomplished by Copenhaver [2] and O'Brien and Boyer [14]. The conversion of high-response data into engineering units is covered in Section 5.

Measurement Uncertainty

The method used to determine measurement uncertainty for the high-response and time-averaged acquisition methods was defined by Abernethy and Thompson [22]. The bias and precision errors were combined using the equation:

$$U_m = \pm\sqrt{(B_m)^2 + (t_{95}S_m)^2}$$

where:

B_m = bias errors based on calibration,
S_m = precision errors associated with the transducer, signal conditioning, and recording devices,
t_{95} = student T distribution weighting factor based on the number of samples used to calculate a measurement average.

The time-averaging of 30 samples resulted in t_{95} being set equal to 2 for the time-

averaged measurements. For this report, the weighting factor used for high-response measurements was also 2 because each measurement was an average of 500 samples. The estimated bias errors, precision errors and measurement uncertainties for the time-averaged measurements used in this report are listed in Table B.1. The estimated precision errors associated with the raw high-response measurements are shown in Table B.2. The bias errors associated with the high-response measurements could not be properly estimated, since all of the signal conditioning and digitization equipment added an unknown offset to all of these measurements. However, the bias errors are not important here, because they are absorbed during calibration. So long as the bias errors are assumed to be constant, the true voltage measurements provided by the high-response instrumentation are not important.

Table B.1 Time-averaged measurement uncertainty

Location & Type	Range	Bias Error	Precision Error	Measurement Uncertainty
Inlet static pressure (near transducer #1)	34.5 kPa (5 psi)	0.1529 kPa (0.02217 psi)	0.03851 kPa (0.005586 psi)	0.1712 kPa (0.02483 psi)
Stage 10 inlet static pressure (near transducer #2)	345 kPa (50 psi)	1.275 kPa (0.1849 psi)	0.2866 kPa (0.04157 psi)	0.1398 kPa (0.02027 psi)
Discharge total pressure (near transducers #3 & #5)	690 kPa (100 psi)	2.548 kPa (0.3695 psi)	0.5715 kPa (0.08290 psi)	2.793 kPa (0.4050 psi)
Discharge static pressure (near transducers #4 & #6)	690 kPa (100 psi)	2.920 kPa (0.4236 psi)	0.8956 kPa (0.1299 psi)	3.426 kPa (0.4969 psi)

Table B.2 High-response precision errors

	Range (after signal conditioning)	Precision Error
Probe Transducer #1	5 volts	7.26 mv
Probe Transducer #2	5 volts	4.33 mv
Probe Transducer #3	5 volts	7.94 mv
Probe Transducer #4	5 volts	4.78 mv
Probe Transducer #5	5 volts	13.25 mv
Probe Transducer #6	5 volts	5.23 mv

APPENDIX C: Surge Data

The high-response surge data used in this report are presented in this appendix. Seven plots showing pressure and discharge valve area as a function of time are presented for each of the 12 surge events. For those who oppose adoption of the Système International d'Unités, 1 psi ≈ 6.895 kPa.

Table C.1 Surge events

Compressor Speed	Plenum Volume	Surge Number	Stall Number*
81%	100%	1	17
		2	18
		3	19
		4	20
		5	70
	120%	6	28
	80%	7	90
82%	100%	8	7
		9	15
	80%	10	87
87%	100%	11	8
	80%	12	86

* Stall number indicates the occurance of the surge or rotating stall relative to other such events during the entire compressor test. For example, stall number 86 was the 86th "stall" of the test.

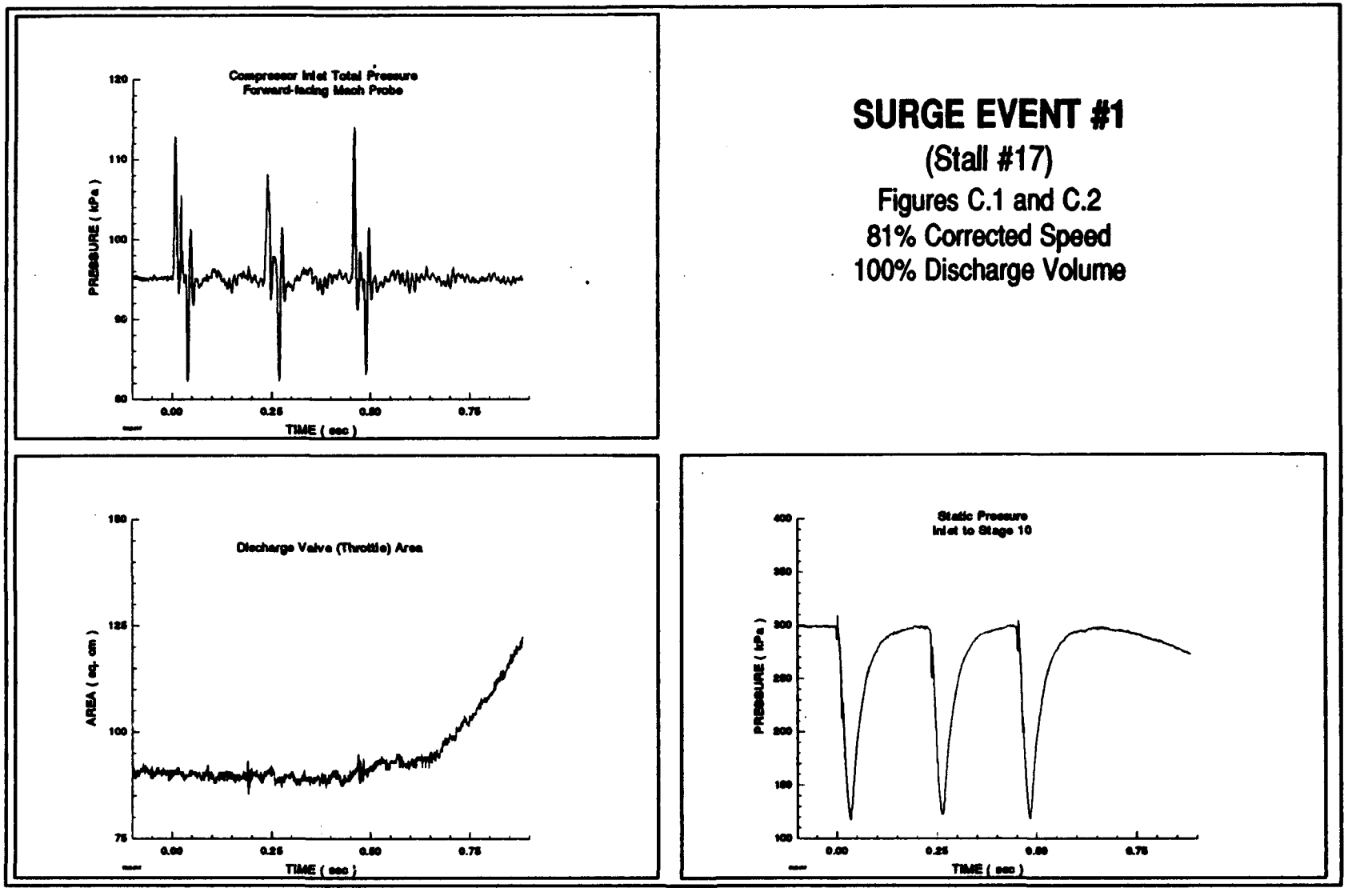

Figure C.1 Surge Event #1 Data

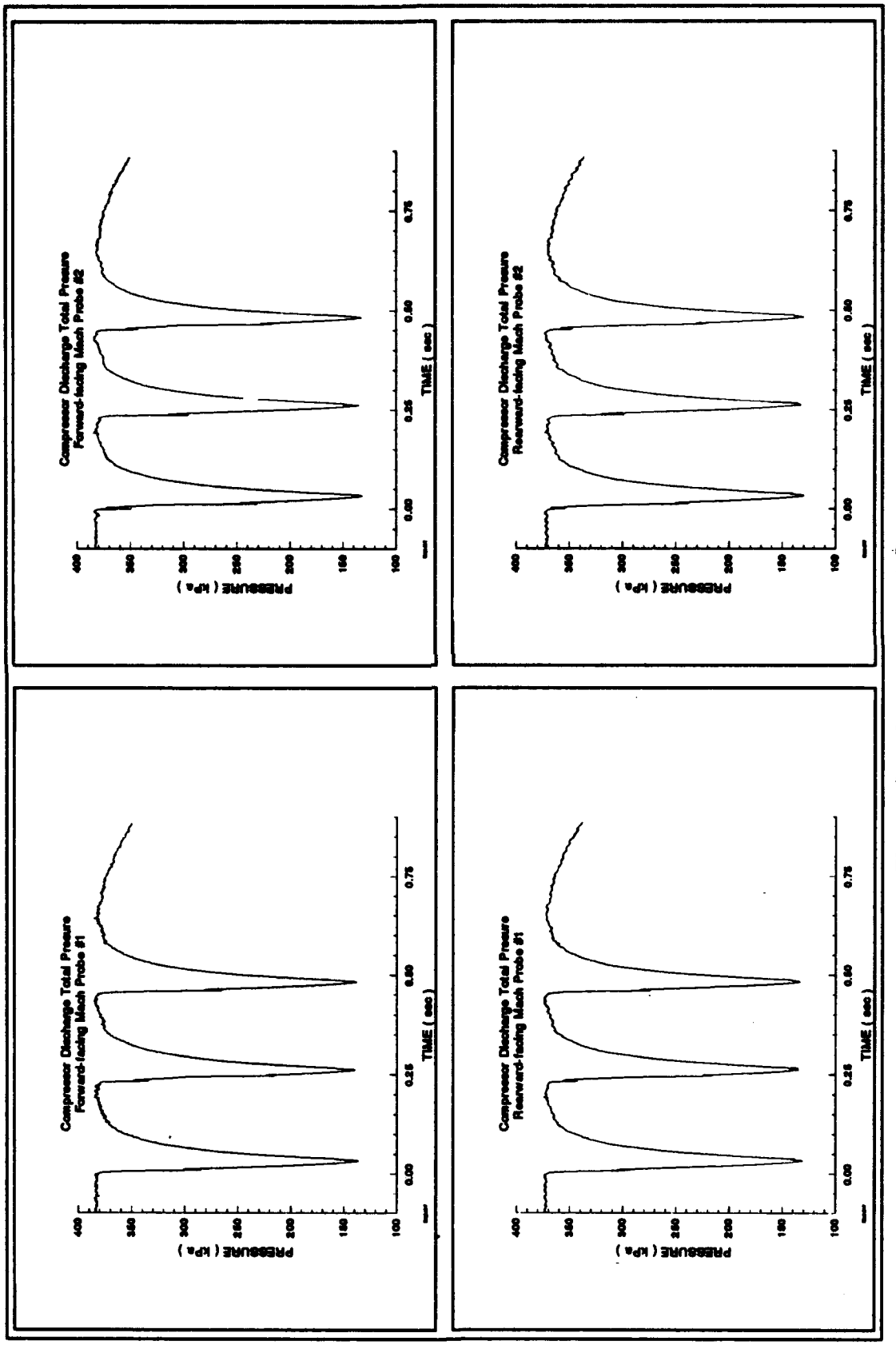

Figure C.2 Surge Event #1 Data

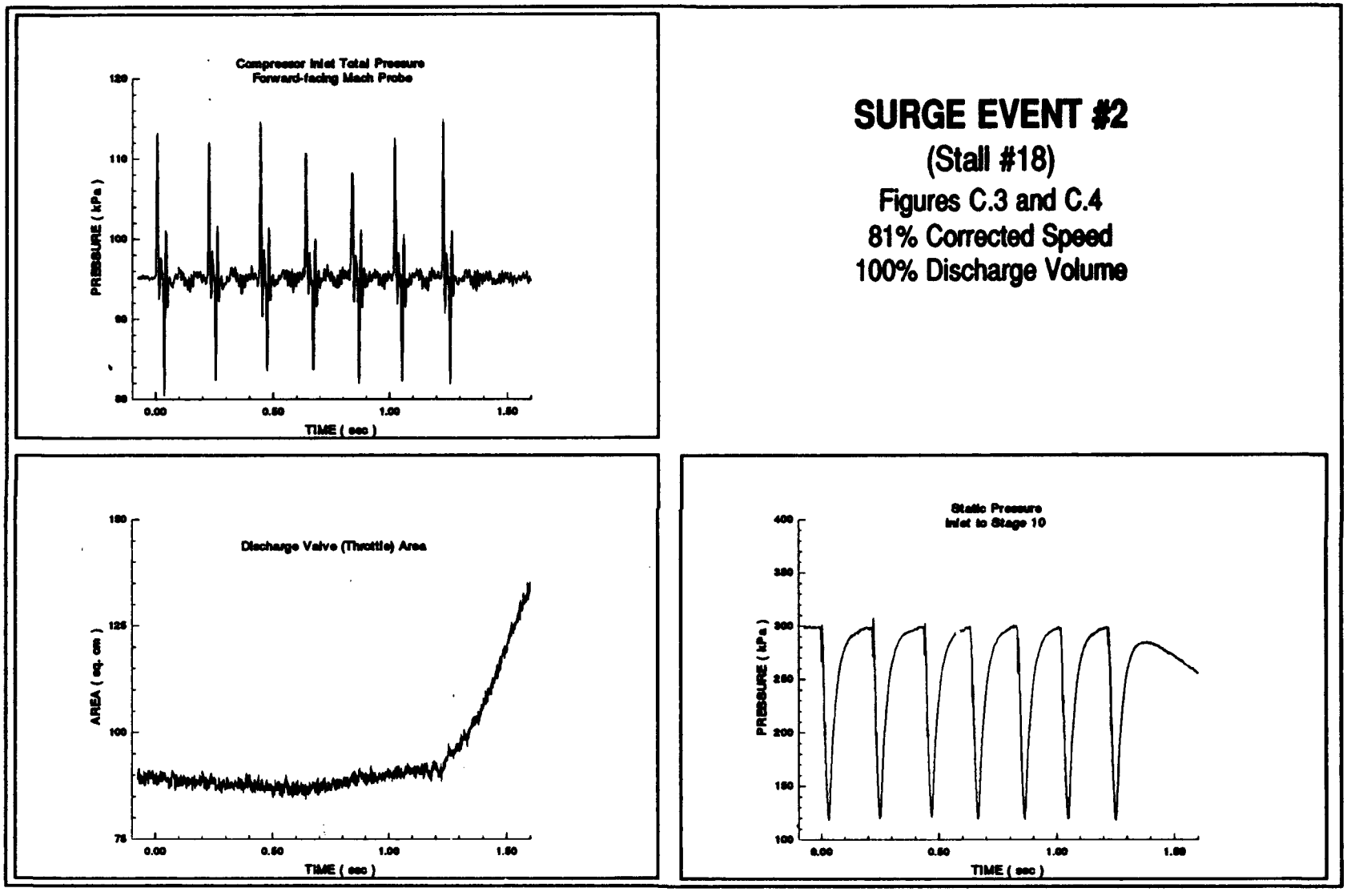

Figure C.3 Surge Event #2 Data

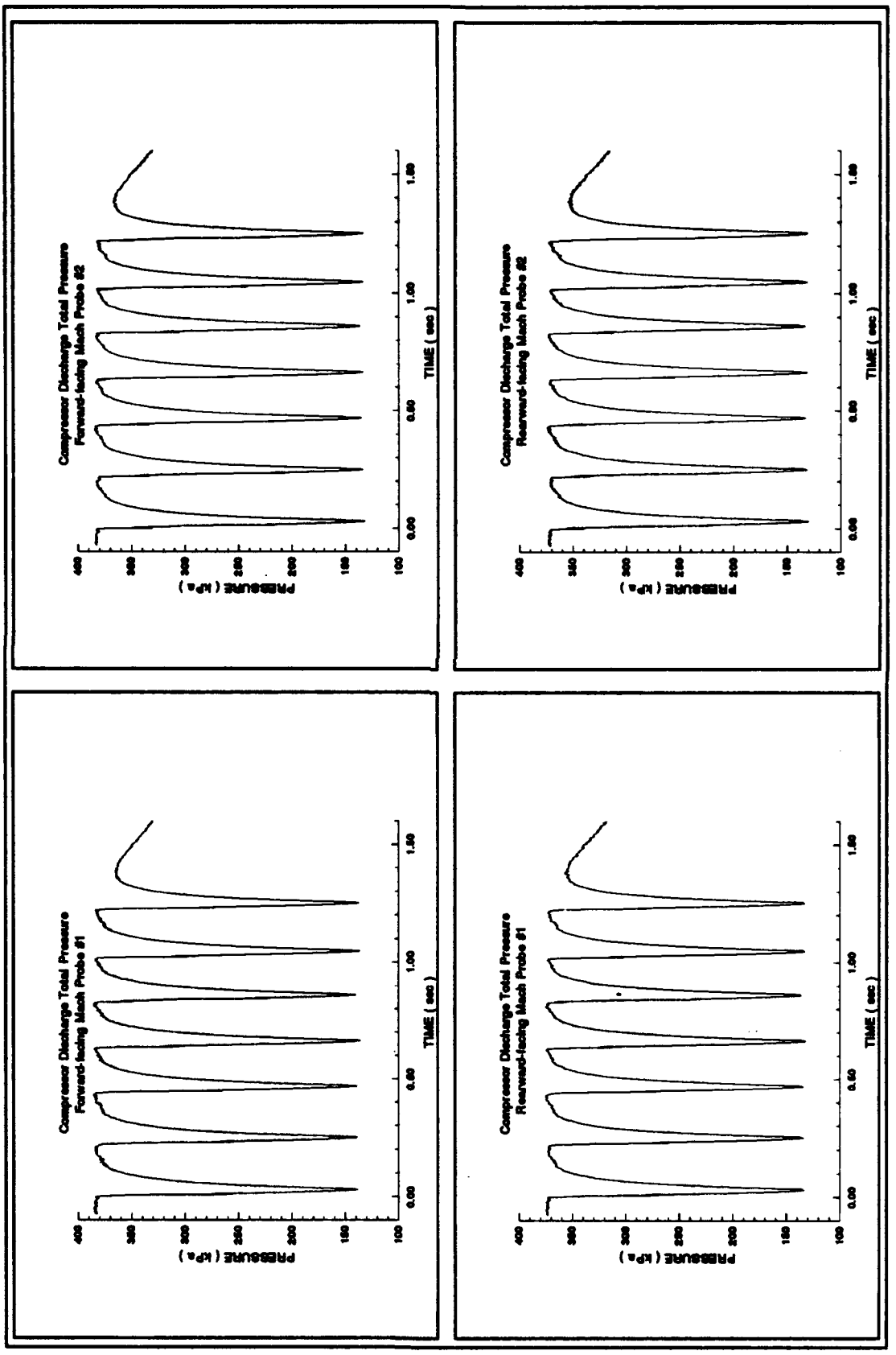

Figure C.4 Surge Event #2 Data

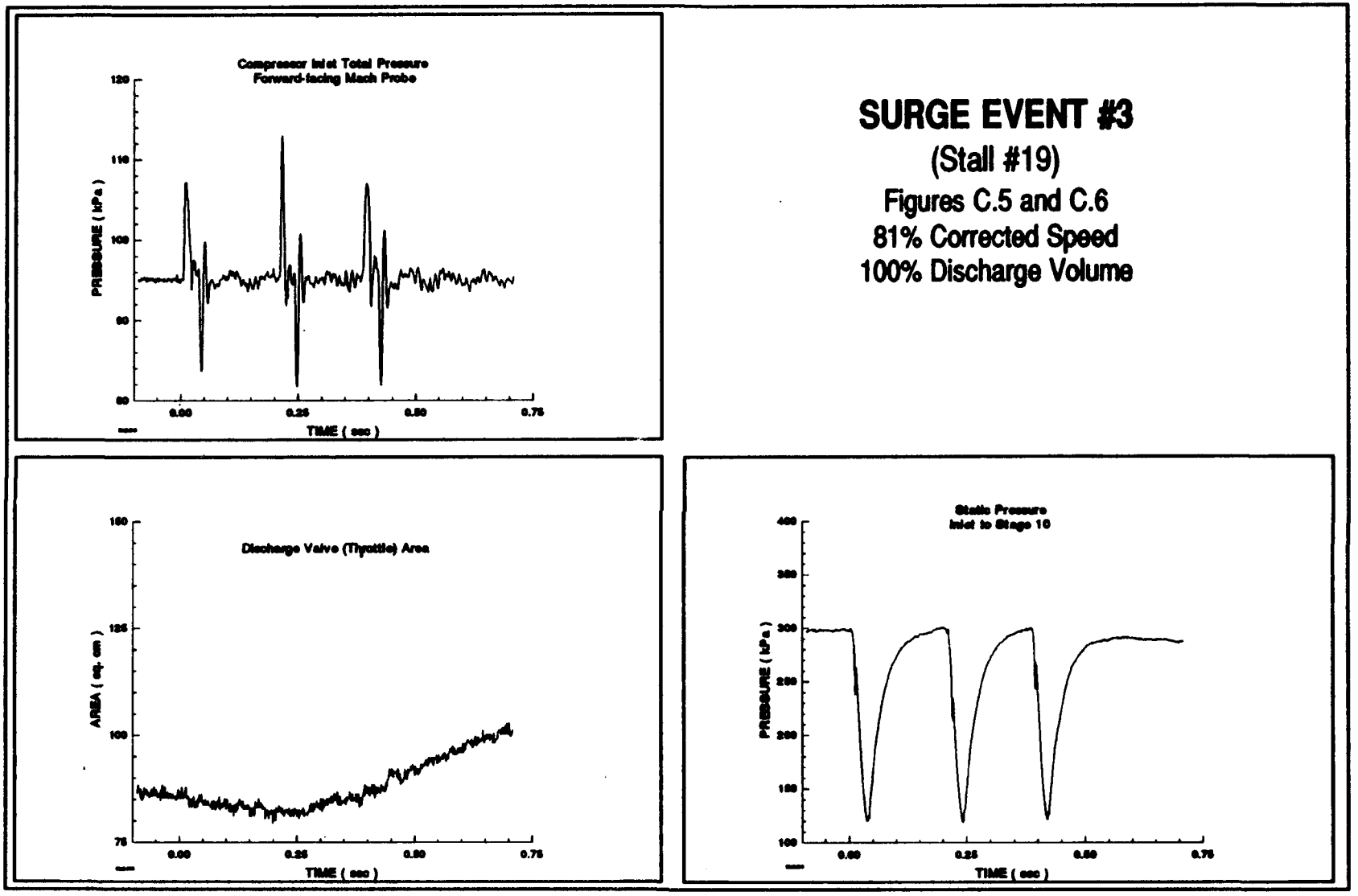

Figure C.5 Surge Event #3 Data

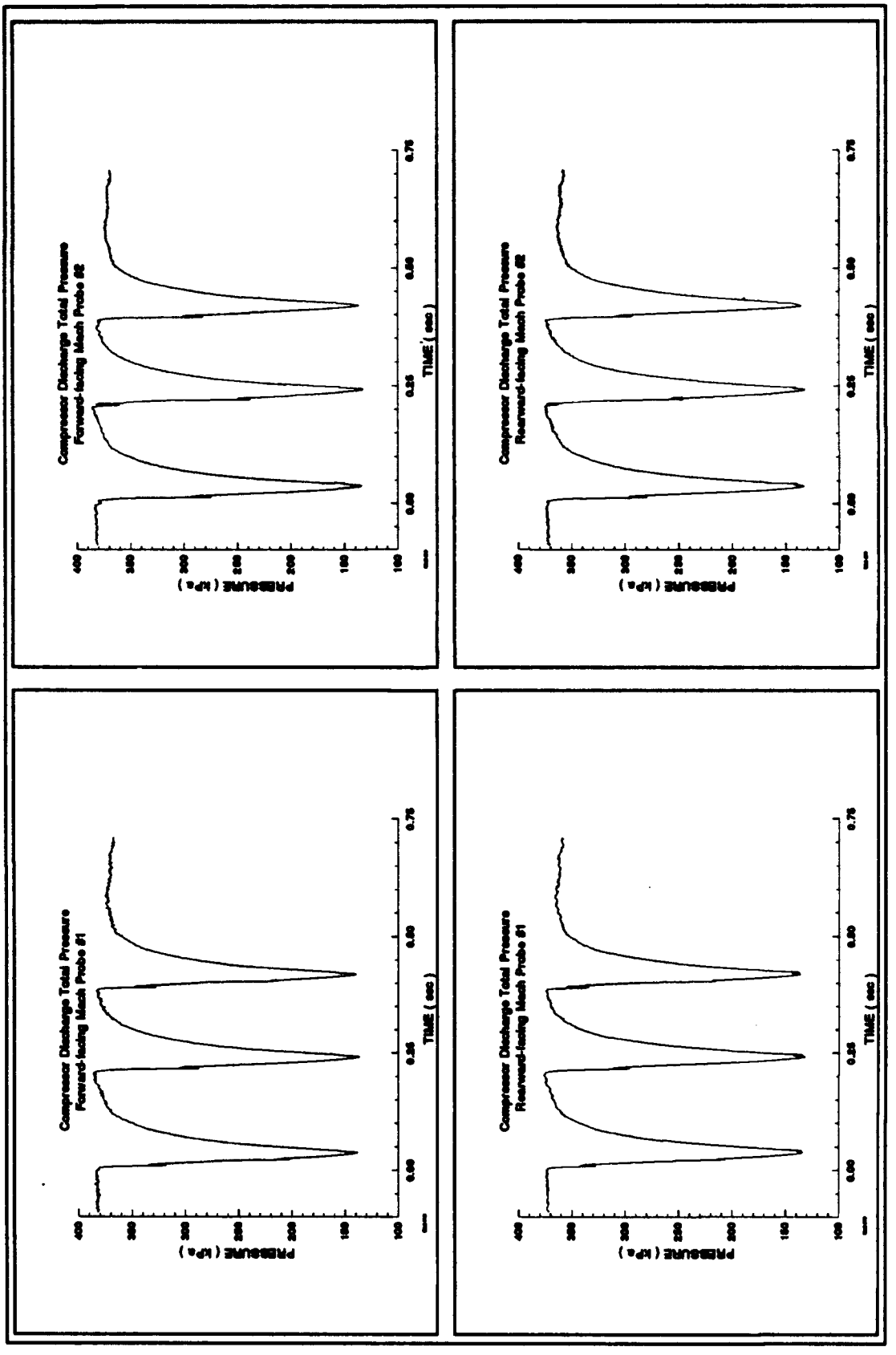

Figure C.6 Surge Event #3 Data

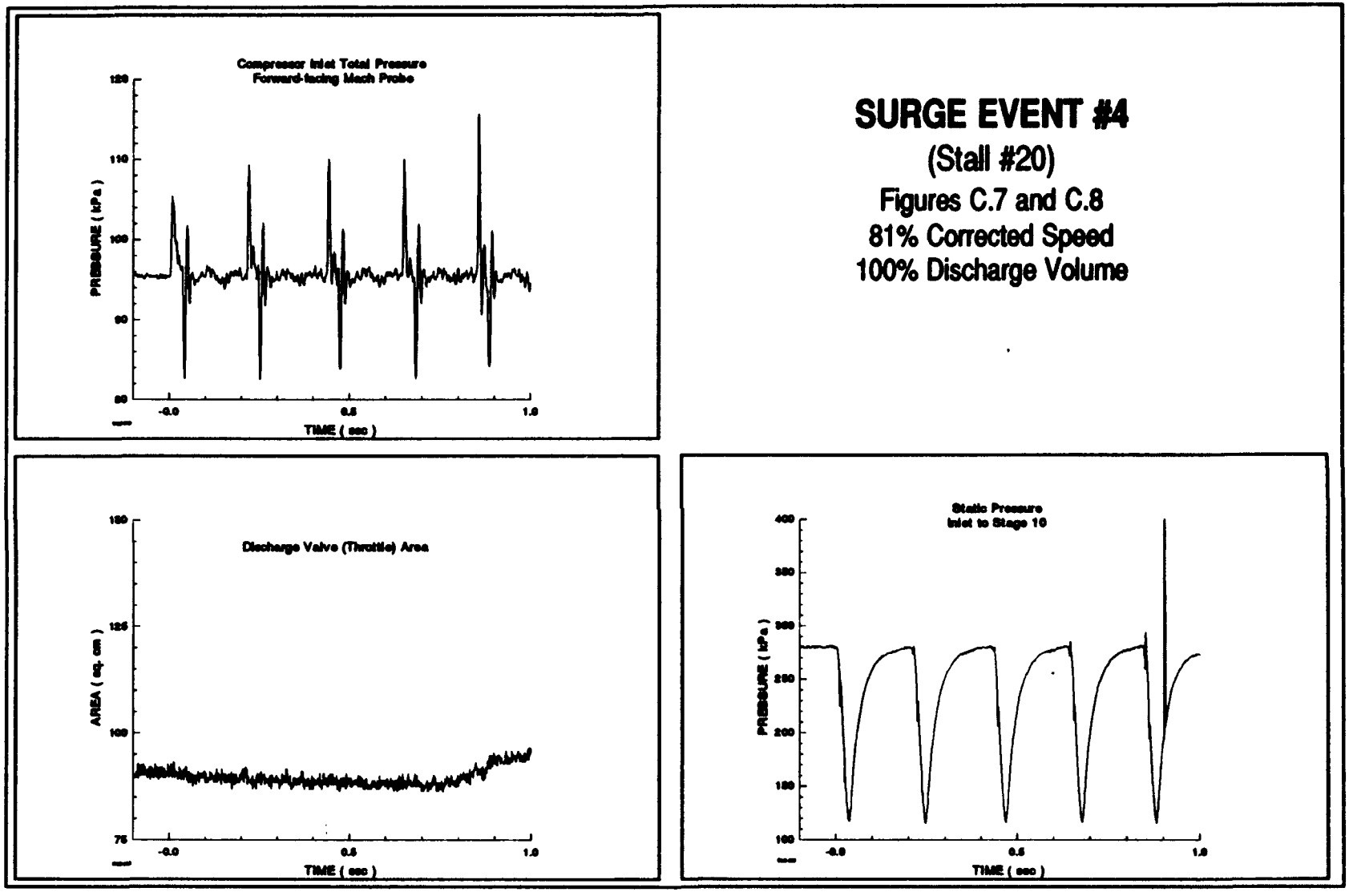

Figure C.7 Surge Event #4 Data

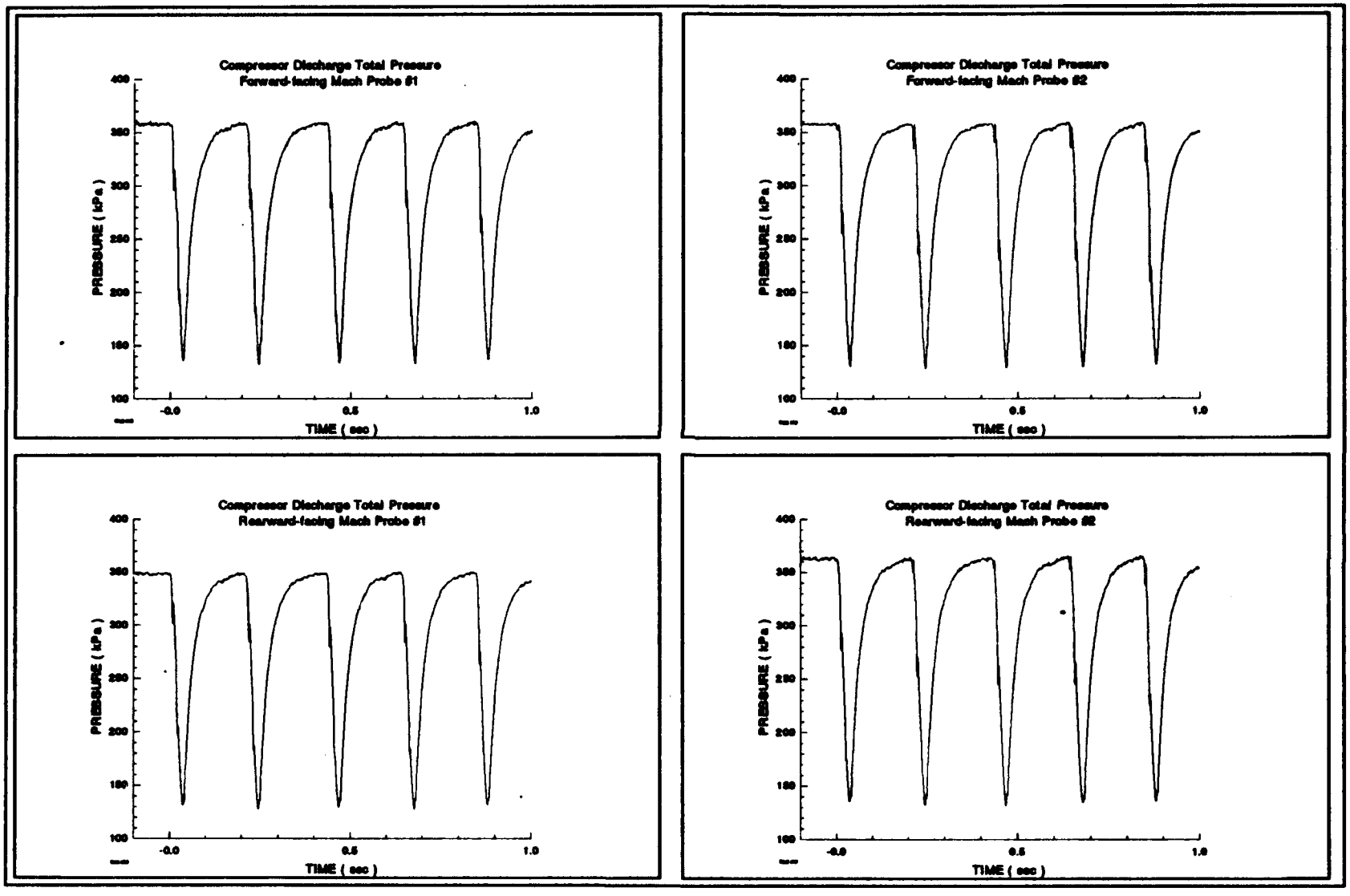

Figure C.8 Surge Event #4 Data

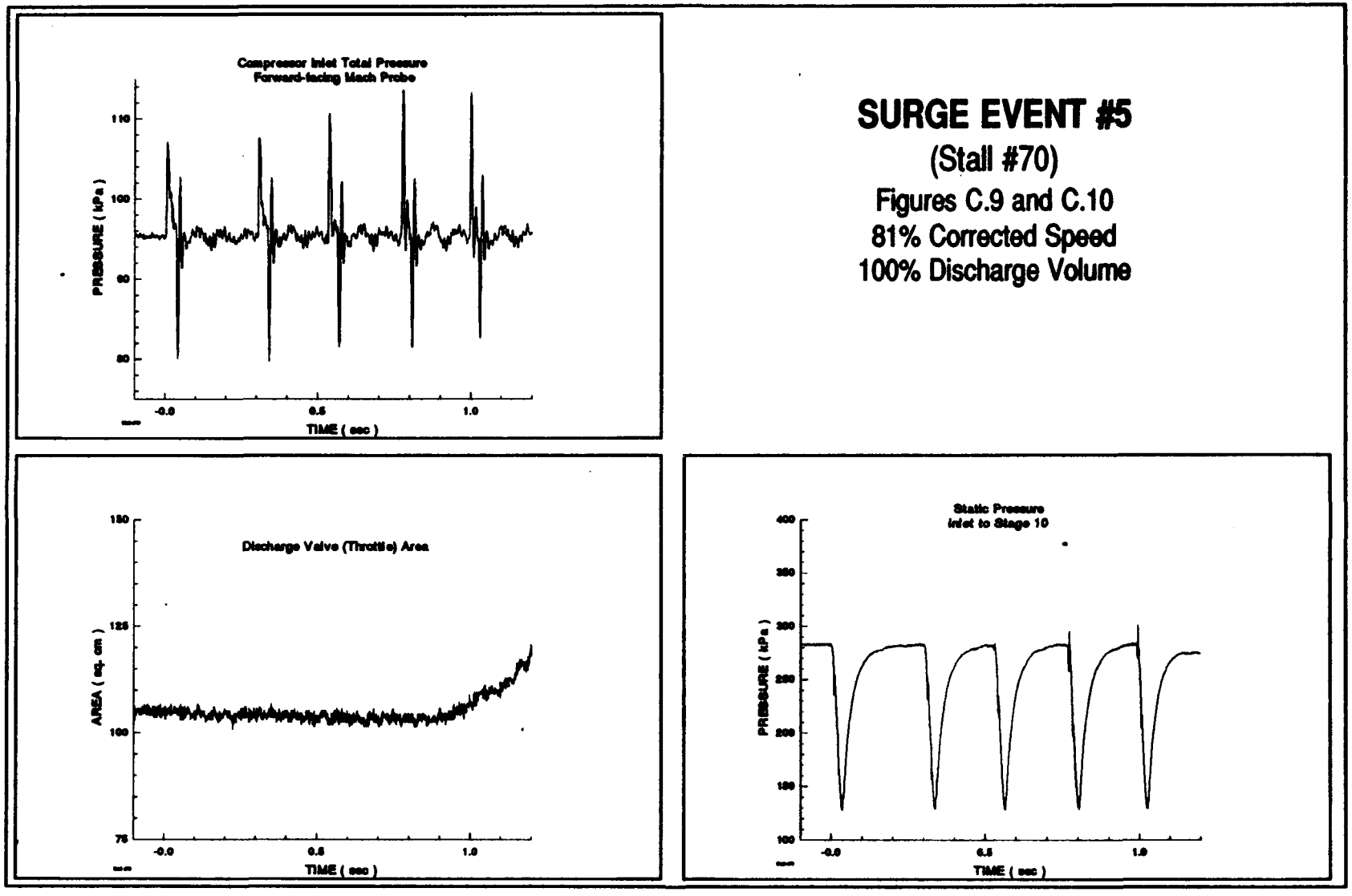

Figure C.9 Surge Event #5 Data

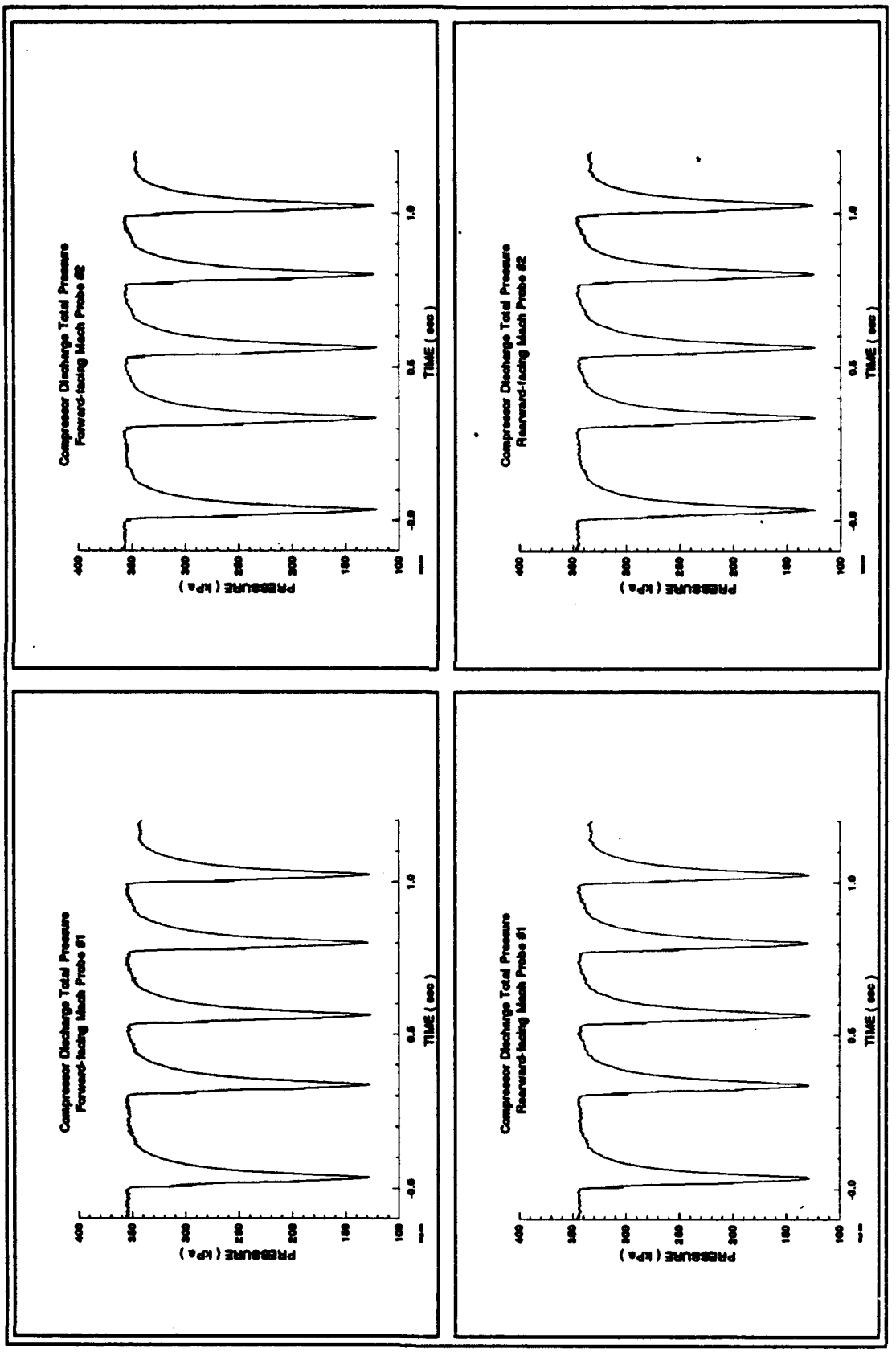

Figure C.10 Surge Event #5 Data

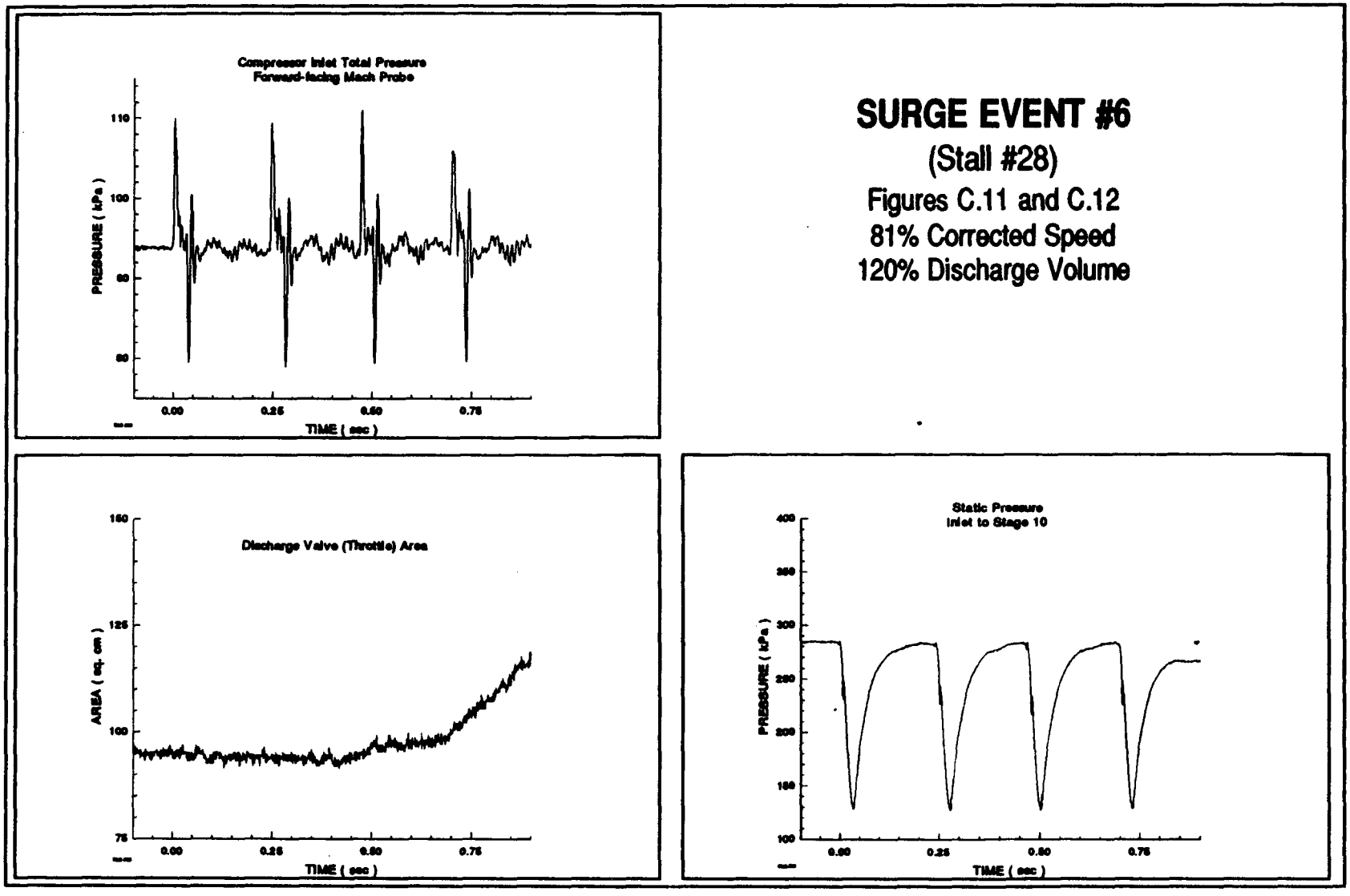

Figure C.11 Surge Event #6 Data

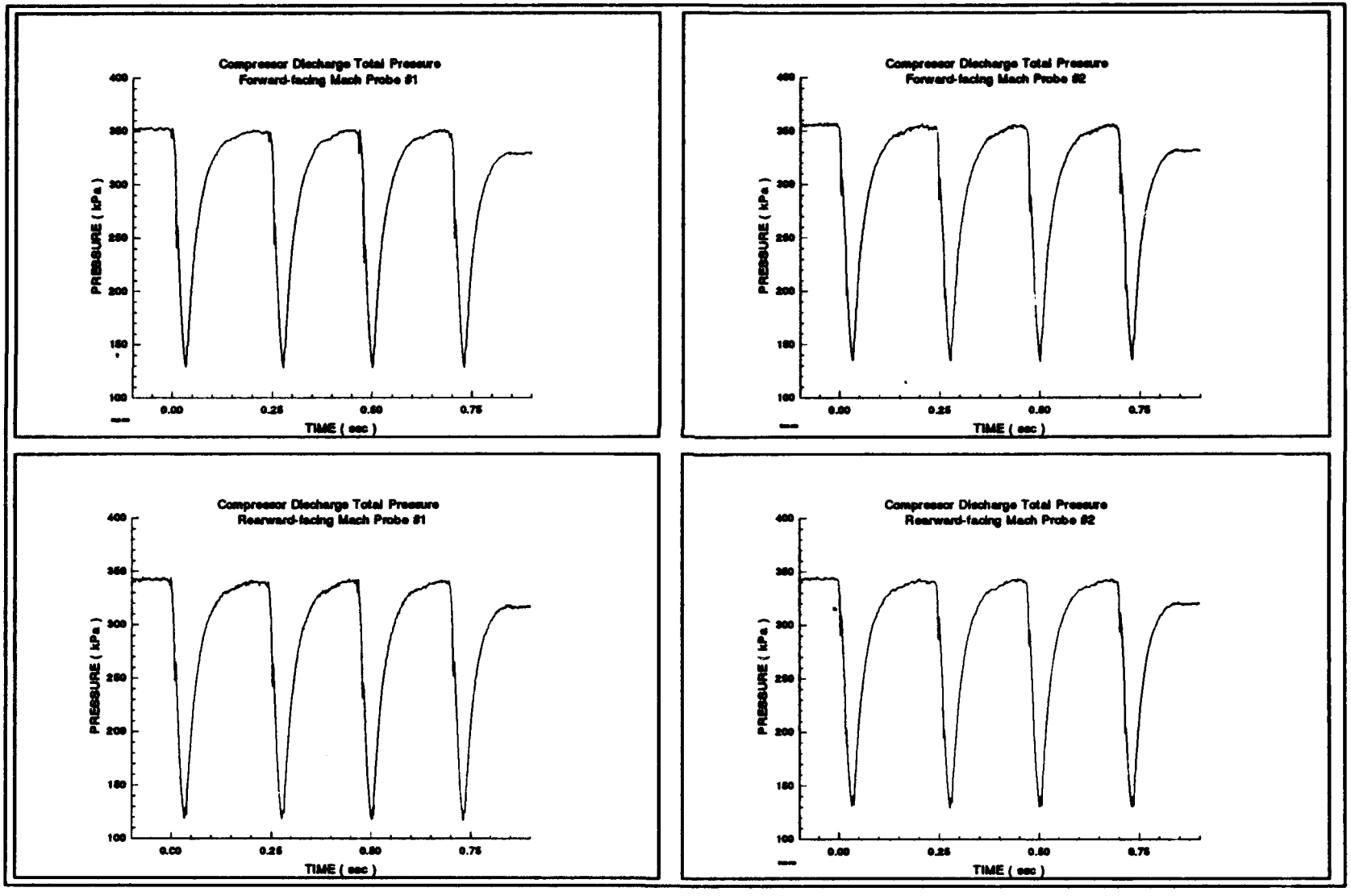

Figure C.12 Surge Event #6 Data

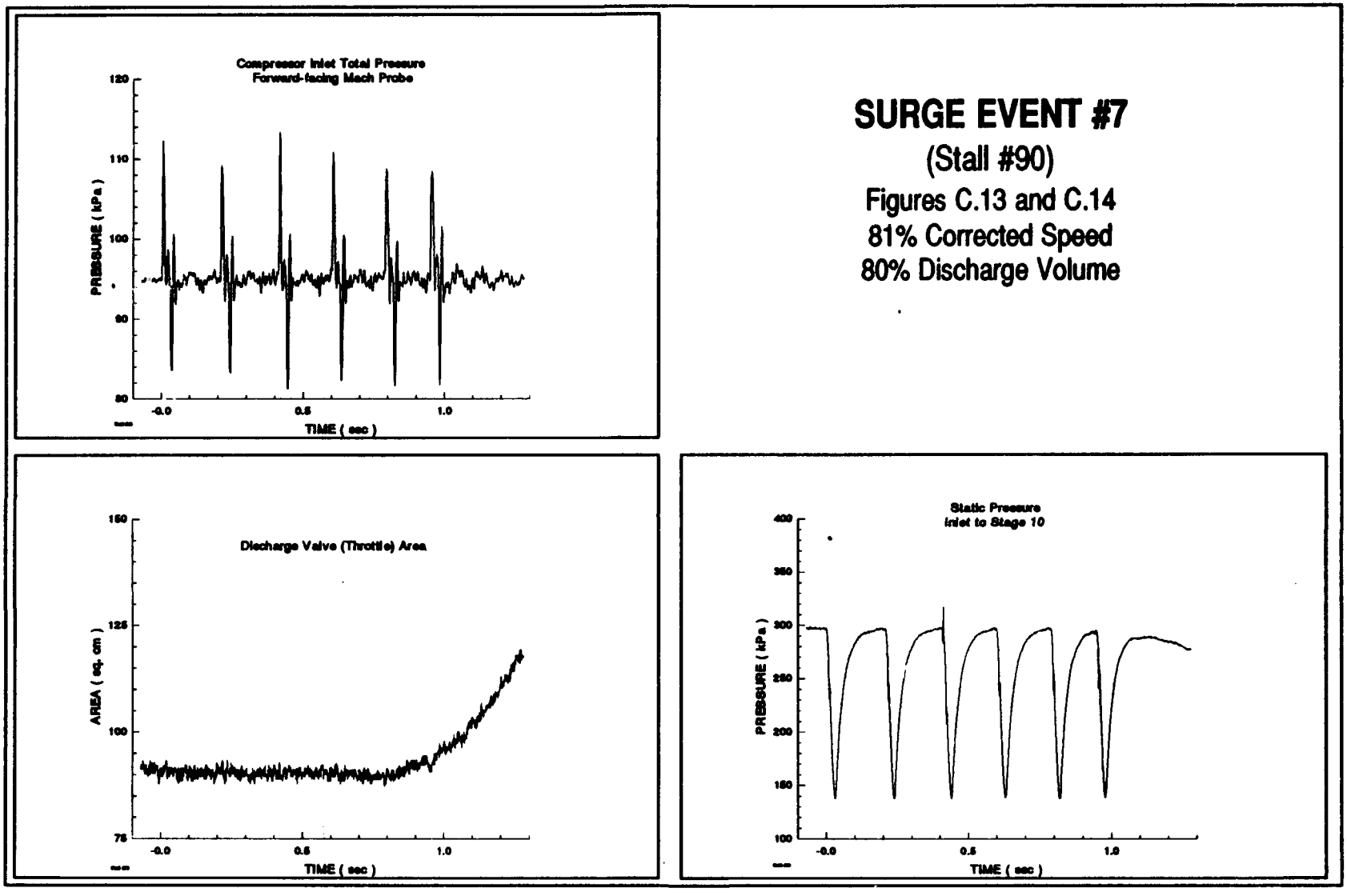

Figure C.13 Surge Event #7 Data

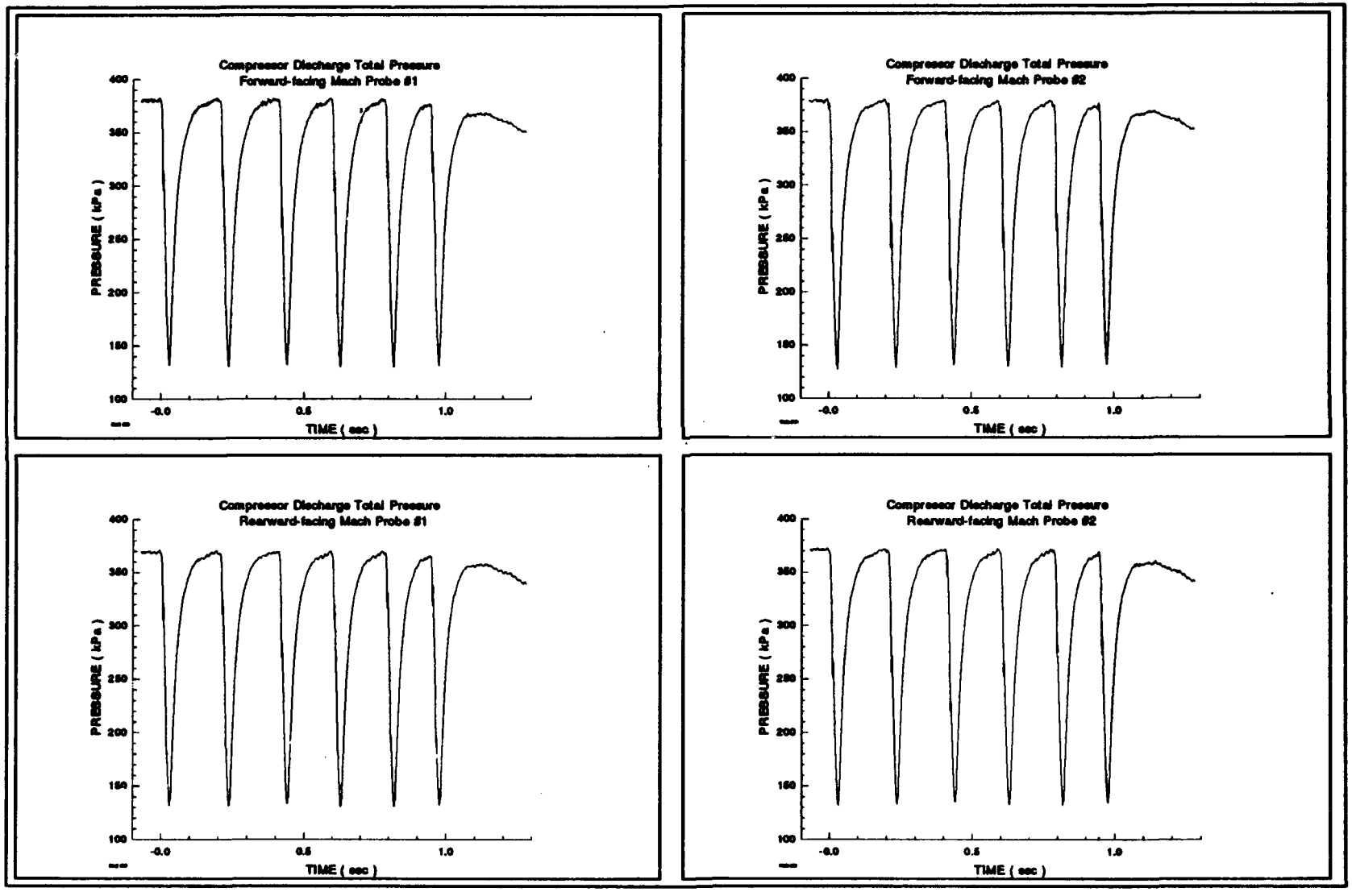

Figure C.14 Surge Event #7 Data

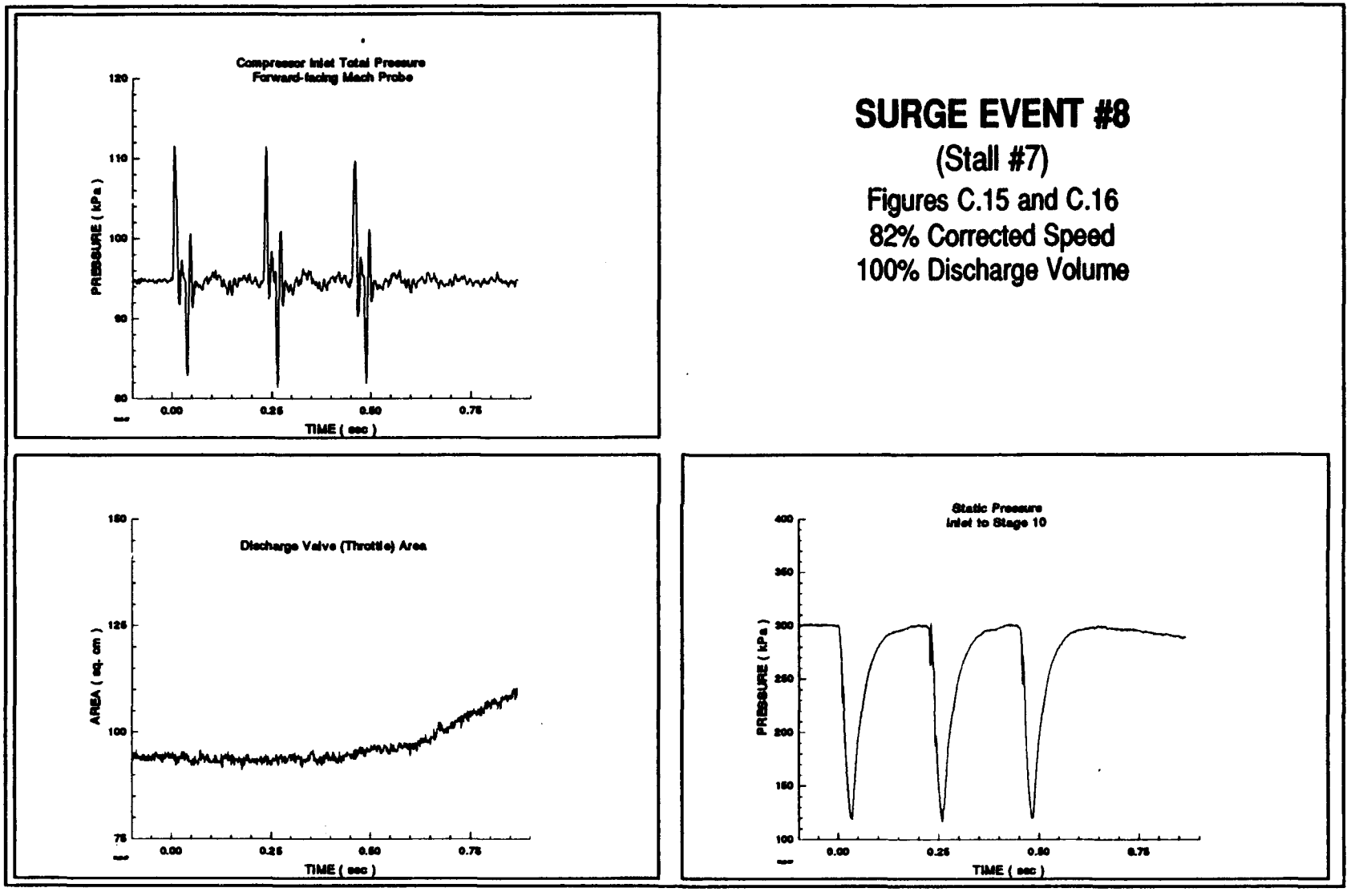

Figure C.15 Surge Event #8 Data

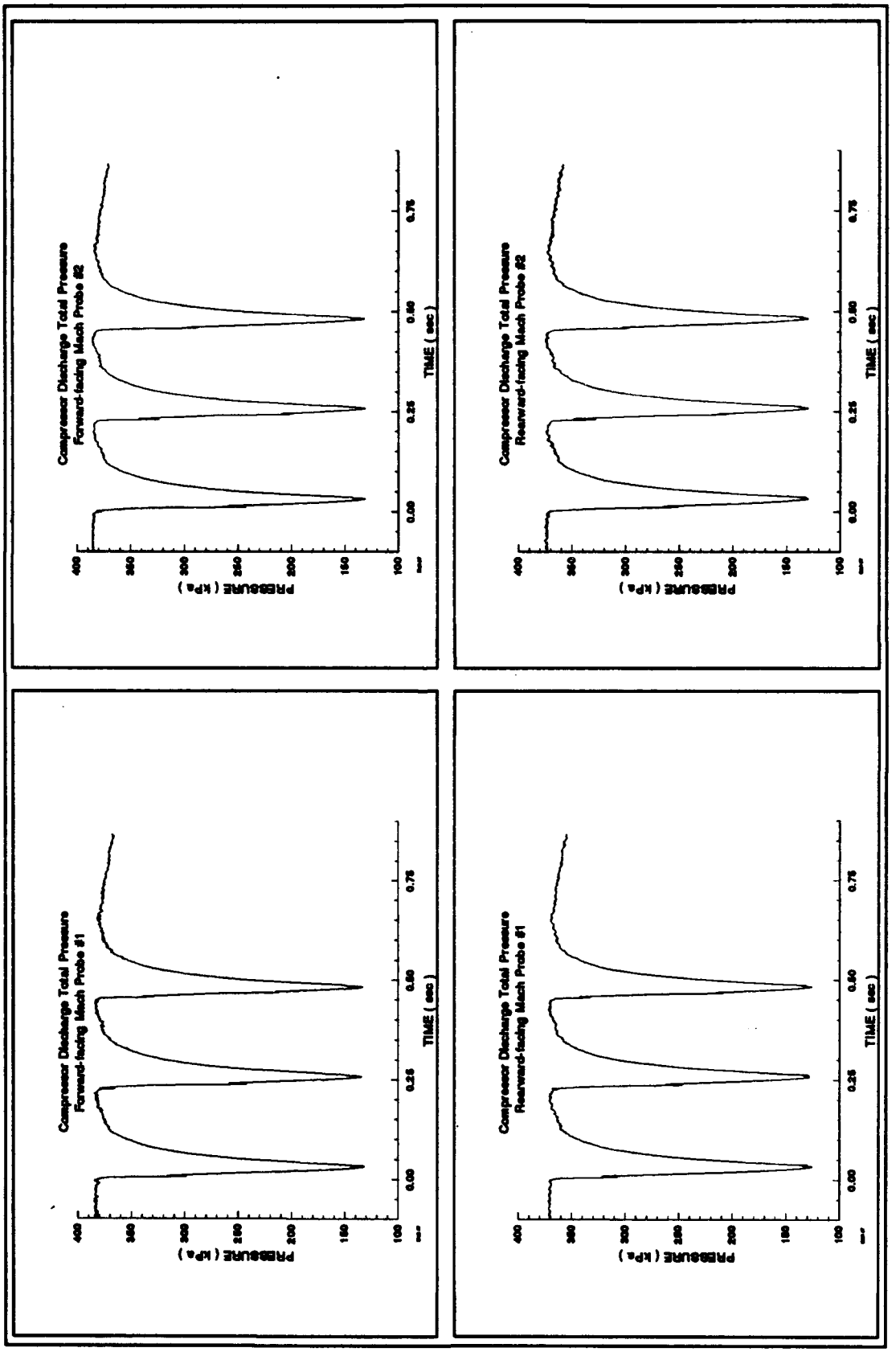

Figure C.16 Surge Event #8 Data

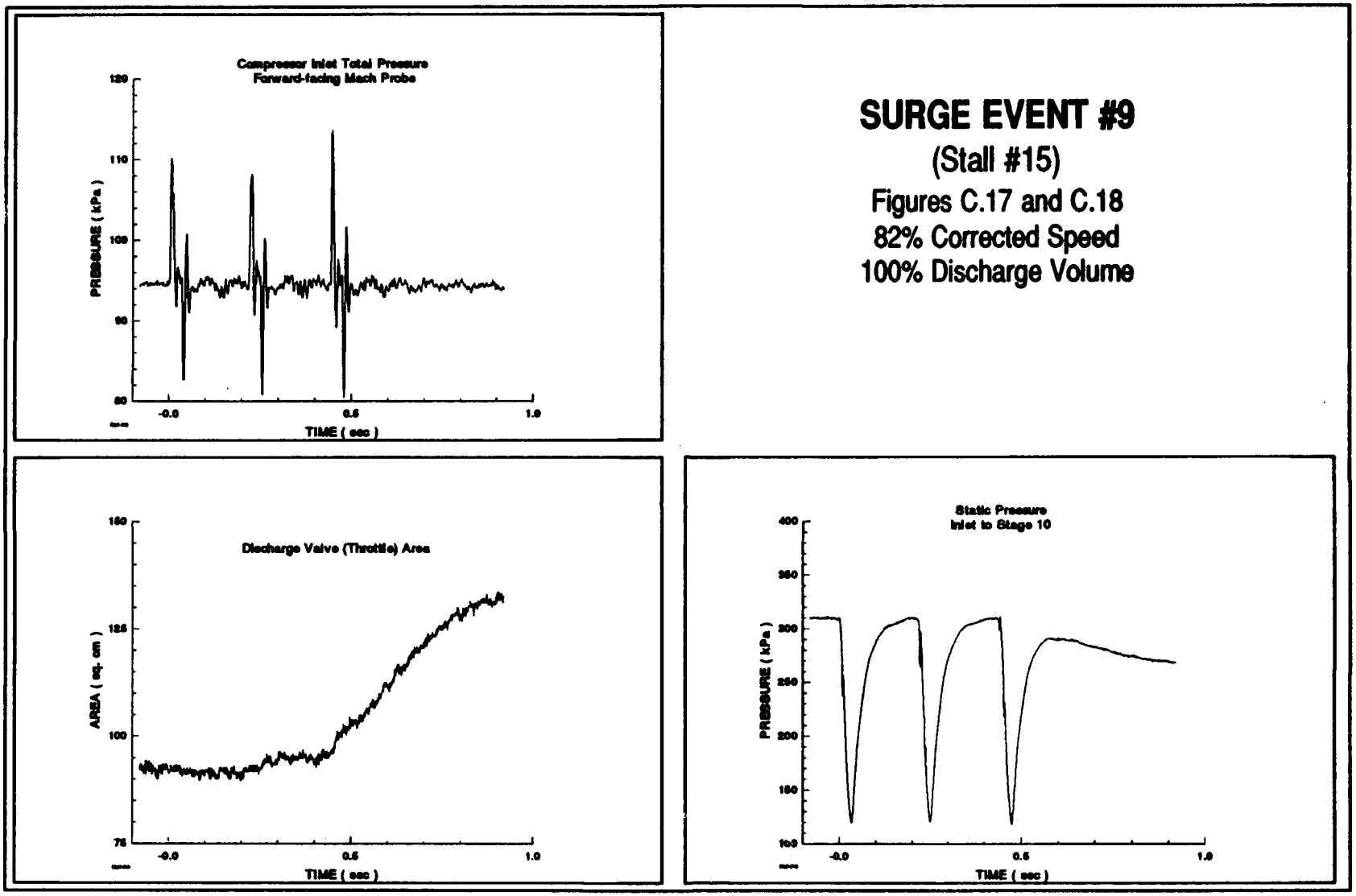

Figure C.17 Surge Event #9 Data

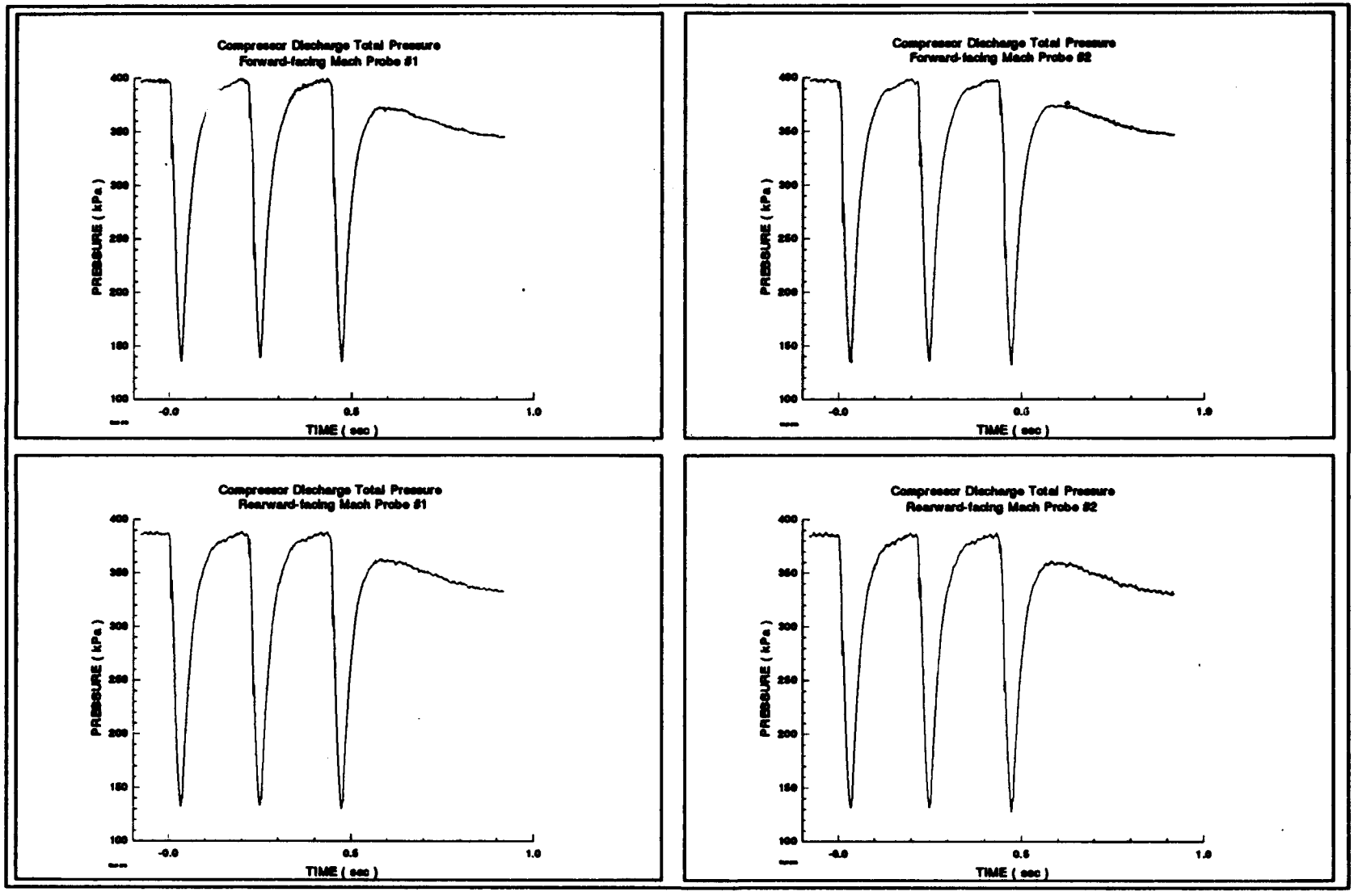

Figure C.18 Surge Event #9 Data

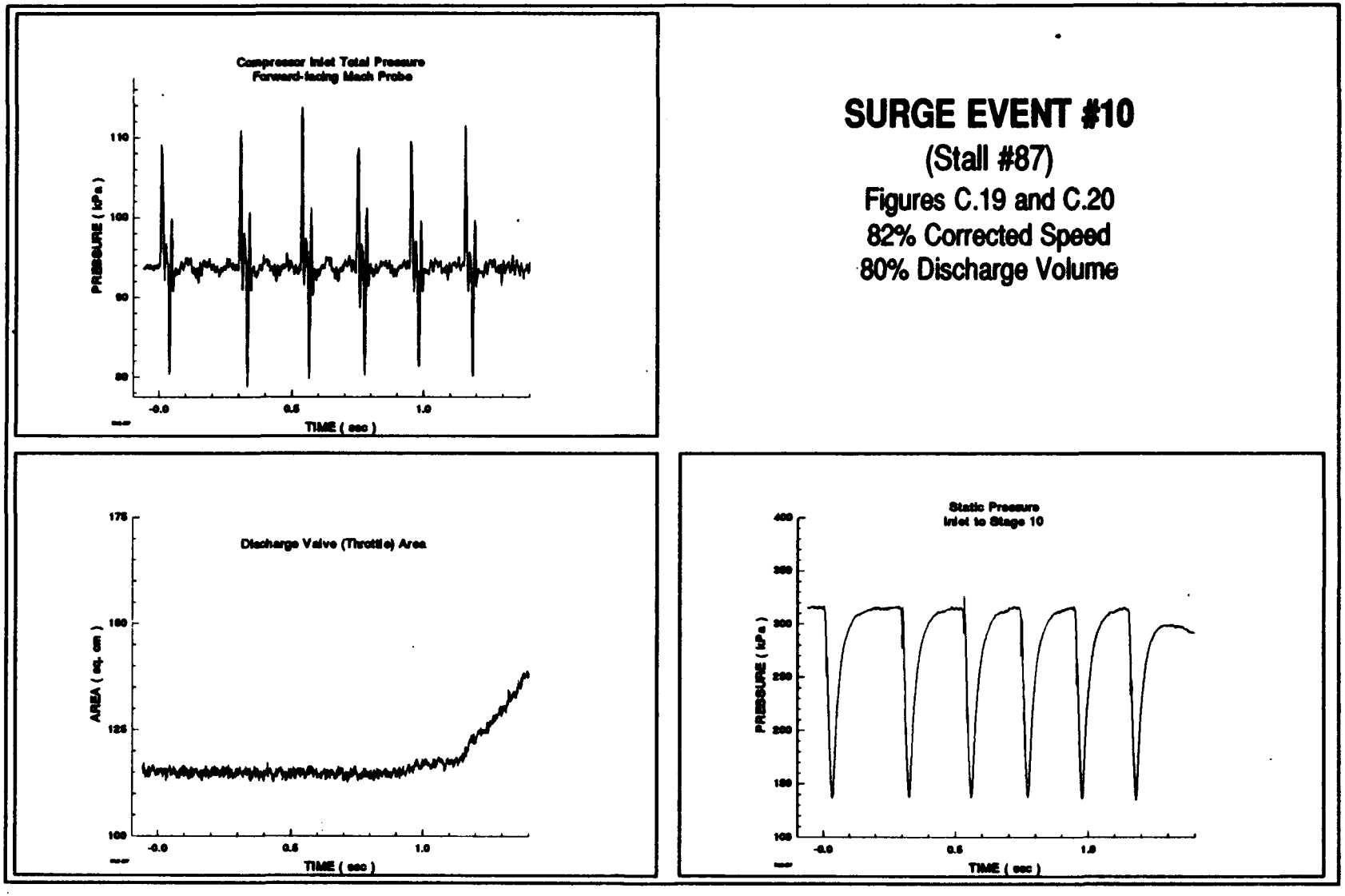

Figure C.19 Surge Event #10 Data

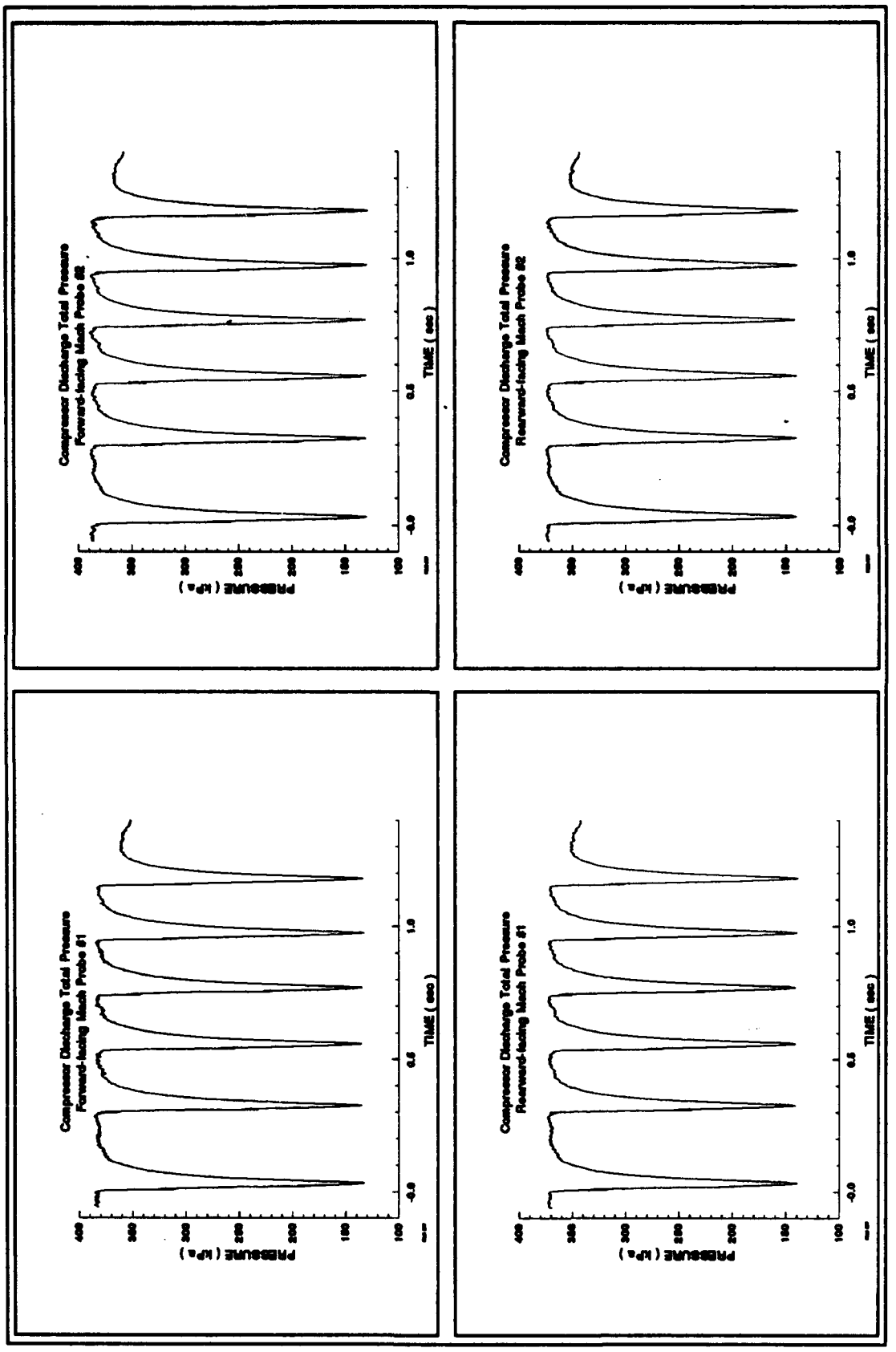

Figure C.20 Surge Event #10 Data

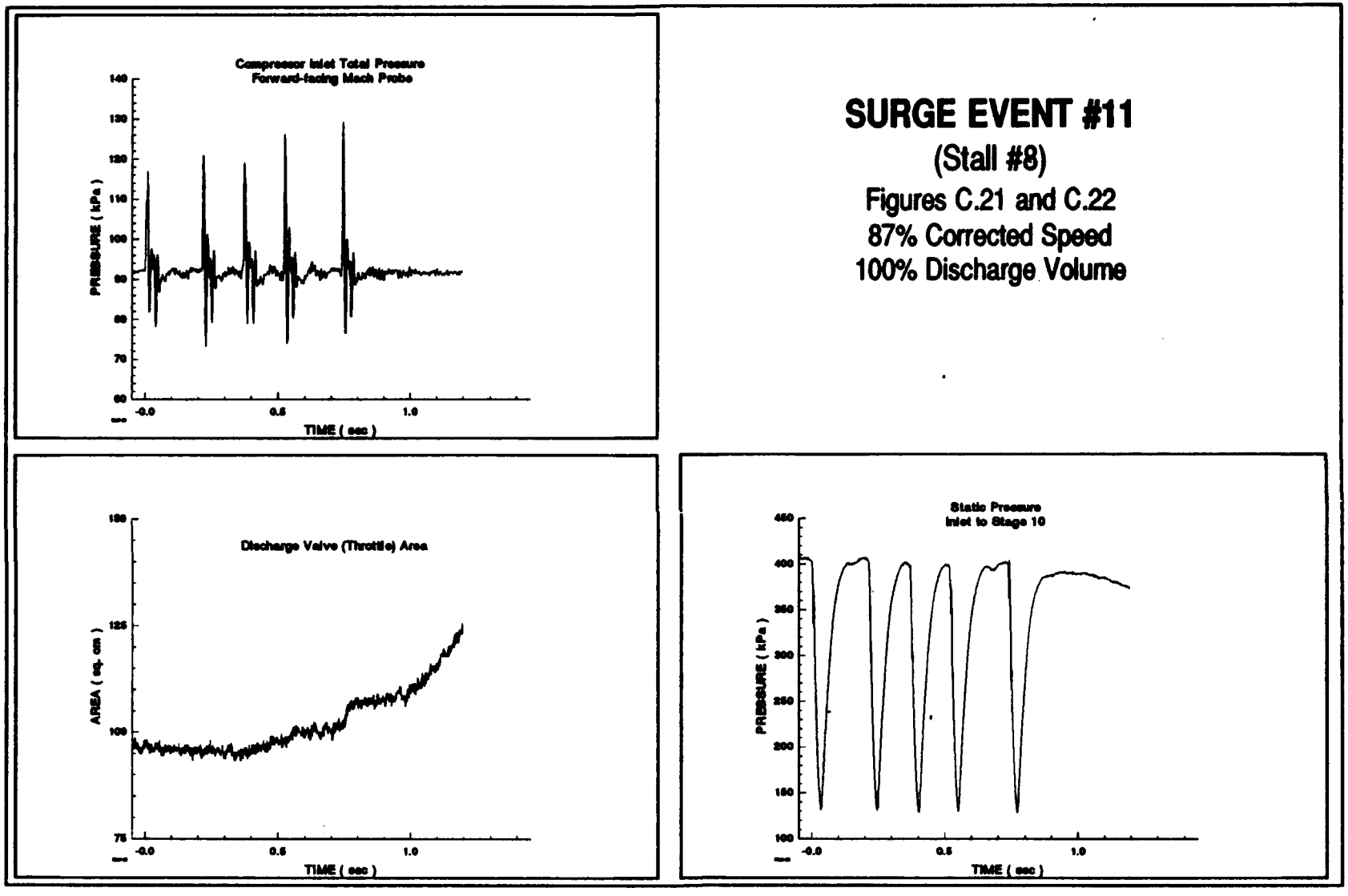

Figure C.21 Surge Event #11 Data

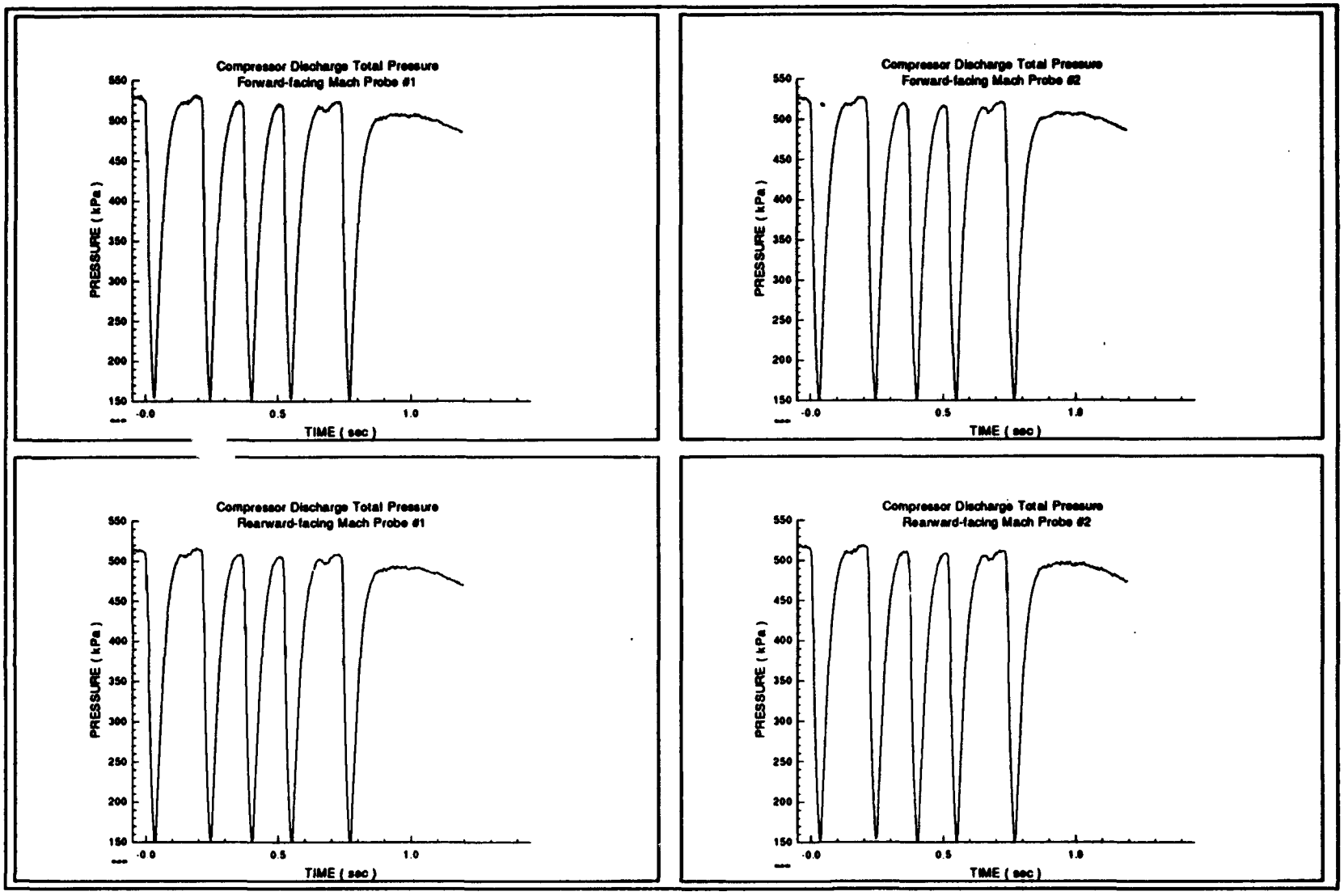

Figure C.22 Surge Event #11 Data

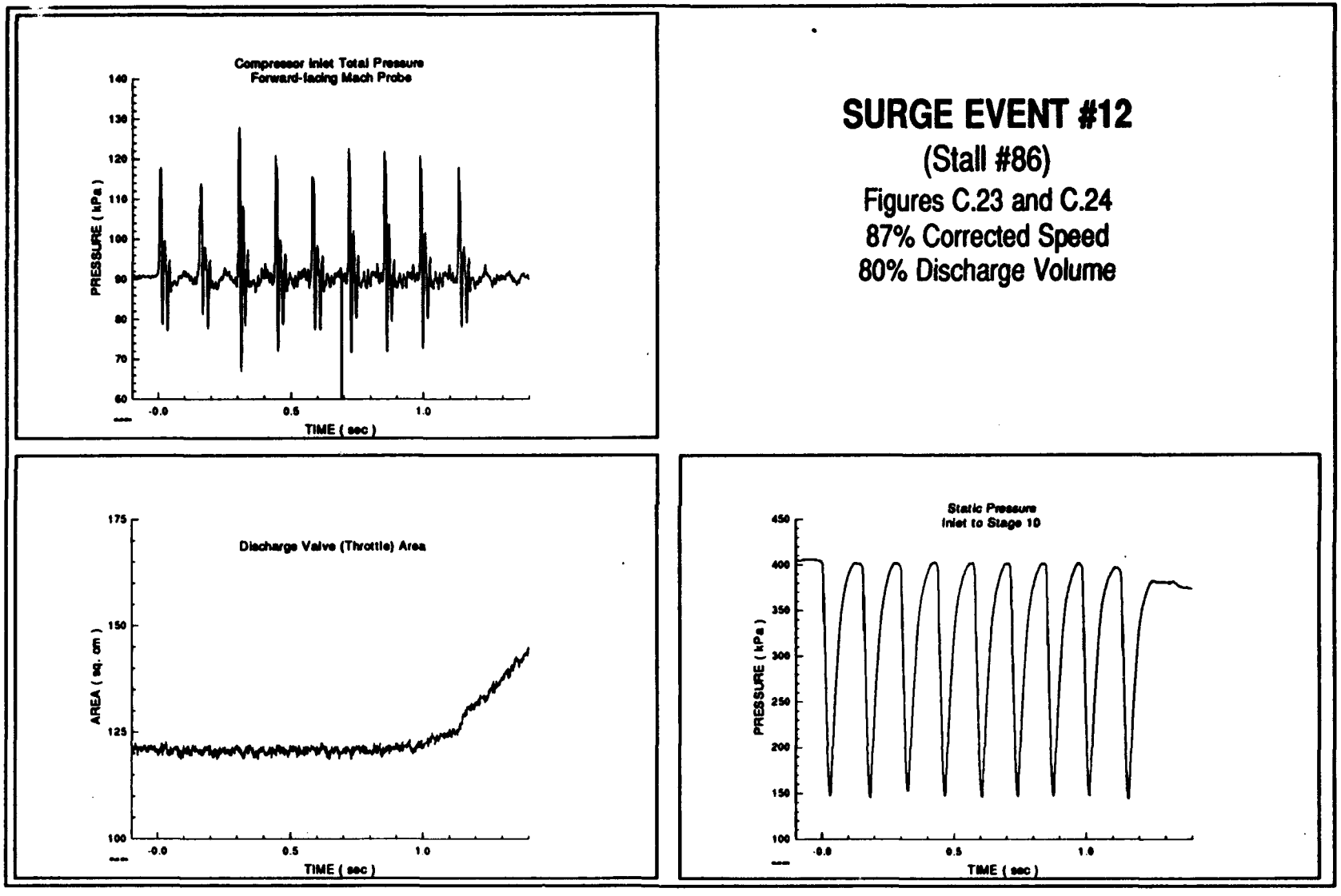

Figure C.23 Surge Event #12 Data

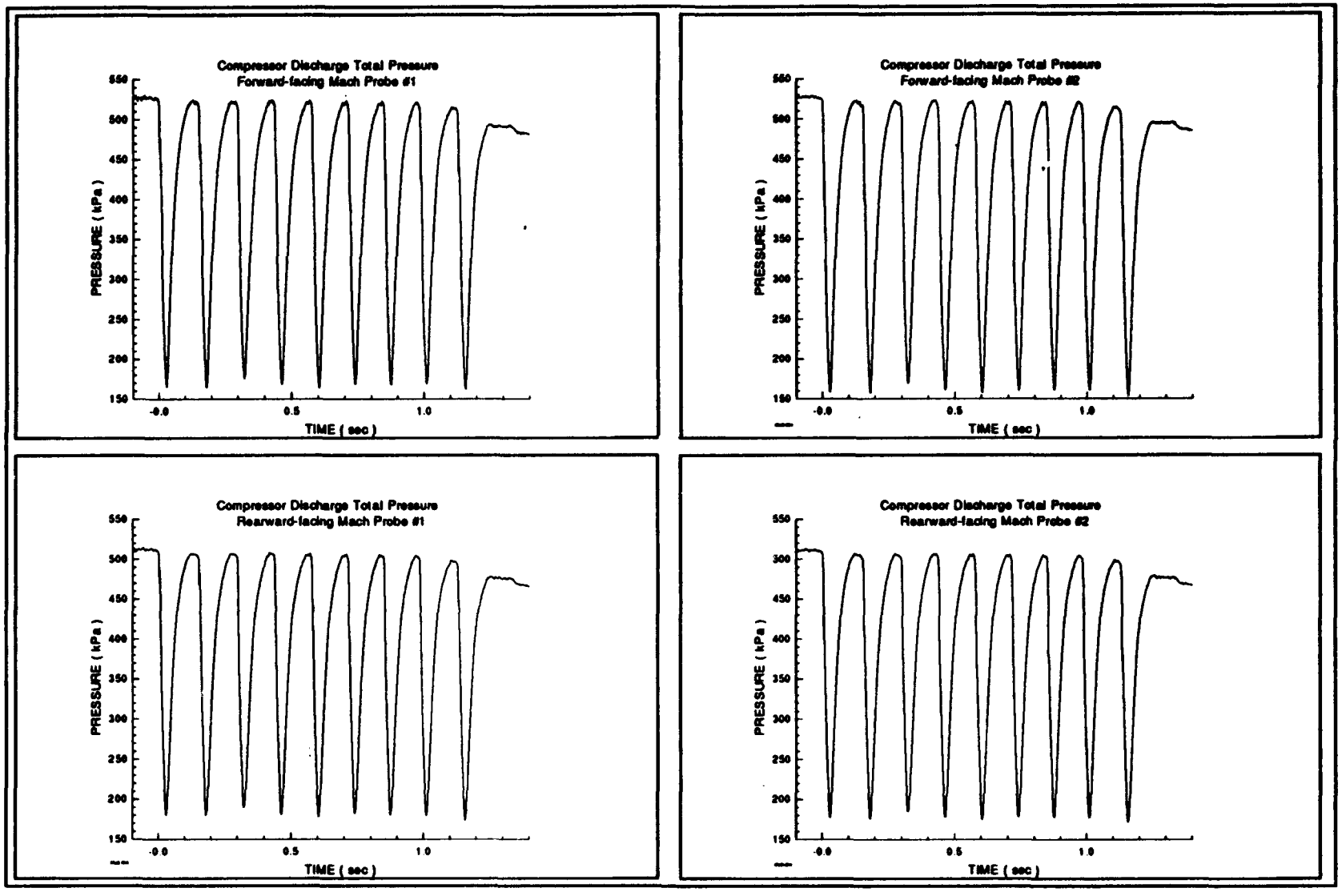

Figure C.24 Surge Event #12 Data